PURDUE UNIVERSITY
GRADUATE SCHOOL
Thesis/Dissertation Acceptance

This is to certify that the thesis/dissertation prepared

By Tanu Tanu

Entitled
HIGH SENSITIVITY NANOTECHNOLOGY GAS SENSING DEVICE

For the degree of Master of Science in Electrical and Computer Engineering

Is approved by the final examining committee:

Maher E. Rizkalla	Ahdy W. Helmy
Chair	
Mohamed A. El-Sharkawy	Brian S. King
Paul Salama	

To the best of my knowledge and as understood by the student in the Thesis/Dissertation Agreement, Publication Delay, and Certification Disclaimer (Graduate School Form 32), this thesis/dissertation adheres to the provisions of Purdue University's "Policy of Integrity in Research" and the use of copyright material.

Approved by Major Professor(s): Maher E. Rizkalla

Approved by: Brian S. King 12/06/2016

Head of the Departmental Graduate Program Date

HIGH SENSITIVITY NANOTECHNOLOGY GAS SENSING DEVICE

A Thesis

Submitted to the Faculty

of

Purdue University

by

Tanu Tanu

In Partial Fulfillment of the

Requirements for the Degree

of

Master of Science in Electrical and Computer Engineering

December 2016

Purdue University

Indianapolis, Indiana

This thesis work is dedicated to my husband Vijeet who has been my source of motivation and has supported me throughout my studies when I was facing challenges. I also want to dedicate it to my parents, my mother-in-law and my siblings who have always loved me unconditionally and who's good examples have taught me to work hard for the things that I aspire to achieve.

ACKNOWLEDGMENTS

Foremost, I would like to express my sincere gratitude to my advisor Prof. Maher Rizkalla for the continuous support of my thesis study and research, for his patience, motivation, enthusiasm, and immense knowledge. His guidance helped me in all the time of research and writing of this thesis. I could not have imagined having a better advisor and mentor for my research.

Besides my advisor, I would like to thank the rest of my thesis committee: Prof. M. El-Sharkawy, Prof. Paul Salama, and Dr. Ahdy Helmy, for their encouragement, insightful comments, and hard questions.

I am grateful to Dr. Brian King for offering me motivation and support for starting my master's degree at IUPUI. I want to acknowledge INDI (Integrated Nano-systems Development Institute) lab for allowing use of sophisticated equipment and apparatus which was necessary for my research work. I also want to acknowledge Richard G. Lugar Center at IUPUI for allowing me to use Xenon flash lamp.

I also want to thanks Dan Minner for training me for using the sophisticated instruments and apparatus. I thank my fellow mate Neeraj Rathi for his support in developing the embedded part of the sensor and Monika Kakani for stimulating discussions, for the sleepless nights we were working together before deadlines.

Last but not the least, I would like to thank my family: my parents Ajay and Mohini for giving birth to me at the first place and supporting me spiritually throughout my life.

TABLE OF CONTENTS

Page

Page

LIST OF TABLES

LIST OF FIGURES

Figure Page

SYMBOLS

m	mass
v	velocity
V	volts
A	ampere
Ω	ohms
Λ	lambda
Δ	delta
$\mathring{A}$	angstrong
μ	micro
ρ	resisivity
ϵ	electrical permittivity
n	nano
p	pico
f	femto

ABBREVIATIONS

VOCs	volatile organic compounds
CNT	carbon nanotube
PWM	pulse width modulation
IoT	internet of things
MCU	micro controller unit
HTTP	hypertext transfer protocol
MQTT	message queue telemetry transport
IP	internet protocol
MAC	media access control
ARM	advanced RISC machines
RISC	reduced instruction set computer
SoC	system on chip
MEMS	micro electro-mechanical systems
NEMS	nano electro-mechanical systems
S/N	signal to noise
CMRR	common-mode rejection ratio
CVD	chemical vapor deposition
MOCVD	metal-organic chemical vapor deposition
PECVD	plasma-enhanced chemical vapor deposition
MBE	molecular beam epitaxy
RF	radio frequency
DC	direct current
CZ	czochralski
FET	field effect transistor

JFET	junction field effect transistor
AuNPs	gold nanoparticles
SEM	scanning electron microscope
ppm	parts per million
ppb	parts per billion

ABSTRACT

Tanu, Tanu. M.S.E.C.E., Purdue University, December 2016. High Sensitivity Nanotechnology Gas Sensing Device. Major Professor: Rizkalla M. Professor.

The nanotechnology materials have been used for high sensitivity sensing devices due to their ability to alter their properties in response to the environmental parameters such as temperature, pressure, gas, electromagnetic, and chemicals. The features of employing nanoparticles on top of graphene thin film have driven the hypothesis of achieving high sensing nanotechnology devices.

This study demonstrates a novel approach for designing a low noise nanoparticle based gas sensing device with internet of things (IoT) capability. The system is capable of minimizing cross-talk between multiple channels of amplifiers arranged on one chip using guard rings. Graphene mono-layer is utilized as sensing material with the sensitivity catalyzed by addition of gold nano-particles on its surface. The signal from the sensing unit is received by an offset cancellation amplifying system using a system on chip (SoC) approach. IoT capability of the sensing device is developed using FRDM K64f micro-controller board which sends messages on IoT platform when a gas is sensed. The message is received by an application created and sent as an email or message to the user.

This study details the mathematical models of the graphene based gas sensing devices, and the interface circuitry that drives the differential potentials, resulting from the sensing unit. The study presents the simulation and practical model of the device, detailing the design approach of the processing unit within the SoC system and wireless implementation of it.

The sensing device was capable of sensing gas concentration from 5% to 100% using both the resistive and capacitive based models. The I-V characteristics of the

FET sensing device was in agreeable with the other models. The SoC processing unit was designed using cadence tools, and simulation results showed very high CMRR that enable the amplifier to sense a very low signal received from the gas sensors. The cross talk noise was reduced by surrounding guard rings around the amplifier circuits. The layout was accomplished with 45nm technology and simulation showed an offset voltage of 17μV.

1. INTRODUCTION

Gas sensing technology is extensively investigated due to its wide range of applications and inherent limitations. Applications in areas such as industrial, medical, residential and homeland security make it a significant area of development due to which it is grabbing attention in industrial as well as academics researches. The studies been established of gas sensing technology have three major areas of investigation, which are different kinds of sensors, sensing principles and fabrication techniques [1].

Gas sensing methods are widely based on variation of electrical properties and optical, acoustic, thermal properties among others. There are varieties of methods based on electrical variation with different materials being used like metal oxide semiconductor, polymer, graphene and carbon nanotubes among others. Metal oxide semiconductor materials like SnO_2, Al_2O_3, TiO_2 etc provide sensing with an advantage of low cost and high sensitivity and have been widely utilized. However, they possess some inherent challenges like poor performance at high temperature and structural instability and defects. Metal oxide semiconductor materials exhibit greater sensitivity to inorganic gases like ammonia etc but they cannot detect some harmful volatile organic compounds (VOCs). On the other hand, polymer material based sensing devices are commonly used to detect VOCs as well as some inorganic compounds. But they also have some disadvantages such as poor selectivity, instability over a long time and irreversibility. Smart nano-materials graphene, carbon nanotubes etc serve in detection of physical quantities such as change in electrical energy, chemical energy, mechanical energy, optical energy etc. Due to unique electrical properties, mechanical properties and high surface to volume ratio, graphene and carbon nano-tubes have been widely explored for gas sensing devices. The change in any of the parameter of the sensor due to change in physical quantity provides us useful information. It may lead us to detect type of gas, its concentration, pressure, temperature, flow, etc.

While designing and applying gas sensors, performance of the sensing device is evaluated from its several properties. Sensitivity of a gas sensor is a vital indicator of its performance, and gives us an estimate of the lowest concentration of gas it can detect. Selectivity of the sensor is another important aspect where the gas sensor is able to detect a particular gas from a mixture of gases. According to researchers [2], approaches which perform changes in composition of sensing materials by decorating them with catalytic metal nano-particles are mentioned to improve sensitivity and selectivity of the sensors. Other performance indicators like response time, power consumption, fabrication cost, reversibility among others are significant factors leading to an efficient sensor. Besides these, a gas sensor needs to ensure a stable and reproducible signal for a long period of time.

1.1 Gas Sensing Devices

1.1.1 Importance of Gas Sensing Devices

Comfort and health

The environment where we live has numerous kinds of gases, some of which are essential to our living and some of which are harmful. An adequate level has to be maintained for all such gases and specifically the level of harmful gases has to be controlled all the time. Pollution in the atmosphere is caused by stationary sources such as residences, factories, refineries, etc or mobile sources such as automobiles, ships, trains and so forth. To detect, monitor, and control damage caused by bad air quality, reliable sensing systems are needed. Therefore, for the enhancement of living standards, gas-sensing technology is developing rapidly to provide people with safer and healthier environment. A similar case of poor air quality appeared in 2001, where the occupants of workplace premises were suffering from a disease called "Sick building syndrome". The symptoms included headache, absenteeism and reduced work efficiency. Some of the factors responsible involved inadequate ventilation, chemical and biological contaminants resulting in bad quality air [3].

To prevent such extreme situations to occur, low cost, high sensitivity gas sensing devices can be employed for air quality monitoring in real time. This can decrease the incidences related to respiratory system illnesses; consequently, people will have a better quality of life. This is particularly important for children and elderly people. This will have an economic impact on society, as it will help to reduce the costs associated with the treatments of these illnesses.

Homeland Security

Gas sensing devices can be applied for homeland security in case of poisonous gas being used creating terror threat. Similar case occurred in Japan in 1995 [4], where early detecting of the poisonous gas could have saved lives. Also terror attacks or accidents concerning gas explosions could prove to be fatal if involving hazardous and lethal gases.Some of the poisonous gases like carbon monoxide are odorless and tasteless, making them undetectable by human senses. In all such conditions, it becomes crucial to have a device which can detect such harmful gases even at a very low concentration.

Household Safety

Gas leakage in residential as well as industrial areas poses a high risk of explosion if fossil fuels or combustibles gases are involved. Cooking appliances, fueling stations and more recent fuel cells using Hydrogen as energy source are a few to name among many, where monitoring of gas leakage is essential. Gas leakage from refrigerator and air conditioners may also pose risk of severe injury and death due to oxygen deprivation if leaked in closed spaces.

Ventilation

In automobile cabins also there is a risk of buildup of noxious gases due to extreme traffic conditions which could harm drivers ability to drive. For ventilation control of kitchen area through vents, sensors can be applied in the hooded vents to speed up the venting process in case of some gases and vice versa. Similarly in microwave oven, in order to optimize and automate cooking process, gas sensor can detect typical gases coming out of food while getting cooked.

Agriculture

In the agricultural areas, gas sensors can be deployed since levels of carbon dioxide have to be maintained and monitored for optimized plant growth in greenhouses.

Transportation

Transport sector plays an important role in contribution to the climate change and air pollution which are major environmental concerns today. It has adverse effect on the environment and serious impact on people's health. Hence emission control regulations are being enforced in various countries to bring the presence of air pollutants down [5]. Major vehicle emissions include CO, CO_2, hydrocarbons, oxides of nitrogen and particulate matters. To control the emissions by different treatment systems, first emission monitoring sensors are necessary. The gas sensors can gauge the levels of pollutants and feedback input to the treatment systems for efficient use.

Medical field

In medical field, gas sensors can be developed to detect presence of some particular compounds in patients breath to diagnose diseases. Human breathe is composed of CO_2, N_2, O_2, H_2O and other traces of gases which include inorganic molecules and other volatile organic compounds (VOCs) [6]. VOCs such as acetone, ethane and isoprene are products of metabolic reactions in the human body while inorganic compounds related to other health conditions can be indicators of other potential diseases. Therefore an abnormally high or low concentration of VOCs and inorganic compounds in human breathe can lead to easy diagnosis of diseases.

1.1.2 Sensor Characteristics

Signal received by the sensor needs to be processed for pulling out useful information from it. For accurate and acceptable processing of the signals, complete understanding of sensor operation, nature of signals received, along with static and dynamic characteristics of the sensing system is required [7]. Having understanding of the nature of signal and sensor, we will be able to perform data acquisition in correct

manner. Following this, the processing of data will be performed using appropriate interfacing circuitry and this will avoid loss of significant information. For correct mapping of output versus input of the sensor and for evaluation of performance of the sensing device, we need to know sensor characteristics behavior. Sensor characteristics for evaluating its performance, can be classified into two categories namely static and dynamic.

Static Characteristics

Static characteristics are the properties of the system after all transient effects have settled to their final or steady state. Important static characteristics of a sensor are as follows:

Accuracy

Accuracy of a sensing system is the capacity of the measuring instrument to give results close to the true value of the measured quantity.

Precision

Precision is the capacity of the instrument to measure the same reading repetitively under the same quantity and same conditions. Figure 1.1 is pictorial explanation of difference between accuracy and precision.

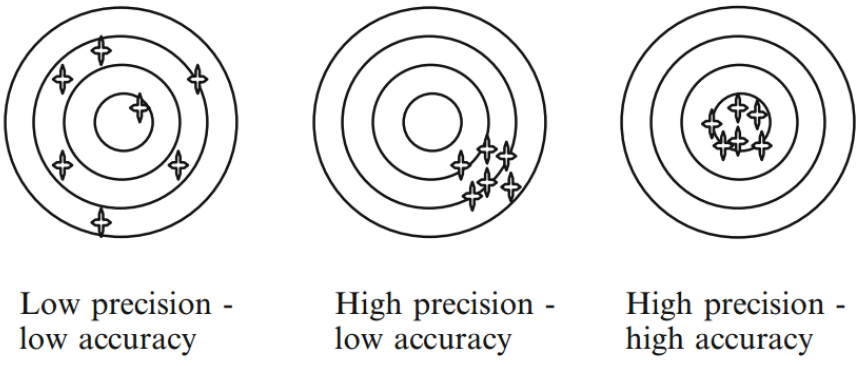

Fig. 1.1. Difference between accuracy and precision.

Repeatability

Repeatability is the sensing systems ability to produce same out when the environmental and operating conditions remain same. It is a long term estimate which is of equal importance like precision of a sensor which is a short term evaluation.

Resolution/Discrimination

Resolution is the minimal change of the input necessary to produce detectable change at the output. It is strongly limited by any kind of noise present in the signal.

Errors

The difference between actual value and the value measured by the sensor is error produced by the sensing device. It can be caused by internal or external sources like random noise, interference from other system etc. It is given by

$$Absolute\ error = Output\ - True\ value$$

Noise

The fluctuations in the output recorded when there is no change in input are referred to as noise. Signal-to-noise ratio is a commonly used figure to represent noise strength in a signal.

$$\frac{S}{N} = \frac{Mean\ value\ of\ the\ signal}{Standard\ deviation\ of\ the\ noise} \tag{1.1}$$

Sources of noise can be either external of internal. External noise can be caused by electromagnetic signal which are coming from power supplies, temperature change, mechanical vibrations etc. Internal noise can be categorized as electronic noise, shot noise, generation- recombination noise, white noise and pink noise. Electronic noise results in current or voltage variations which is caused by agitation of carriers due to thermal energy above 0 K.

Drift

Drift is a gradual change in output with time, when the input remains the same. It is usually attributed to aging of the electronic components, instability in temperature etc. Drift is assessed with respect to a baseline which is the standard output value when the sensor is not exposed to stimulus.

Calibration Curve

A sensor has to be calibrated to achieve best possible accuracy. Calibration of the sensor can be done by applying known inputs and recording the outputs. An ideal calibration curve is shown in Figure 1.2.

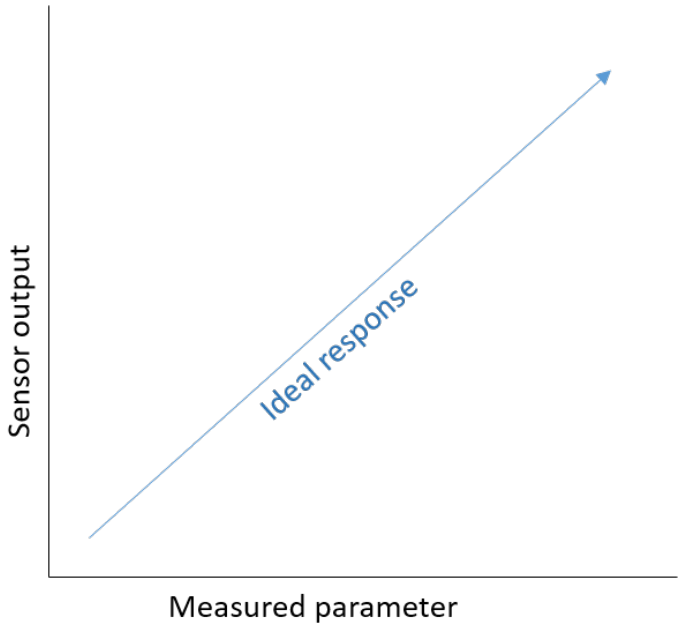

Fig. 1.2. Calibration curve for ideal response

Sensitivity

The ratio of incremental change in sensor output with incremental change in input signal is evaluated as sensitivity of the sensor. It can be calculated by taking slope of the calibration curve. An ideal sensor has a high and constant sensitivity. In practical applications, sensor eventually reaches a region of saturation where it no longer responds to stimulus.

Linearity

The closeness of the calibration curve to a straight line shows how linear a sensor is.

Hysteresis

Hysteresis is exhibited by sensors when the trajectory followed by the sensor is

different while reading output values. Some sensors tend to read low when increasing signal and high when decreasing signal. Hysteresis has to be taken in account to avoid false and inaccurate readings. Figure 1.3 shows a typical hysteresis curve.

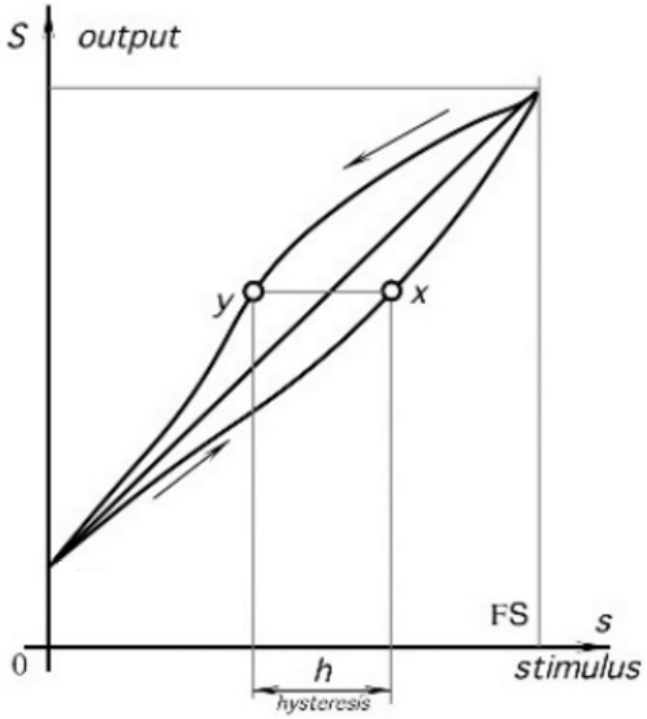

Fig. 1.3. A typical hysteresis curve

Dynamic Characteristics

Dynamic characteristics of a sensing system describe the response of the system when it is exposed to a signal that changes with time. The system transient response can be represented by quantities such as:

Rise time (t_r)

Rise time is the time taken by the signal to rise from 10% of its value to 90% of its value.

Fall time (t_f)

Fall time is the time taken by the signal to decrease from 90% of its value to 10% of its value. Figure 1.4 depicts both rise time and fall time for a signal.

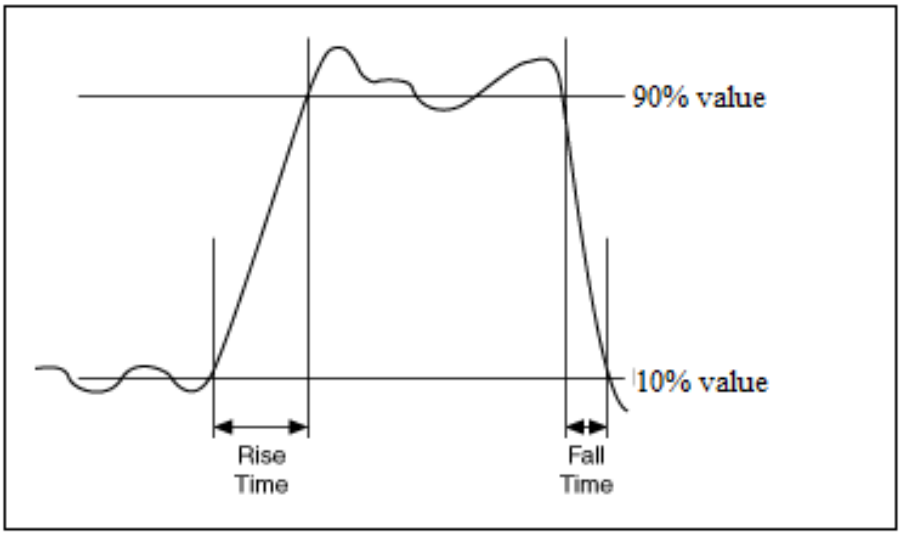

Fig. 1.4. Rise time and fall time of a signal

1.2 Issues and Limitation of the Existing Technology

Due to miniaturization to the nano-scale, there is an issue of cross talk that appears in processing multi-channel devices these days. According to [8], at reduced dimensions, cross talk is fundamentally coulomb interaction which has strong influence on the behavior of devices. Poisoning of the gas sensor is another issue which affects recovery of the gas sensor after sensing. Gas sensing by a smart material occurs due to adsorption of gas molecules on the material surface. Once the gas is detected, the sensor recovery process starts in which desorption of molecules takes place in presence of air. Poisoning of sensor happens when the sensor does not recover to its initial condition.

1.3 Employment of MEMS and NEMS in Sensing Devices

MEMS/NEMS is a system that is reducing the world down to chip size machines. MEMS stands for micro-electro-mechanical system, which refers to micro-scale devices offering attractive characteristics such as reduced size and weight, low power consumption and high speed and precision. MEMS have a characteristic length scale between 1mm and 1μm and MEMS industry is already valued in tens of billion dollars and is growing rapidly. Similarly, NEMS, nano-electro-mechanical system, refers to nano-scale devices. NEMS devices have a characteristic length between 1μm-100nm and there are discussions if it could go even below 1nm. Research on NEMS is extremely active and field of NEMS is said to be currently in its infancy. The entire device can be of a higher scale but if the functional part of the device lies in the micro or nano-range, it is referred to as MEMS/NEMS device. Applications of MEMS/NEMS devices include sensors, actuators and passive structures. MEMS/NEMS technology have the ability to miniaturize the machines and devices while keeping the cost effectiveness in control, and this gives this technology incredible power. MEMS/NEMS have the right scale for interacting with the material world outside in the macro-world and small enough to interact with the biological systems [9]. MEMS/NEMS sensing or actuation can use many methods for sensing such as change in electrical resistance, change in capacitance, piezo-resistive, piezoelectric methods etc. The physical parameters such as electrostatic, capacitance, thermal, magnetic etc, are manipulated at the micro/nano-scale.

1.4 Research Hypotheses

Graphene is popularly called miracle material because of its unique properties. Graphene is being widely explored for the fabrication of gas sensors. Because of its 2D structure, high conductivity and large surface to volume ratio it proves to be the best available nano-structure for sensing devices. According to [10], the reactions and interactions of the gaseous molecules with the graphene layer can be catalyzed

by using nano-particle materials such as Gold, Platinum, and Lead that may provide enhanced sensitivity for the devices. According to [xx], due to consistent size and narrow size distribution, gold was the choice for formation of nano-particles. Xenon flash annealing process is a faster and convenient method to perform de-wetting of thin films as compared to thermal de-wetting process which takes few hours to perform. Due to reduced size of the SoC, presence of noise becomes an unavoidable issue to be addressed. Guard rings were used to stop minority charge carriers from resulting in noise. The features of the xenon annealing as compared to the thermal process. In order to increase the sensor performance, the sensor needs to detect a lower concentration of gas. To ensure very low changes to be detected and amplified by the amplifier, the amplifier itself needs to have very low offset. So to identify lowest change in resistance values in presence of gas, offset cancellation techniques were used. For further improving the utility of the gas sensor, the sensor was integrated with a micro-controller board featuring high speed and low power consumption. The board exhibits a plenty of other attractive features, which can be focused with the gas sensing capabilities for creation of a higher degree of sensing.

1.5 Our Approach

1.5.1 Integrated Gas Sensor Design

The gas-sensing device is a nano-particle based gas sensor, which comprises of a sensing unit and a processing unit. The sensor in a further step works practically as an embedded system device demonstrating IoT (Internet of things). The integrated device components are shown in Figure 1.5. The sensing unit was formed at IUPUI and the Interface circuit was simulated using software such as cadence spectre, Cadence Virtuoso and PSpice. The embedded systems device was designed and working prototype was created using a NXP development micro-controller board. Due to its unique materialistic properties, graphene was selected to be the sensing nano-material in the study, and the sensitivity was further enhanced by formation of nano-particles

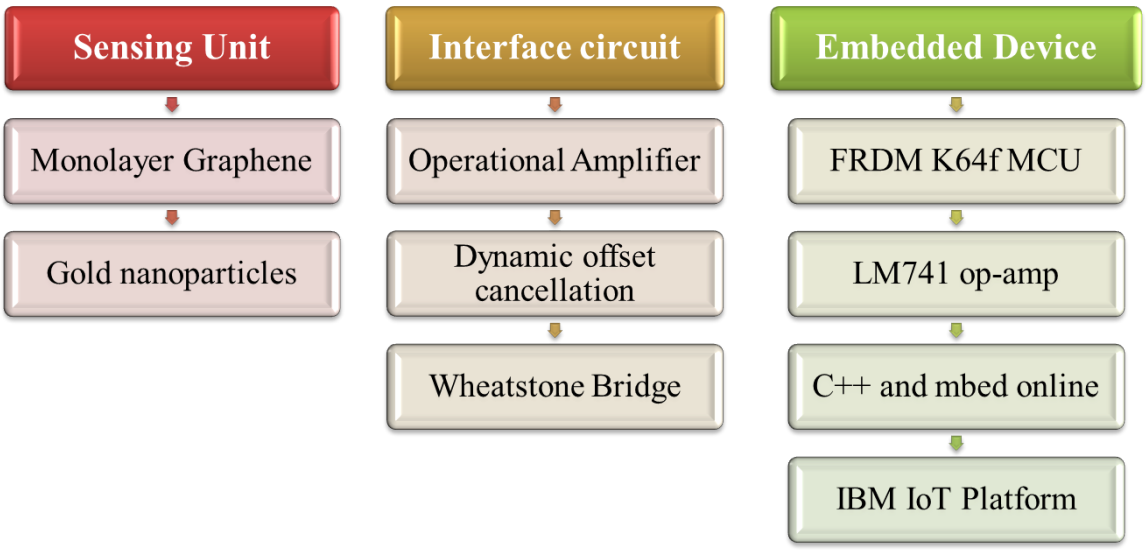

Fig. 1.5. Components of integrated gas sensing device

on its surface. The sensing unit was prepared after a series of steps and was found to be highly sensitive to carbon dioxide gas. The sensor was able to detect a change in resistance of graphene sheet. This change in resistance needs to be processed for conversion into useful information. Since the change in resistance values can be very small for a lower concentration of gas, amplifier needs to be employed. According to the requirement, the amplifier has to be a high offset and high gain amplifier. To convert the change in resistance values to change in voltage values, a bridge circuit was used. A simple wheat stone bridge outputs a proportional change in voltage for a change in resistance in one of its arms. The differential voltage from the bridge circuit was fed into the amplifier. A low offset amplifier with a high gain amplifies the differential voltage from the sensor and gives us an amplified output signal. As the integrated gas sensor as discussed is sensing and processing the presence of gas, the next step to be accomplished was to utilize the IoT technology using FRDM K64f micro-controller development board. The amplified voltage signal is sent as a pwm (Pulse Width Modulation) signal to the board. The board is then coded to

perform comparison and communication tasks. Machine-to-machine communication is achieved, when gas sensor is able to send signals and information to a machine wirelessly.

1.5.2 Thesis Organization

Chapter 2 covers the fabrication technique adopted for the gas sensing device. It talks about the structure and composition of the wafer. It also describes graphene as a smart material and how it is the best suited material for the gas sensor investigated in this work. Deposition technique for graphene and fabrication technique for our sensing unit will be detailed for the practical device used for this study. Chapter 3 details the instruments and apparatus used for the characterization and testing purposes, while chapter 4 elaborates on the mathematical model designed for sensing and various gas sensing configurations. Chapter 5 introduces the integrated gas Sensor, which includes the amplifying circuit, its schematics and layout design for the gas sensor. The software design using cadence is also detailed. The hardware design and approach using the interfacing of wheat stone bridge circuit, amplifiers, and the processing unit is detailed. This chapter also discusses means of reducing cross talk noise techniques, which were utilized for the integrated device. Chapter 6 covers description about incorporation of a micro-controller board for wireless application of the gas sensor. Significant real life applications of a gas sensor are described in chapter 7. The software and hardware results with the research findings were reported in chapter 8. The thesis then concludes our findings with proposed future work in chapter 9.

2. FABRICATION OF THE SENSING DEVICE

In this research work, graphene was chosen as the sensing material for developing the gas sensing device. Graphene is defined as a material which consists of a single atomic sheet of conjugates sp^2 carbon atoms [11]. Graphene was first extracted using 'Scotch Tape' method using mechanical exfoliation by Geim and Novoselov in 2004, and received Nobel prize for their work on graphene in 2010. It gained popularity due to its high thermal conductivity, highest possible surface to volume ratio, high electron transfer rate, unique mechanical properties, high thermal stability and highly-sensitive detection. Graphene family has several materials related to graphene which have been synthesized using various techniques, have unique properties. Some of them including graphene are graphene oxide, reduced graphene oxide, graphite, graphite oxide etc, where all of them are well known for ultimate adsorption capabilities for gases, ions, vapors etc [12]. This has been researched by numerous researchers for sensing gases such as NO_2, NH_3, CO, H, O_2, water vapor and VOCs. Charge transfer between adsorbed molecule and surface leads to sensing of the gas. Tailoring sensitivity and selectivity along with other properties of sensors can be done by combining two or more materials. According to [13] & [14], due to mutual attraction, the adsorption of gases is enhanced if graphene sheets are decorated with metals.

2.1 Graphene Vs CNTs

Smart materials such as graphene and carbon nano-tubes (CNTs) with innate nano-scale sizes offer potential applications. Although both are made up of carbon, but their structures differ as shown in Figures 2.1 [15] and 2.2 [16]. Their one of a kind electrical properties show magnificent electron mobility higher than any known material at room temperature. Additionally, the novel mechanical attributes of car-

bon materials demonstrates that they are to a great degree strong and stiff contrasted with other silicon based materials. Both demonstrate a high sensitivity towards any progressions in their chemical surroundings. The structural features in terms of their high electron mobility at room temperature make them ideal over others. Graphene is picked over CNTs for gas sensing in light of the fact that although CNTs have high aspect ratios, graphene has most noteworthy conceivable surface area every unit volume (hypothetically 2630 m^2/g) for single-layer graphene [17] giving them better sensing capability. The capacity of gas sensing with graphene is high because of the adsorption or desorption of gaseous molecules that go about as donors or acceptors on the graphene surface. That may create disturbance in graphene conductance permitting devices to identify those progressions. In outcome, graphene is an astounding material appropriate for applications identified with surface related phenomena. According to [2], there is variation in gas sensor signals that were better detectable with three different gases, citing good quality gas sensing devices at room temperature.

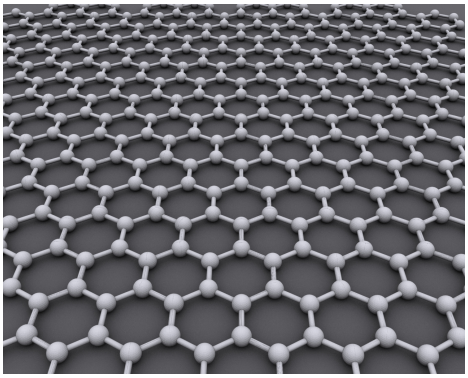

Fig. 2.1. Graphene structure

Oxidizing gases such as NO_2 enhance hole conduction and generate a significant decrease in resistance, and reducing gases such as Ethanol and Ammonia cause depletion of holes and hence raise the resistance of carbon material [18].

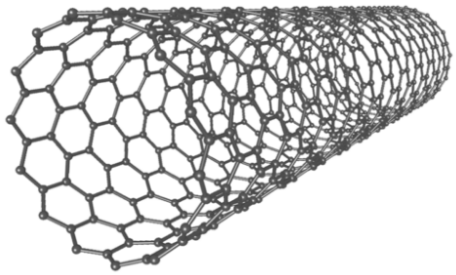

Fig. 2.2. Structure of carbon nano-tube

Table 2.1
Gas sensing effects according to researchers

Gas	**Concentration (ppm)**	**Change in Resistance**	**Type of gas**
NH_3	1000	Increase	Reducing
NO_2	1000	Decrease	Oxidizing
Ethanol	1000	Increase	Reducing

2.2 Wafer Structure

The structure of wafer comprises of a sensitive layer of mono-layer graphene over a silicon substrate with thin silicon dioxide layers on both sides of it as shown in Figure 2.3. The wafer was prepared by p-type doped silicon, CVD based graphene film and oxidation layer in between. The description of the graphene based wafer is as follows:

Graphene film

- Growth Method: Mono-layer graphene was deposited on the wafer surface using CVD synthesis technique.
- Transfer Method: Clean transfer method.
- Quality Control: Optical Microscopy and Raman checked.
- Size: 1 cm x 1 cm.

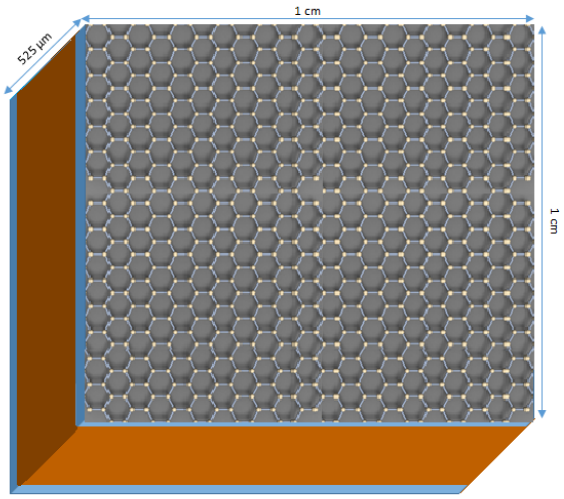

Fig. 2.3. Components of Integrated Gas Sensing Device

- Appearance (Color): Transparent.
- Transparency: more than 97%.
- Appearance (Form): Film.
- Coverage: more than 95%.
- Number of graphene layers: 1.
- Thickness (theoretical): 0.345 nm, one atom thick.
- FET Electron Mobility on SiO_2/Si (expected): 4,000 cm^2/Vs.
- Sheet Resistance: 600 Ω/[sq].
- Grain size: Up to 10 μm.

Substrate

- Type/Dopant: P-type/Boron.
- Orientation: 100.

- Growth Method: CZ method is used to obtain single crystals of semiconductors.
- Resistivity: 1-30 Ω-cm.
- Thickness: 525 +/- 25μm.
- Front Surface: polished.
- Back Surface: etched.
- Coating: 300 nm thermal oxide on both wafer sides.
- Size: 1 cm x 1 cm.

2.3 Thin Film Technology

Thin film technology is a modern technology which requires thin films for different applications. The thin layer of material may range from fractions of a nano-meter to several micrometers in thickness. According to [19], a film is considered to be a thin film when its properties are different from bulk. The change in properties may result from high surface to volume ratio or structure of thin film which depends on the substrate thin film is deposited on. Progress in this technology depends on the ability to controllably deposit thin films. There are various methods of thin film syntheses available today. Figure 2.4 categorizes major thin film deposition techniques.

2.3.1 Chemical Vapor Deposition

For creating high quality graphene film, the most efficient way is by chemical vapor deposition (CVD). CVD is simply deposition of gaseous reactants on a substrate. It takes place in a reaction chamber where a carrier gas is combines with the source material in gaseous form. In the next step, it reacts with the substrate inside the reaction chamber creating a material film on the substrate surface. Temperature of the substrate is a vital condition for this process to occur. The CVD process, usually

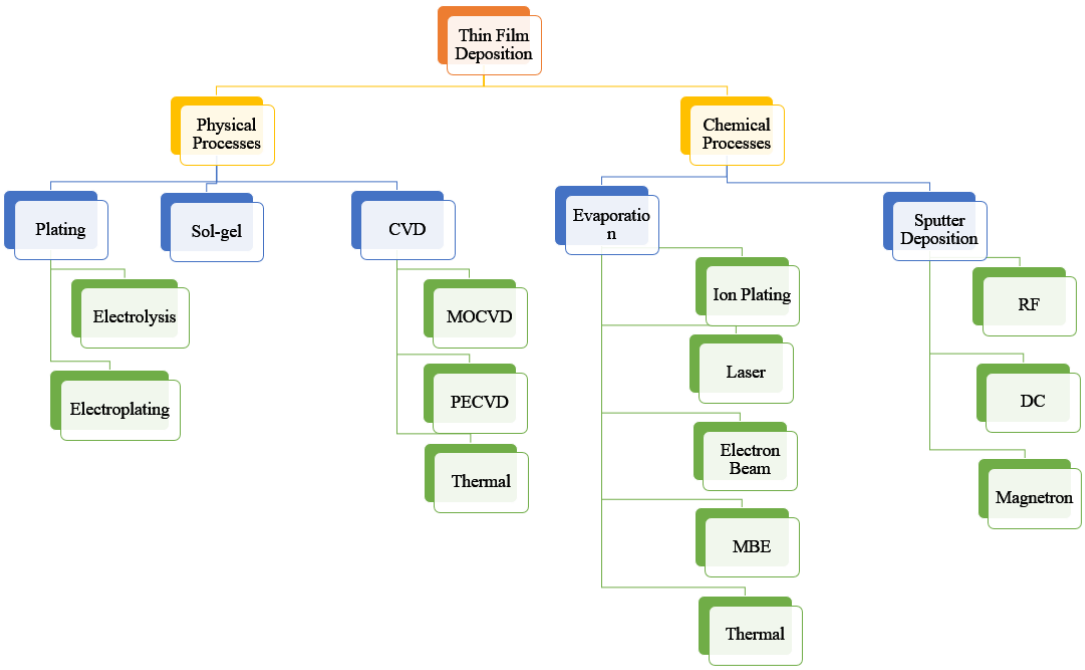

Fig. 2.4. Thin film deposition methods

coats a very small amount, at a very slow speed, often in microns of thickness per hour. Advantages of using CVD is high quality film, high purity, fine grain and more hardness over other methods.

2.3.2 Sputtering with Gold

A "Denton Desk V turbo" sputtering machine is shown in Figure 2.5. It is specific gold standard system for electron microscopy sample preparation. It delivers consistent, highly repeatable and exceptional results. This particular sputtering coater is suitable for oxidizing or non-oxidizing metals. The high resolution magnetron sputter deposits a uniform conductive coating precisely. It has a mechanical pump which can reach upto a 50 mtorr process pressure. Desk V Turbo sputters with a 2 inch cathode and it is driven by dc power supply. It has a colored touch screen monitor

for easy use and process can be changed in real time. The screen provides intuitive and simple operation, features include timed sputter which was a significant feature for our research. Sputtering technique was used to deposit gold thin film over the

Fig. 2.5. Keithley characterization system

mono-layer graphene. The gold thin film needed to be tested for different thickness, so the timed sputter feature was utilized for sputtering for varied time periods.

Sputtering Vs Evaporation

Sputtering is a process where target material is bombarded on a substrate by ionized gas such as argon in a vacuum chamber whereas in evaporation technique the metal after sufficient heating, evaporates to the wafer to form the thin film. Figure 2.6 demonstrates the comparison between the two processes pictorially.

- **Coverage Area**: The coverage area is larger while sputtering than thermal evaporation because of the nature of their deposition method. The vapors used in thermal evaporation are directional; while the ion bombardment of the sputtering is over a larger area.

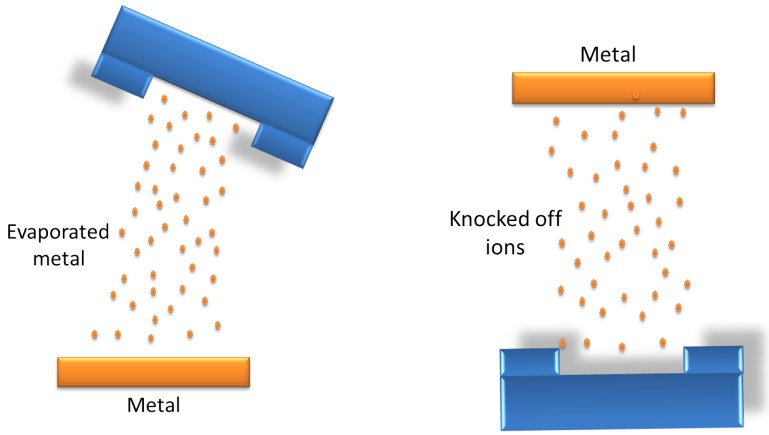

(a) Thermal evaporation (b) Sputtering

Fig. 2.6. Comparison between the two thin film deposition processes

- **Deposition Rate Control**: Deposition rate can be controlled by a lot of factors in sputtering such as gas pressure,temperature, and potential difference between the material and the wafer. Whereas in evaporation one can only control the temperature to vary the deposition rate.

- A significant advantage of sputtering over evaporation is that materials with very high melting points can be coated easily using sputtering technique while evaporation of these materials is difficult and problematic process.

- Higher energy atoms are produced by sputtering technique over lower energy atoms produced by evaporation technique.

- Sputtering provides better adhesion on the substrate over evaporation.

- Decomposition of material is uniform in sputtering while the material decomposition is high in evaporation.

2.4 Dewetting with Xenon Flash Lamp

Further functionalization of graphene coated with gold thin film was done using xenon flash induced solid-state dewetting. For formation of gold nano-particles (AuNPs) dewetting was performed on Gold thin film. Generally, dewetting describes the rupture of a thin film on the substrate (either a liquid itself, or a solid) and the formation of droplets. Similarly, the xenon flash annealing can dewet a thin film into spherical nano-particles. The intense pulse light system to be used is a commercial xenon flash system shown in Figure 2.7. It is capable of ionizing Xenon gas to generate up to 50 J/cm^2 of flash energy density. The power supply and trigger circuit are designed to deliver up to 15 flashes per trigger with a maximum trigger rate of 1Hz. Flash duration and delay between flashes can be adjusted between 0.5 ms to 30 ms and 1 ms to 10 ms, respectively. Further exposure to larger energy may lead to evaporation which eliminates existing smaller particles but also create them simultaneously because to size reduction of larger particles. This process to be performed has variable parameters like energy, number of pulses, duration of pulses and gap duration between two pulses. The minimum dewetting energy and the evaporation energy are function of the initial film thickness. One of the advantages of using a

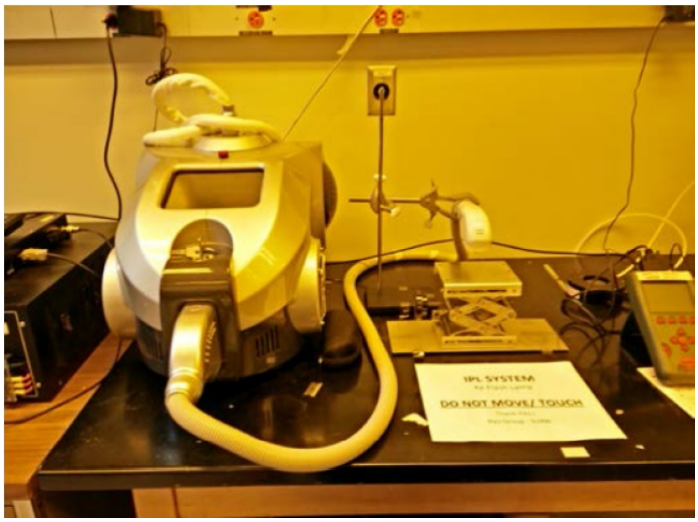

Fig. 2.7. Xenon Flash Lamp

xenon flash lamp for annealing over conventional thermal annealing process is that it is faster. A thermal annealing process is time consuming and may take hours to process.

3. PRACTICAL MODEL CHARACTERIZATION

For specific purposes some scientific instruments are used for testing and characterization. On the basis of precision, accuracy, high speed and other specific capabilities the instruments are chosen to perform specific tasks. All the equipment used in this research work were available at IUPUI facility. The following characterization apparatus were used for testing the functionality of the system, presence of thin films at nanoscale, the multi layers of the device, the mono-layer structure of graphene and the presence of nano-particles on top of graphene.

3.1 Keithley Characterization System

Keithley 4200 Parameter Analyzer is a high performance instrument which accelerates testing of devices pertaining to materials research, semiconductor devices and process development. It is a modular and fully integrated analyzer which provides I-V (Current-Voltage), C-V (Capacitance-Voltage) and ultra fast pulsed I-V characterization. It has a multi-switch module which enables it to switch between I-V and C-V measurements effortlessly. Figure 3.1 is a picture of Keithley 4200 characterization system [20]. Some unique features which make it best choice for device modeling and characterization are listed below:

- The device has windows interface which is user friendly and no training is required to use it.
- The testing does not require any complex programming and works on single click.
- Measurement range is wide with a high resolution and low noise.
- It is a cost effective system with software upgrades.

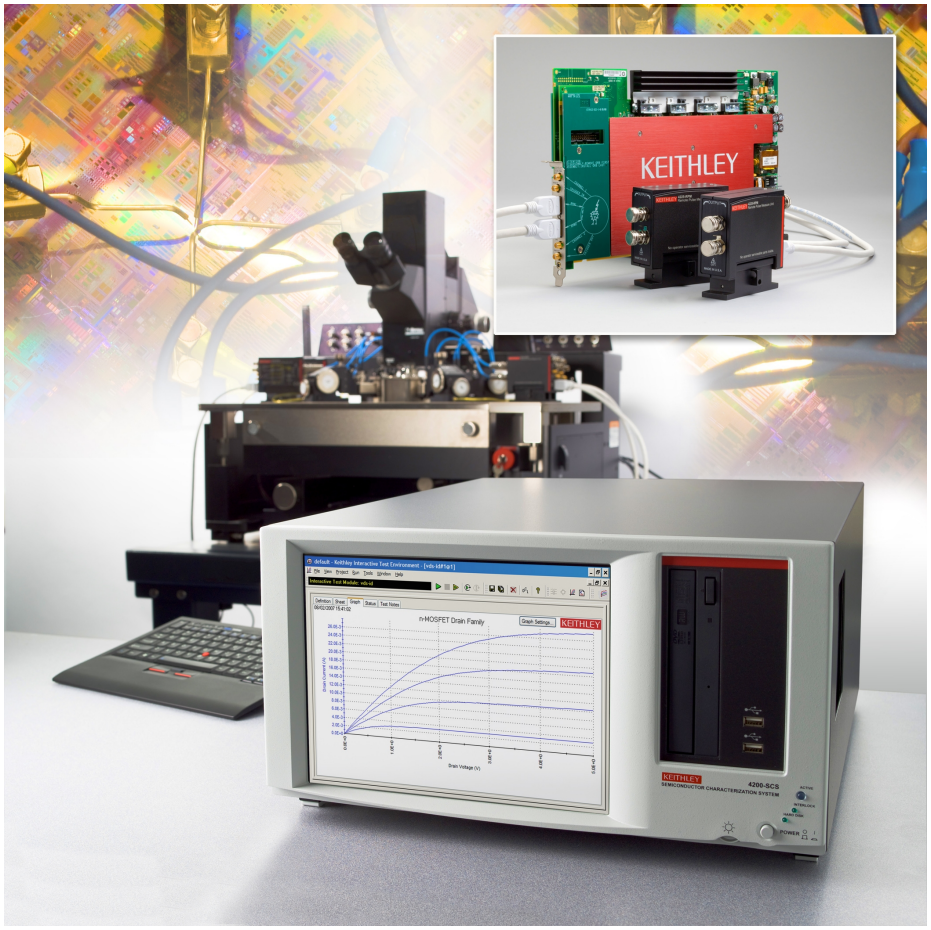

Fig. 3.1. Keithley characterization system

The Keithley system was used in our research for making resistive measurement, capacitive measurements and FET configuration. The four-point collinear probe was used to make measurements on the Silicon wafer. The output data obtained can be easily exported in excel workbooks and the plots can be obtained in .bmp, .jpg and .tif formats for offline analysis. The range of the measurements by the device for various characterizations are:

- Current-Voltage (I-V) Range: 0.1 fA to 1 A and 0.2 μV to 210 V.
- Capacitance-Voltage (C-V) Range: 1 kHz to 10 MHz.

3.2 Scanning Electron Microscope

A Field Emission Scanning Electron Microscope JEOL 7800F possesses unmatched resolution and stability for imaging and analysis. It is an appropriate choice for observing structural morphology of nano-particles since it provides 1,000,000x magnification with a sub-1nm resolution. Figure 3.2 is a picture of JEOL 7800F SEM. It is capable of performing a low kV imaging of highly magnetic samples.

Fig. 3.2. Field emission scanning electron microscope JEOL 7800F

Main features of the JEOL 7800F SEM are listed below:

- Principal Resolution 1.0nm at 15kV.
- 0.8nm at 15 kV (GB mode).
- 1.5nm at 1.0kV.
- 1.2nm at 1.0kV (GB mode).
- 3.0nm at 0.1kV (GB mode).
- Analytical Resolution 3.0nm at 15kV (5nA).
- Accelerating voltage: 0.01 to 30kV.
- Beam Current Range: 1pA to 200nA at 15kV.

- Magnification Range: 25x to 1,000,000x (at 4x5 print size).
- Short Working Distance Retractable Solid-State Back-scatter Detector (SRBE) Composition (Z-contrast), Crystal Orientation, Topography.
- Scanning Transmission Electron Detector (STEM) Detector (0.8 nm resolution at 30kV).
- Energy-Dispersive X-ray Spectroscopy.

SEM was used to observe the presence of gold nano-particles on the mono-layer graphene silicon wafer.

3.3 Raman Spectroscopy

A Foster and Freeman micro laser raman spectrometer was utilized to perform raman spectroscopy on the graphene mono-layer as well as gold nano-particle samples. Raman spectrum exhibits lots of features which are specific to the molecular structure of the sample. It provides peaks which can be used to analyze, identify and differentiate between materials. Figure 3.3. shows the raman spectrometer used in this study. It has a 785nm, 2.5 mW laser and both 20x and 35x objectives. The 785 nm infra-red laser has better ability to suppress florescence.

3.4 X-Ray Diffraction

Figure 3.4 shows a Bruker D8 discover X-ray diffraction instrument was used for performing X-ray diffraction for gas sensing samples. It is an advanced X-ray diffraction system which works in real time and is easy to use. Due to a bigger window sie of the 2-D detector, the speed of data collection is high. X-Ray diffraction is a phenomenon of scattering of X-rays by the regularly spaced atoms of a crystal. It is useful in obtaining information about the structure of the crystal. Diffraction of X rays by the crystal is described by Bragg's condition, $n\lambda = 2d\sin\theta$ where θ is

Fig. 3.3. Foster and Freeman micro laser raman spectrometer

the scattering angle, n is a positive integer and λ is the wavelength of incident wave. The intensity of the diffracted wave depends on the crystal structure of that specific material. Diffracted pattern is the basis of the primary use of the technique which leads to identification and characterization of compounds.

Fig. 3.4. Bruker D8 discover X ray diffraction instrument

The thickness of the gold layer was estimated by the sputter time and the energy applied to the coater. The graphene mono-layer thickness was determined by the X-ray diffractor. The characterization system was used to check the functions of the various configurations of the device including resistive capacitive and FET configuration. The details of these configurations are given in chapter. 4. Raman spectroscopy was used in this study to confirm presence of all the multiple layers of the device.

4. GAS SENSING CONFIGURATIONS AND MODELING

Various sensing mechanisms and configurations can be used to measure change in one of the properties of the sensing material. Thin layer configuration of graphene based sensors was utilized due to numerous unique properties of graphene monolayer. During gas sensing, the phenomenon happening on sensing surface of graphene is called adsorption. Adsorption is adhesion of gas atoms or molecules to the surface of graphene. Based on the kind of interaction between the adsorbed molecules and substrate, strength of adsorption can be either physisorption or chemisorption. The interaction is van der waals in the former case and chemical bonds for the later one. The presence of gaseous molecules, creates disturbance in its molecular structure, and accordingly affects the graphene conductance. Change in conductivity of graphene sheet further permits devices to identify the unknown parameters. Various compositions of the gaseous molecules interact with the graphene layers in various modes. The reactions and interactions of the gaseous molecules with the graphene layer can be catalyzed by using nano-particle materials such as gold, platinum, and lead [6] that may provide enhanced sensitivity for the devices.

4.1 Mathematical Modeling

The goal of this research is to design a gas sensing signature array (GSSA) to be used as a model array for sensor identification of the various applications including gas sensing or mixture of gases. Pattern recognition methods are very promising when gases are identified by means of gas sensor arrays. In this study, we have demonstrated the device performance with CO_2 gas of 100% and 5% concentrations. The parameters taken into consideration are mainly type of gas, concentration of the gas (c_1, c_2, and c_3 etc), static response, and dynamic response. Static response is

the magnitude of the change in resistance due to presence of gas, as time approaches infinity steady state. Since the response of the sensor does not change immediately, but following some rise time or fall time, we will record the dynamic response of the sensor. In this approach, the change in resistance (ΔR) at different time intervals say t_0, t_1, and t_2 were recorded. The following GSSA for an instance is given for different concentration of gases. Likewise the GSSA for other gases and different time instances can be obtained.

$$GSSA_{t_0} = \begin{pmatrix} \Delta R_{g_1,c_1} & \Delta R_{g_1,c_2} & \Delta R_{g_1,c_3} \\ \Delta R_{g_2,c_1} & \Delta R_{g_2,c_2} & \Delta R_{g_2,c_3} \\ \Delta R_{g_3,c_1} & \Delta R_{g_3,c_2} & \Delta R_{g_3,c_3} \end{pmatrix}$$

In the above matrix, $\Delta R_{g_1c_1}$ represents the change in resistance of gas g_1, with concentration c_1 at a time t_0. The Signature Array data will lead to the optimum gas sensing device. In our study we obtained the data for two concentrations 100% and 5% of CO_2, based on the available gas concentrations in the IUPUI facility. Data is presented in the results section.

4.2 Sensor Models Used in the Study

4.2.1 Resistive Modeling

In resistive type of sensing, the resistance of sensing material is altered due to presence of gas. Change in resistance is attributed to either geometric or material changes in the sensing material. As can be noted from the expression below, for a conducting surface we have,

$$R = \frac{\rho L}{A} \tag{4.1}$$

In presence of gas sensor act as a variable resistor as can be seen in Figure 4.1. Different gases in the surrounding of the sensor causes it to change its resistance value either up or down from its nominal resistance value at zero input. According to [18], oxidizing gases such as nitrogen dioxide (NO_2) enhances hole conduction and

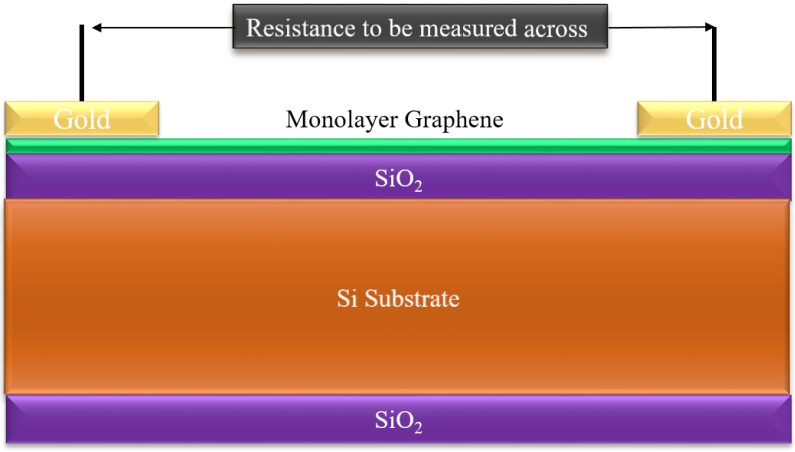

Fig. 4.1. Resistive Configuration of the sensor

generates a significant decrease in resistance, and reducing gases such as ethanol and ammonia (NH_3) may cause depletion of holes and hence raise the resistance of carbon material.

4.2.2 Capacitive Modeling

Capacitive sensing is based on determination of change in capacitance of the device in presence of gas. Due to presence of gas, changes in dynamics occur from enhanced or depleted number of carriers in the device. This may result in formation of depletion layers. The depletion layers in the nano-sensing devices act as insulating layers between the conducting plates forming a parallel plate capacitor kind of structure. After such formations, capacitive coupling takes place due to one or more such formations resulting in changes in overall capacitance of the device. Simple capacitive sensing configuration is shown in Figure 4.2.

4.2.3 FET Configuration

The three terminal field effect transistor devices are gaining popularity and as a result FET based nano-structure sensors are being researched a lot. In our gas

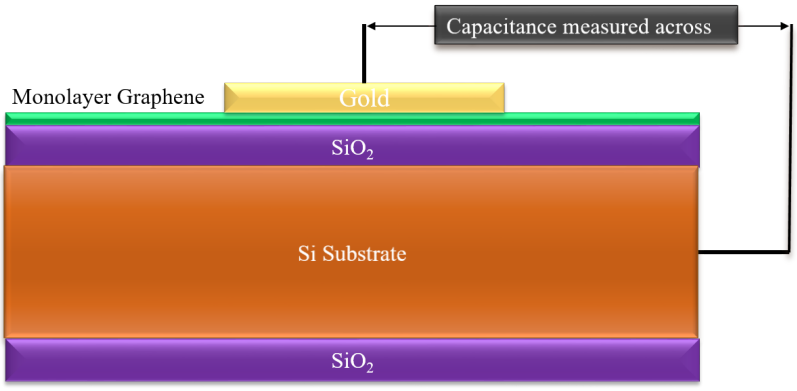

Fig. 4.2. Capacitive Configuration of the sensor

sensing device, mono-layer graphene acts as channel for the FET device whereas gold film at the center is acting as gate terminal of the FET. Due to change in electrical conductivity of the channel, the current flowing through the channel alters in presence of gas as shown in Figure 4.3. The current-voltage (I-V) characteristics can be noted for different gases for sensing. The conducting channel in our device is made up of graphene whereas gate terminal is made from gold thin film deposition. Silicon substrate being a p-type doped with Boron metal have high holes concentration, attracts electrons. That positively impacts the performance of the device. The details are give in the results and discussions section.

On application of gate voltage or drain voltage of varied polarities, the mobility of carriers starts forming or reducing size of conductive channel in the FET. The Drain current (I_d) for different drain voltage (V_d) at constant gate to source voltages (V_{GS}) can be recorded for plotting output characteristics. Similarly drain current (I_d) vs gate-source voltage(V_{GS}) at constant drain voltages (V_d) can be plotted for transfer characteristics.

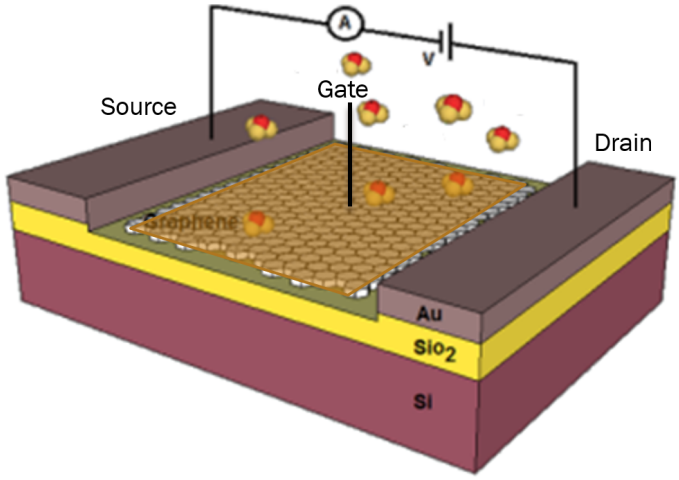

Fig. 4.3. FET configuration of the sensor [21]

5. THE INTEGRATED SENSING SYSTEM

5.1 System Modeling

The processing unit includes the interface circuitry and instrumentation amplifiers. The interface circuitry functions as energy conversion from the chemical energy of gas into electrical energy in the form of voltage signal, reflecting the information described in ΔV. The second stage of the processing unit is the amplifier stage, which provides the noise suppression cross talk between the various signals of the assemblies, and the amplification factors of the signals.

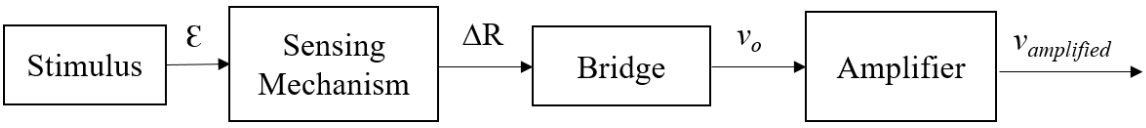

Fig. 5.1. Block diagram of Integrated Gas Sensing Device

5.2 Software

For the simulation of the processing unit, virtuoso layout editor, virtuoso schematic editor and spice software were used. The interface circuitry was designed on PSpice. Schematic and layout of operational amplifier was designed on cadence spectre and virtuoso respectively.

5.2.1 Layout and Schematic

Cadence design system is a electronic design automation (EDA) software and services company which produces software and hardware for designing integrated

circuits, systems on chips (SoCs) and printed circuit boards. One of the platforms offered by Cadence is its virtuoso platform which contains tools for designing full-custom integrated circuits; includes schematic entry, behavioral modeling (Verilog-AMS), circuit simulation, custom layout, physical verification, extraction and back-annotation. It is used mainly for analog, mixed-signal, RF, and standard-cell designs, but also memory and FPGA designs. In this study, virtuoso schematic editor was used first to create a schematic of a operational amplifier with offset cancellation capabilities. Virtuoso layout editor was used to design layout of simple operational amplifier.

Virtuoso Schematic Editor

Cadence Virtuoso Schematic Editor is a fast easy design entry software with speeds up the design entry task upto 5 times faster. The component libraries at transistor level are available with sophisticated wire-routing capabilities. Schematic of operation amplifier was designed on Cadence Spectre with offset cancellation circuitry at transistor level. For the offset cancellation circuitry, a clock generator was designed.

Virtuoso Layout Suite

The cadence generic process design kits (GPDK) provide device and semiconductor process level information for use with Cadence Virtuoso L, XL, and GXL products. PDK documentation covers layout design rules along with information about process technology to do device level design. A 45nm technology was used and a 'gpdk45' cell library was used. The procedure followed is described below.

1. **Starting the virtuoso layout editor:** The window appearing on starting the virtuoso layout is given in Figure 5.2.

2. **Cell layout:** The schematic generated can be used to generate layout sub cells by choosing 'Generate' and 'All from Source' options in 'Connectivity' tab. The

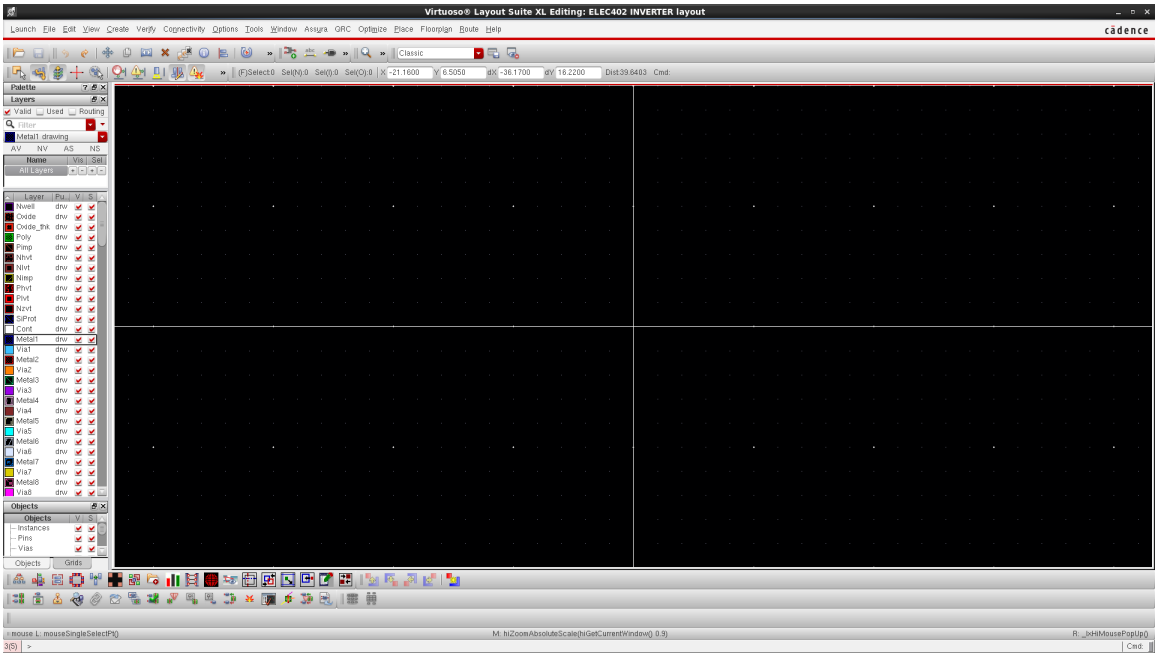

Fig. 5.2. Pad frame showing pin arrangement

sub cells get added to the layout editor window. The connections and vias have to be made and a ruler can be used to match the layout to the floor-plan.

3. **Verification and checks**: The designed layout has to satisfy the fabrication constraints and this will be checked by performing a task called design rule check (DRC). We also need to ensure match in schematic and the layout designed and for that layout versus schematic (LVS) check is performed. In the last step the layout is ready for performing QRC extraction.

4. **Pad frame:** For fabrication the layout should fit in a pad frame which is provided by MOSIS. Image of the 40-pin pad frame is shown in Figure 5.3. The dimensions of the chip with the pad frame are 1.5mm x 1.5mm. The inside area of the pad frame that is available to place your circuit is 900μm x 900μm. Each pin/pad in the pad frame has these 8 kind of pads:

    - PAD-FC: Pad frame corner, non-usable.

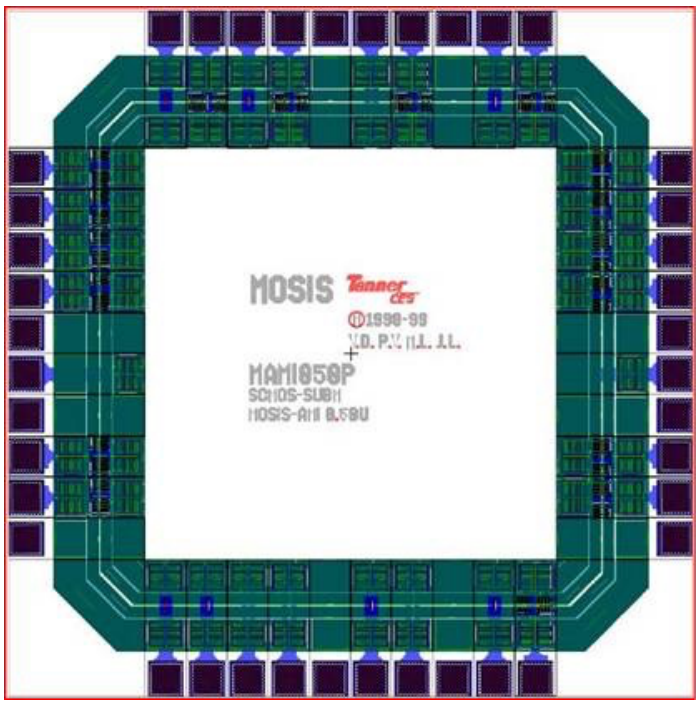

Fig. 5.3. 40 pin pad frame

- PAD-AREF: Analog reference pad, non-usable.
- PAD-GND: Pad ground, 1 pad.
- PAD-INC: Buffered input pad: The input signal to chip received at the pad is buffered and the signal and its complement made available to the circuit inside, 9 pads.
- PAD-IO: Input/output pad, 7 pads.
- PAD-NC: Spacer pad, non-usable.
- PAD-OUT: Output pad with buffer, 8 pads.
- PAD-VDD: V_{dd} power pad, 1 pad.

So the total number of pads available to are V_{dd} (1), Gnd (1), Input (9), Output (8), Input/Output (7). The arrangement of these pads in the pad frame is shown below:

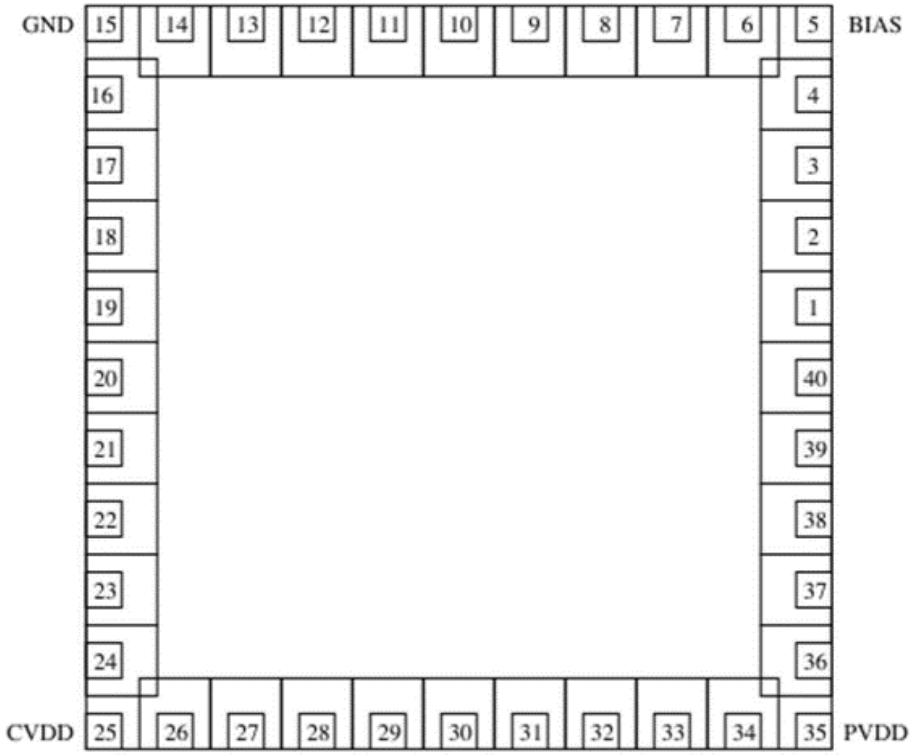

Fig. 5.4. Pad frame showing pin arrangement

5.3 Wheatstone Bridge

A bridge circuit was utilized to translate the slight change in resistance value to change in voltage across the two output terminals of the bridge as shown in Figure 5.5.

5.4 Operational Amplifier

Operational amplifier in differential mode shown in Figure 5.6 was used for amplifying the difference in voltage coming from the Wheat stone bridge. The gain of differential amplifier is given by,

$$v_{out} = \frac{R_3}{R_1}(v_2\text{-}v_1) \tag{5.1}$$

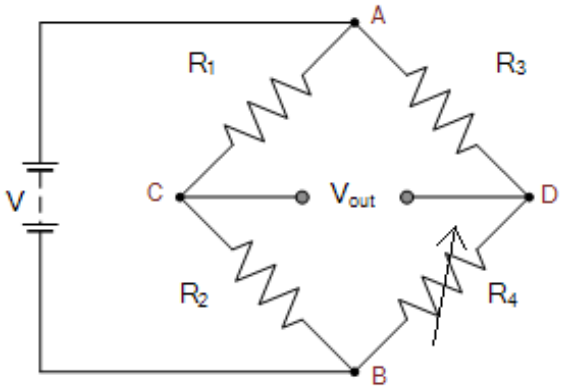

Fig. 5.5. A simple Wheat Stone Bridge

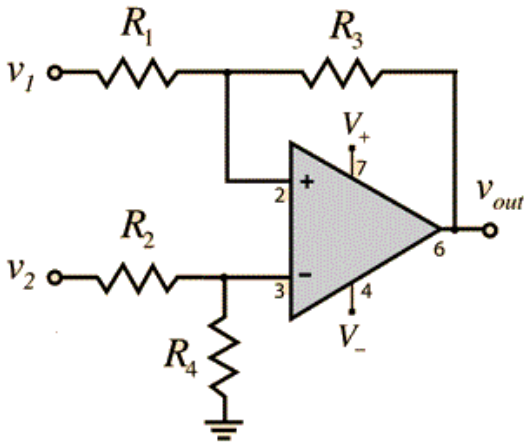

Fig. 5.6. Differential mode amplifier

5.4.1 Dynamic Offset Cancellation Circuitry

In CMOS technology, errors such as offset, drift and 1/f noise become dominant specially at low frequencies. In systems with low input, offset voltage becomes a serious drawback and can go upto 10mV. In our gas sensing device, there was a need to bring offset noise to minimum since it can produce very low change in voltages which needs to be considered. To solve this problem, an offset cancellation circuit was incorporated in the operational amplifier as shown in Figure. 5.7.

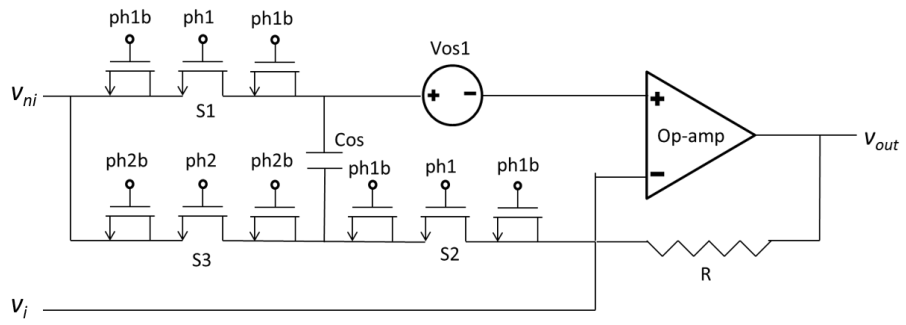

Fig. 5.7. Dynamic offset cancellation circuit

Offset cancellation circuit uses non-overlapping clock generator to control the NMOS switches. It works in two phases depending upon the clock: When ph1 goes high, switches S1 and S2 are closed, the op-amp is in the offset storage mode, and the offset voltages of op amp stored across capacitor Cos. In the next phase, ph1 goes low and ph2 goes high, switch S3 is closed, and the circuit is in the offset cancellation mode. Pre-charged voltage stored in the capacitor in one phase cancels the input offset voltage in the other phase. The two dummy transistors on either side of switch transistor are releasing and removing the charge present in the switch transistor when it is turned off. Those two are also controlled by clock signals in opposite phases.

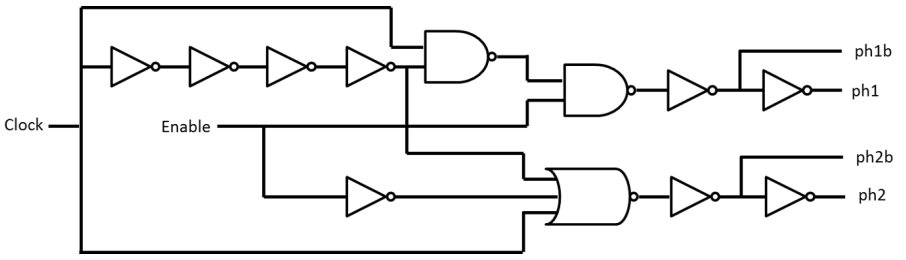

Fig. 5.8. Non-overlapping clock generator

Figure 5.8 shows the circuitry that generates the non-overlapping clocks ph1 and ph2. The static CMOS design is used to implement the NOT, NAND and NOR gates for the clock generator. A static CMOS gate is a combination of the pull-up network (PUN) and the pull-down network (PDN).

5.5 Guard Rings to Prevent Cross-talk Coupling Noise

Due to reduced size of the process-technology, the spacing between adjacent interconnect wires keeps shrinking, which increases cross talk in a multi-channel device. Cross-talk is basically unwanted signal transfer between communication channels. Multi-channel devices provide more number of signals in one package giving more sensing data as compared to single-channel sensing device. This may lead to a highly sensitive and selective gas sensor. For a highly sensitive device and occupying less area, the device need to have sufficient cross talk attenuation. Cross talk between multiple inputs of different instrumentation amplifiers are attributed to parasitic bipolar junction transistors. A guard ring is used to completely surround the device that induces parasitic current. The guard ring is formed in a semiconductor body layer such as an epitaxial layer and has a central guard ring of the same type conductivity as that of the body layer and additional flanking rings of the opposite type conductivity. Guard rings work as dummy collectors by collecting the the minority charge carriers coming from input terminal of one amplifier i.e. emitter leg, which would have been otherwise collected by the second amplifier input i.e. collector terminal. Since in gas sensing devices, where sensitivity is an important parameter, it is significant to have very low cross-talk noise. In such devices, the input can be very small and if the cross talk is high, it may lead to distorted output signals.

In our experimental results only one sensor was developed to test one type of gas at a time. Therefore, one high sensitivity amplifier was used, accordingly the cross talk issue was not practically address since we have only one input coming into amplifier. In case of multiple sensing function are to be performed, the guard rings should be implemented.

6. EMBEDDED SYSTEM AND INTERNET OF THINGS

An IoT gas sensing device was designed and developed for wireless applications of the sensor. The gas sensing device was integrated with a micro-controller board to develop a wireless gas sensing device. Internet of things (IoT) platform was used to receive information from the micro-controller board and send it over the internet. Figure 6.1 shows an overview of the wireless device technology and process adopted.

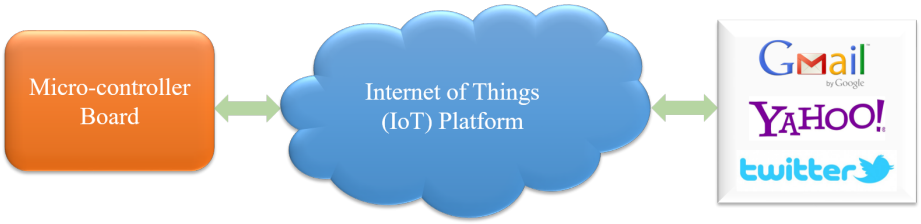

Fig. 6.1. Overview of Wireless device and technology

6.1 Micro-controller Board

The Freedom K64f is a hardware development board produced by NXP [22]. FRDM-K64F is an ultra-low-cost development platform for Kinetis K64, K63, and K24 MCUs. Peripherals enable rapid prototyping, including a 6-axis digital accelerometer and magnetometer to create full eCompass capabilities, a tri-colored LED and 2 user push-buttons for direct interaction, a microSD card slot, and connectivity using on board Ethernet port and headers for use with Bluetooth and 2.4 GHz radio add-on modules. The main components of the development board are shown in Figure 6.2. The Input/Output pin configuration of FRDM K64F are shown in Figure 6.3.

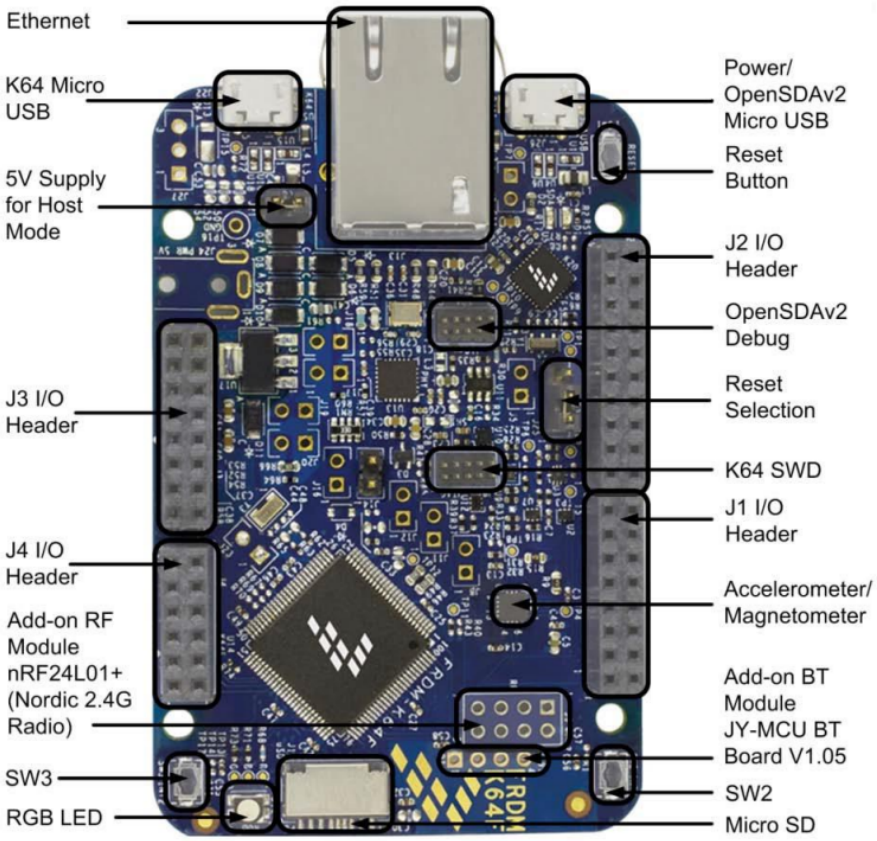

Fig. 6.2. FRDM K64f main components

6.2 System Integration

ARM mbed online compiler was used to write the code and compile the algorithm using C++ language. The system overview is shown in Figure 6.4. Input signal from the gas sensing device was received by the micro-controller board at an analog-in input pin. Input is processed by the ARM cortex M4 MCU and if the sensing conditions are above the defined threshold, the output is sent to IBM IoT platform through MQTT (Message Queue Telemetry Transport). The IBM IoT platform is an amalgamation of IBM Bluemix and IBM Watson. The data from FRDM is received by IBM Watson which acts as a server that takes data from devices connected to it in real time. To further process the data, an application in IBM Bluemix is created

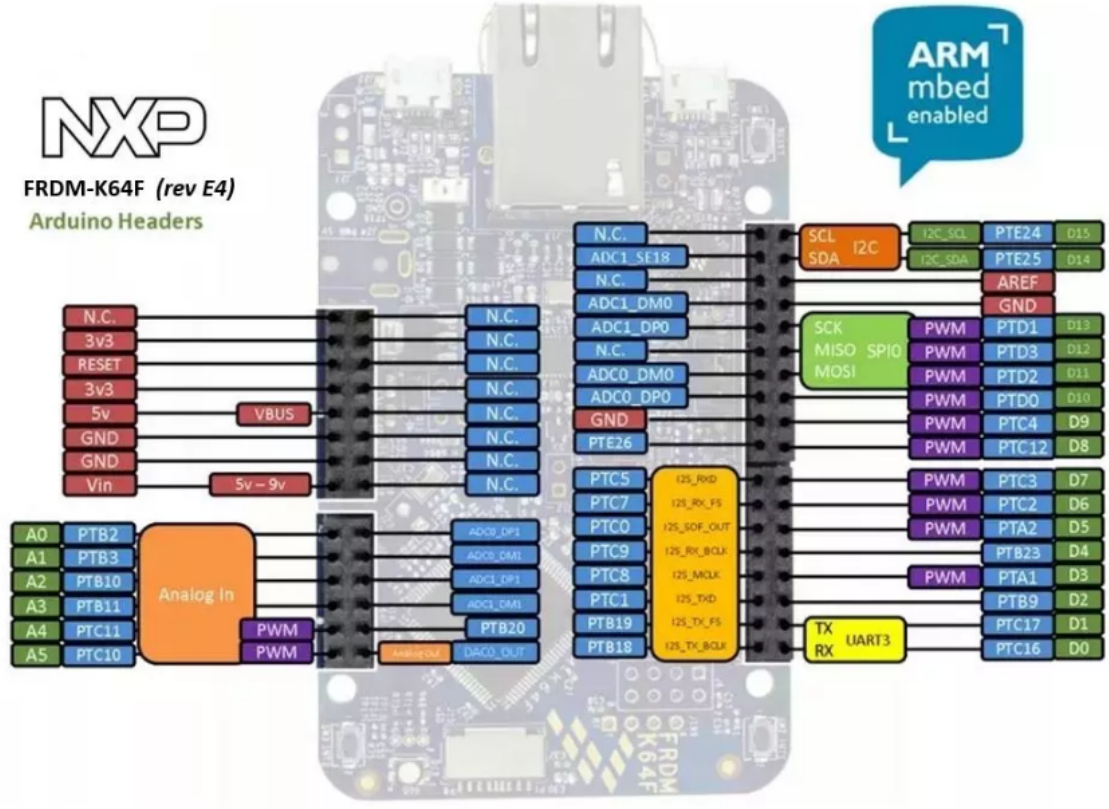

Fig. 6.3. Pin configuration of FRDM K64f

and bounded to IoT Watson services. The application is designed using Node-Red to send the notification as well as data to client servers such as gmail, twitter, yahoo etc via HTTP (Hypertext Transfer Protocol).

6.2.1 Sending Data to Cloud

The flow diagram shown in Figure 6.5 depicts the wireless implementation of the gas sensing device. In the first step, when the device is powered up, all the peripherals are initialized. Next, the Ethernet connection is established when the FRDM is connected to the internet. On successful Ethernet connection, IP address, MAC

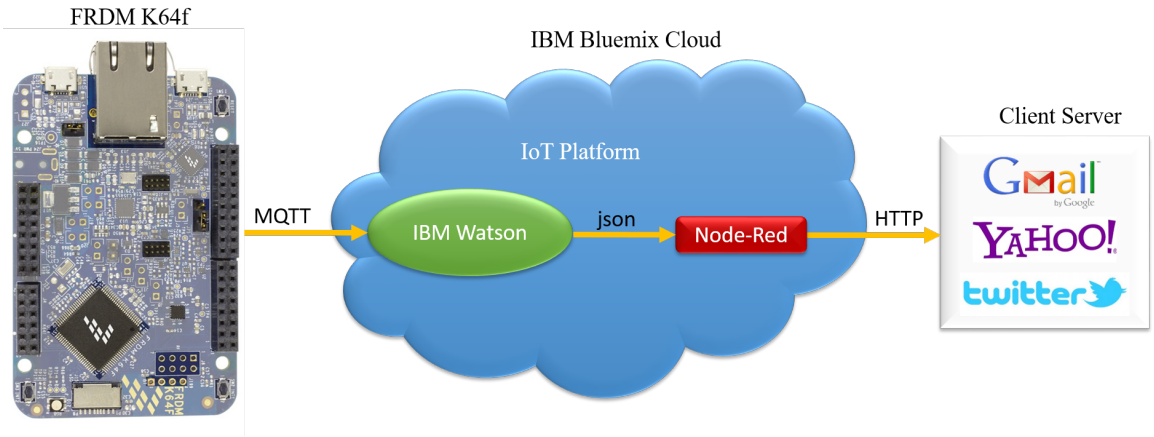

Fig. 6.4. System overview

address and Device ID is obtained. Device ID is significant since it is used to register the device on IBM Watson IoT platform. On adding device to IBM Watson platform, we will obtain organization ID, authentication token and Device type which is used to ensure correct destination address. Once the destination address is identified, the FRDM K64f is in ready position to publish data. If the gas sensor receives voltage higher than the threshold, the data is published on IBM server using MQTT. The procedure followed is described in the below steps.

1. In the first step, we burn the code in the FRDM K64f MCU and obtain the Device ID, which will be used to create the device type on IBM Watson as shown in Figure 6.6.

2. In the next step, we create the Device Type on IBM Watson IoT platform, using the Device ID we obtained in the previous step. Figure 6.7 shows the particulars obtained on creating the device type. These particulars will be used in the code to identify the correct destination.

3. In order to synchronize both the ends, we need to use the credentials from Figure 6.7 in our code. After successful compilation of the code, we burn the

updated code into the FRDM K64f MCU. Now the device tries to connect with the destination as can be seen in Figure 6.6. Once the destination successfully recognizes our device, the system enters into the publishing state.

4. When the sensing condition is met, the data is published on IBM Watson IoT platform as seen in Figure 6.8.

6.2.2 Receiving Data from Cloud

Figure 6.9 displays the IBM Bluemix application designed using Node Red Flow editor. The block 'IBM IoT App-in' uses the data from IBM Watson IoT platform published by FRDM K64f earlier. The data is sent to a 'function block' where we can define the messages to be sent according to defined conditions. Once the conditions are met, the data can be sent to clients through emails, messages and twitter. We have used a 'msg.payload' block for displaying data on the console window.

The procedure followed is described in the steps below.

1. We create an application in order to receive data from IBM Watson and send it to Client server. The application is created in IBM Bluemix by going to catalog section, selecting IoT platforms and assigning a unique name to it.

2. Add IBM Watson service to IBM Bluemix app we created in order to receive real time data from IBM Watson into our application. Confirmation of the services bonded with the application created can be seen in the screenshot in Figure 6.10.

3. To process the data in application, we use Node-Red editor. It consists of blocks to perform various functions such as receive the data from IBM Watson, send the data to IBM Watson, send the data to social networking sites, perform comparisons etc. To build our application to send data to client, we use the node red block shown in Figure 6.9.

4. The first block takes data from IBM Watson and sends forward in the specified format. The particulars like Device ID and format of the data are to be entered in the window shown in Figure 6.11.

5. In the second block we use a function and store the data in a variable 'st' as shown in Figure 6.12. It passes the data to the next block.

6. The data received from the previous block is sent in a form of message via email. The particulars of the email ID through which the email has to be sent and on which it has to be received, are to be entered in the window shown in Figure 6.13. The password has to be of 8 characters.

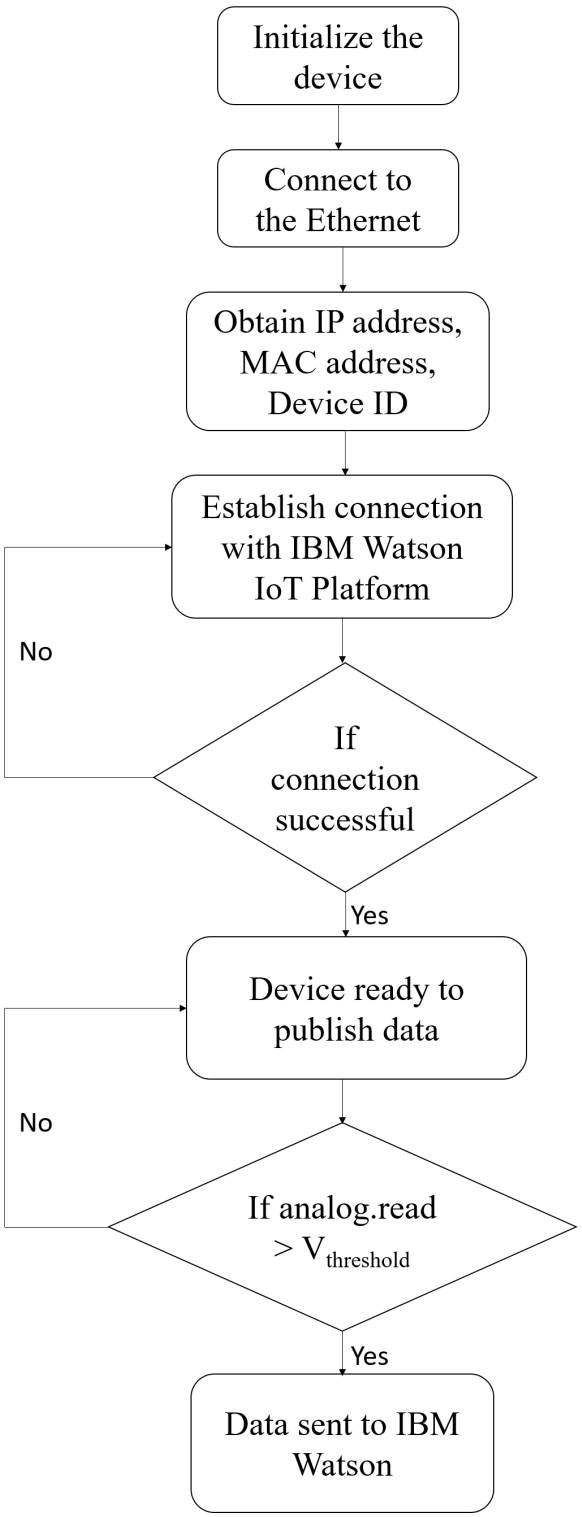

Fig. 6.5. Flowchart for sending data from FRDM K64f to IBM Watson IoT Platform

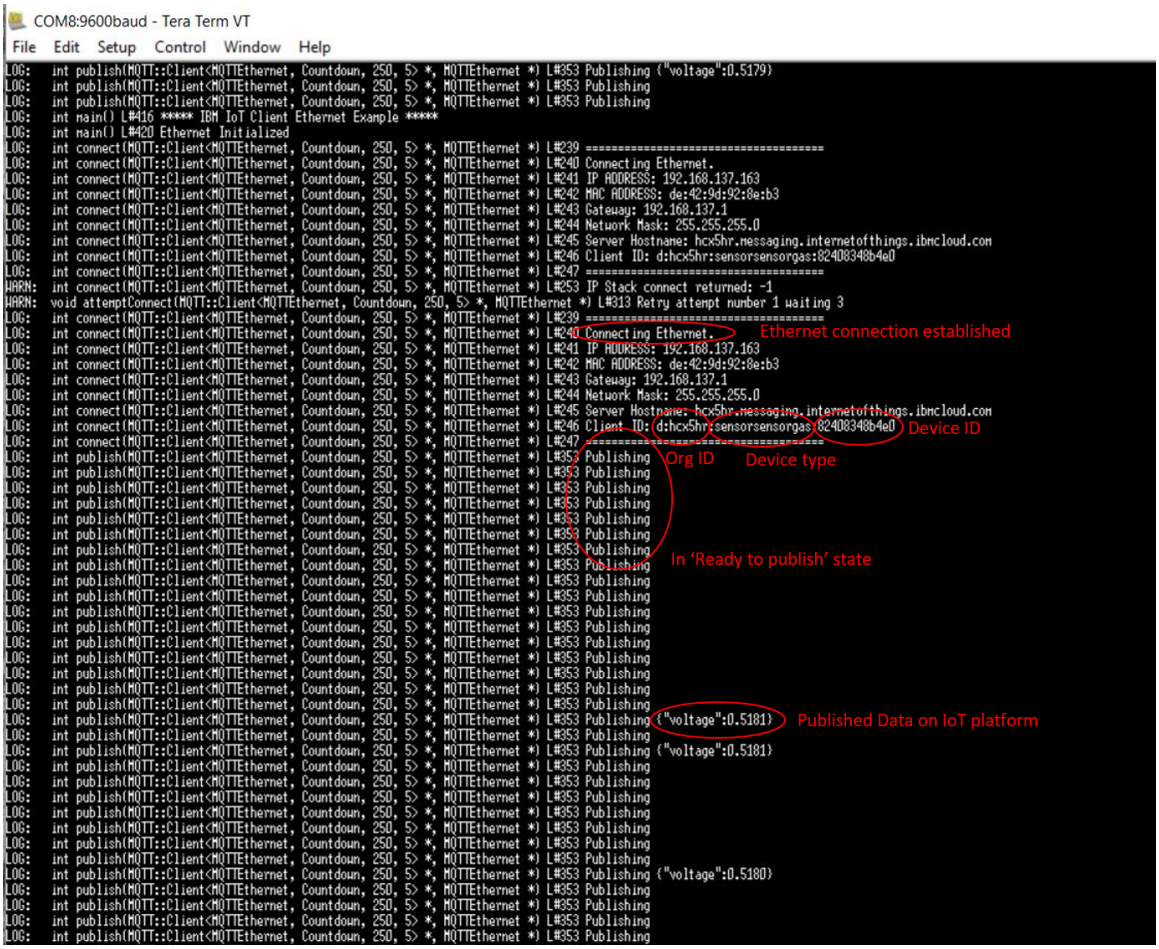

Fig. 6.6. Image highlights particulars obtained from tera-term window

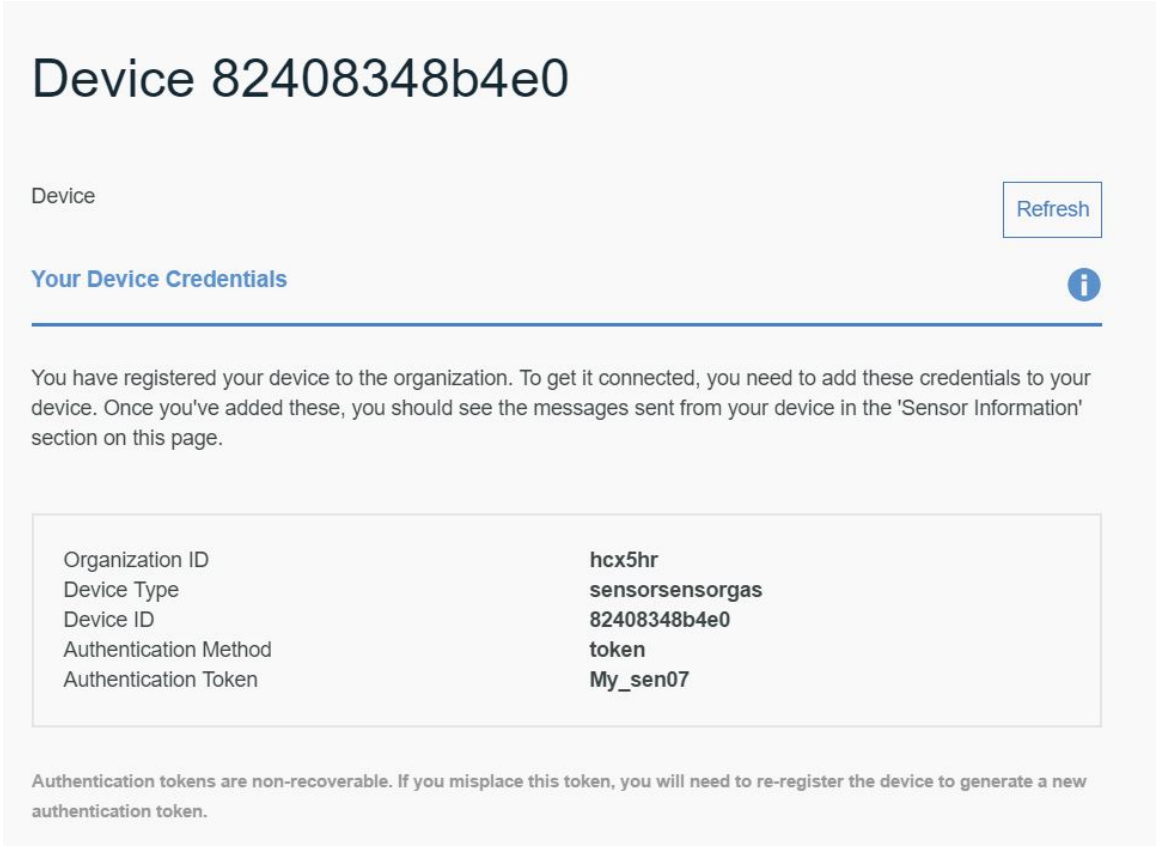

Fig. 6.7. Screenshot of Device type creation window

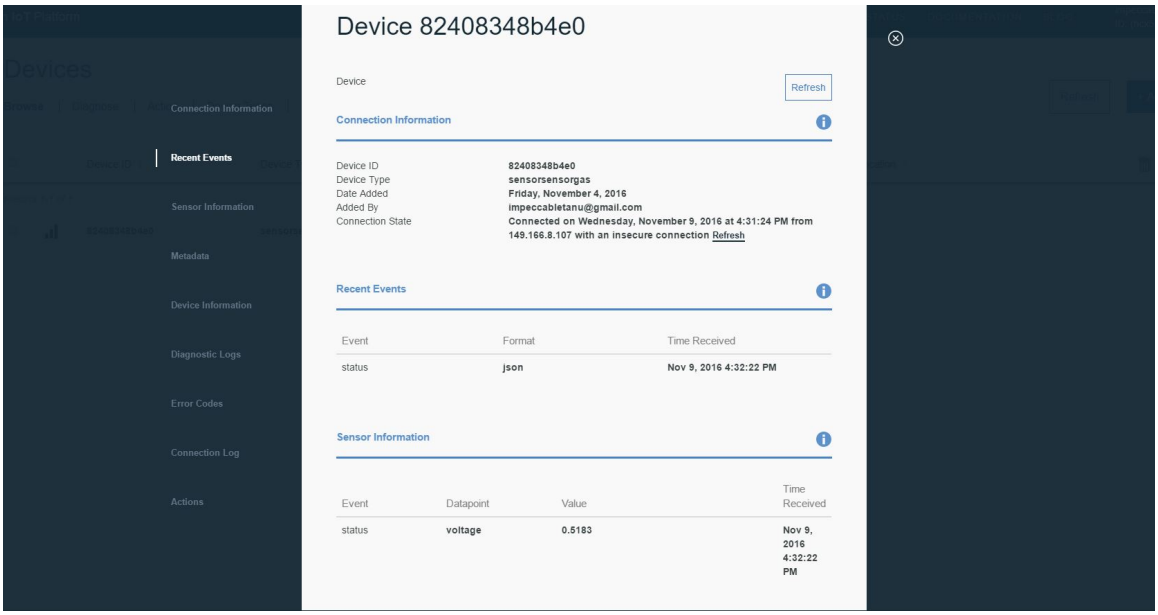

Fig. 6.8. Screenshot taken of window when data is received on IBM Watson IoT platform

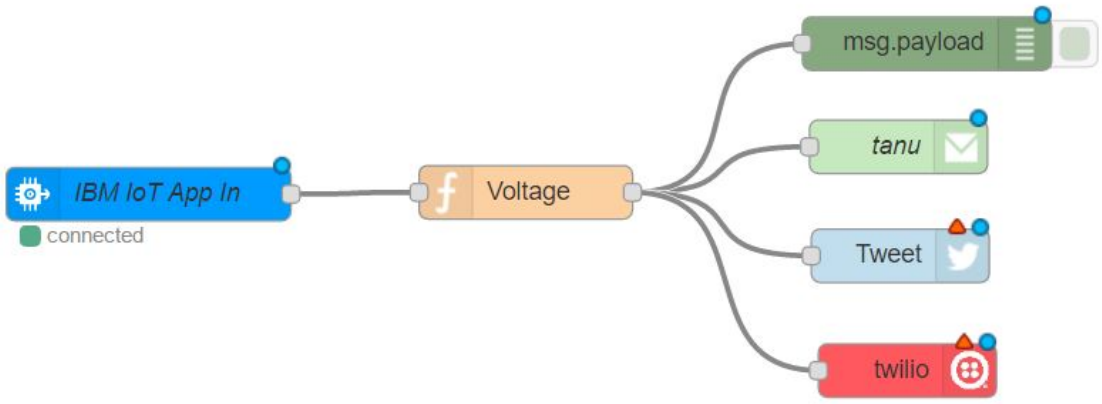

Fig. 6.9. Node-Red Blocks for receiving the data from IBM Watson

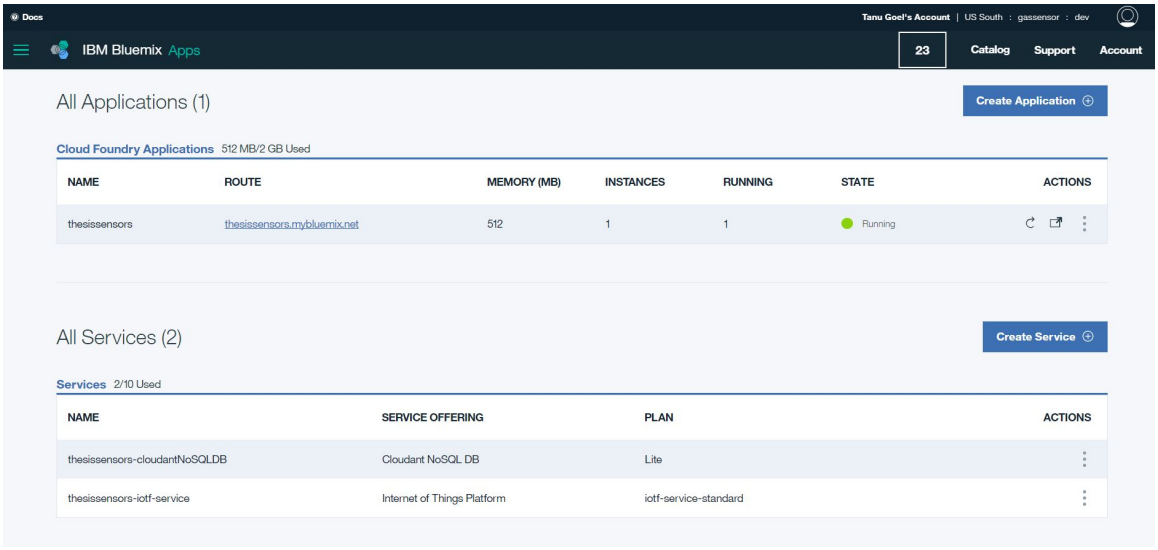

Fig. 6.10. Screenshot displaying the created application and IBM Bluemix services linked to it.

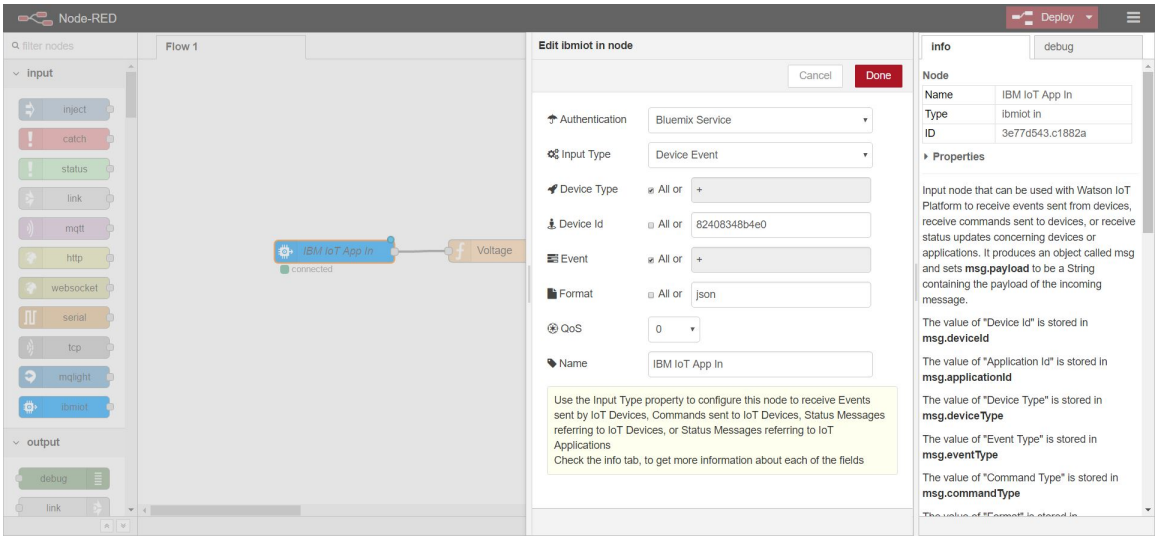

Fig. 6.11. Window screenshot displaying details of 'IBM IoT App-in' block on Node-red

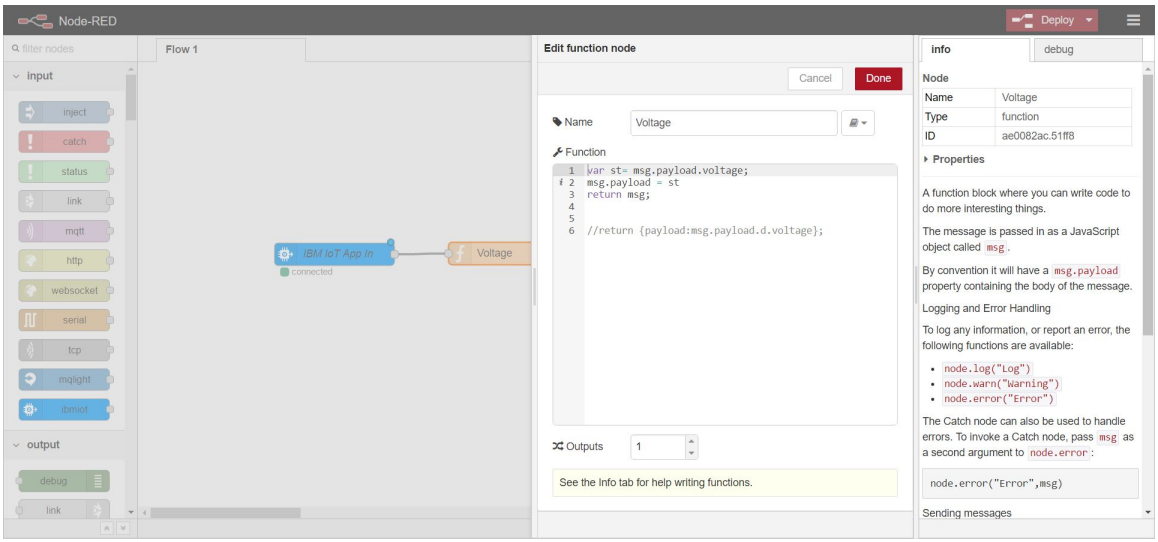

Fig. 6.12. Window screenshot displaying code written for function block on Node-red

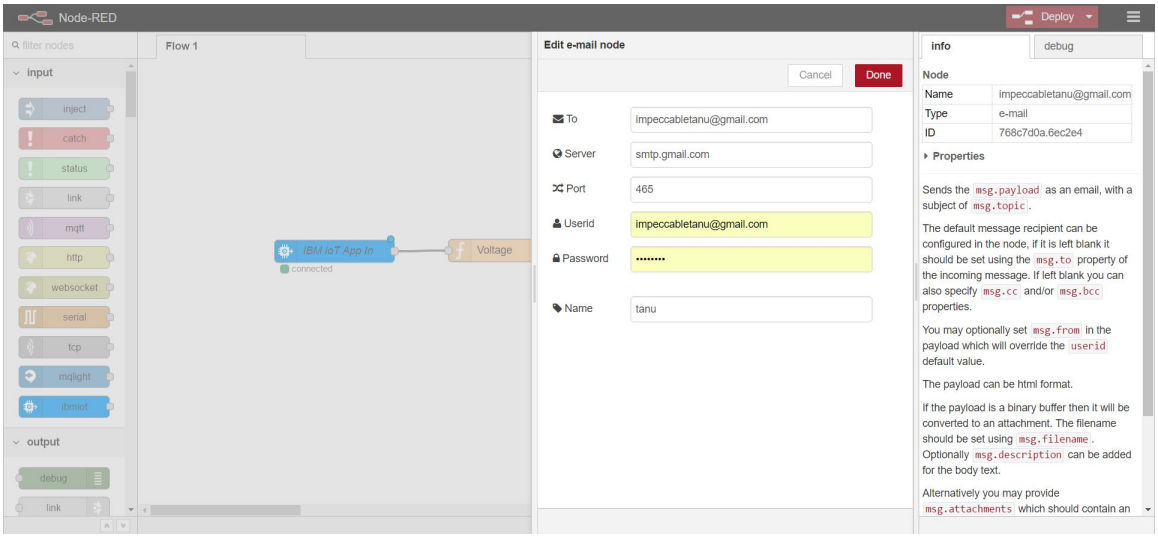

Fig. 6.13. Window screenshot displaying details of client server information block on Node-red

7. APPLICATIONS

7.1 Health Sciences

Identification of disease markers by using highly sensitive gas sensors is being researched now a days. Diagnostic 'breathalyzers' are being developed and researched upon. Breath based analyzers can become a tool of the future, enabling non-invasive means of disease detection. Breath exhaled from human body is composed of a mixture of N_2, O_2, CO_2, H_2O, inert gases and hundreds of other traces of gases. The traces of other gases include low concentration of other volatile organic and inorganic compounds. Presence of volatile organic compounds (VOCs) is due to the metabolic processes inside human body. Whereas inorganic molecules are related to other health conditions. An abnormal concentration of these compounds can be an indicator and act as potential diagnostic tool in future. Researchers are working towards developing an electronic nose to detect VOCs and other bio-markers. Due to high sensitivity of sensors which were being developed earlier to water, presence of moisture interferes with the detection of target gases. Metal oxide semiconductors solve this issue of sensing in presence of water are not stable sensors at elevated temperatures, therefore researchers are moving towards smart materials like graphene and use of metal nanoparticles for improved sensitivity [23].

Characterization of Human Breath for Endocrinology Applications

- Presence of VOCs in human breathe can be used to study human metabolism which can further be extent to early identification of metabolism related diseases. Abnormal concentrations of specific VOCs may become markers of oxidative stress in the human body such as asthma and lung cancer. Currently

only invasive procedures being present for such type of diagnosis, a non-invasive method like breath-analyzer can lead to early assessment of disease, its severity and response to treatment for pulmonary diseases [6].

- Acetone concentration correlates with insulin levels in the body. Small amounts such as 0.1-10ppm of acetone in human breath may lead to exacerbation of diabetes.

- A diseases like diabetes, that threatens lives of millions of people around the world, may be detected by non-invasive means due to abnormal levels of acetone in the breath of human suffering from it. Presence of ethanol has also been linked to diabetes detection.

Various Bio-markers for Non-invasive Detection of Diseases

- Inflammation and oxidative stress in the lungs may result in abnormal concentration of bio-markers like NO, NO_3^- and NO_3^-. For instance, the concentration of nitrogen oxide in human breath as a bio-marker for asthma and related lung diseases can be as low as 2-100ppb.

- For cardiovascular diseases, diabetes, nephritis and bilirubin production, CO exhaled in the breath may act as a bio-marker for its detection.

- Isoprene concentrations are affected by diet and may indicate on abnormal cholesterol levels and increased breath and heart rate.

- H-plyori and renal diseases may be detected by presence of ammonia and amines.

Major disadvantages of the few breath analysis instruments available in market are that they are bulky, costly and require large volume of sample. The most important characteristics for this application are very high aspect ratio of the sensing surface along with a high sensitivity and resolution of the sensor.

With a nano-particle based sensor array having high sensitivity and selectivity, a compact breath analyzer can be developed for performing a quick check-up and it can be used like a pre-diagnostic tool for early detection of various diseases.

7.2 Renewable Energy

Renewable energy sources like hydrogen fuel cells where hydrogen is the main fuel which produces electricity. It is renewable because the fuel isn't burned but it is combined in a chemical process. FCVs (fuel cell vehicles) use hydrogen gas as fuel, combines it with oxygen to produce water. It has zero emission harmful substances when driven and hence it sounds perfectly clean and green option. But hydrogen used is generated typically by reforming natural gas, gasoline or ethanol, which introduce carbon monoxide into the hydrogen gas. For this reason a sensor capable of sensing hydrogen and carbon monoxide is necessary. The main factors which need to be worked upon are low cost, high durability, fast response time, good selectivity, lower drifts and flexible operating temperatures. Such a sensor is essential as a feedback element in FCVs for safety.

7.3 Homeland Security

At places like airports, sea ports and other public places, gas sensing technology for homeland security from incidents involving poisonous gas being used as a threat. Similar incident took place in 1995 in Tokyo, Japan [4] , referred to as Subway Sarin Incident where a poisonous chemical called Sarin was released during rush hours in Tokyo Metro which killed 12 people, severely injured 50 people and causing temporary vision problems for 5,000 others. Along with high sensitivity, a very fast response time is desirable in such situations. Selectivity is another important characteristic which needs to be high to minimize number of false alarms. A wireless gas sensor may meet the requirements for such applications.

7.4 Automotive Industry

Due to increased number of vehicles in the world today, automobiles are contributing in air pollution with a large share. Emissions from vehicles are majorly divided into five categories:

- Carbon monoxide (CO) is the produced due to incomplete combustion of carbon based fuel and higher concentrations of its are poisonous. Carbon based fuel can be bio-fuel or fossil fuels.

- Carbon Dioxide (CO2) is produced in a large proportion due to combustion of carbon based fuel.

- Hydrocarbons (HCs) come from unburnt fuel and they are also referred to as VOCs. Presence of HCs in air may cause ozone depletion and photo-chemical smog. VOCs in the air on the other hand may cause respiratory illnesses such as asthma.

- Oxides if Nitrogen (NO_x) is produced inside engines which work at high temperatures. NO_x becomes a serious air pollutant due to its reactions with HCs being a highly reactive chemical. It produces secondary pollutants such as ozone and photo-chemical smog in presence of sunlight. Ozone when inhaled can damage lungs and small amounts may cause chest pain. coughing and irritation in throat. Photo-chemical smog is an issue of modern industrialization because of its common presence in all modern cities with sunny,warm, dry climate Because it travels with the wind, it can affect sparsely populated areas as well. The link between automotive exhaust and photochemical smog was discovered in the 1950s by Arie Hagen-Smit as seen in the picture in Figure 7.1 [24].

- Particulate matters (PM) are small particles which include unburnt carbon, heavy metals, dust, smoke and other toxic substances. They increase risk of cardio-pulmonary diseases. In order to do combustion control and monitoring of emitted gases, gas sensors are necessary. Tail pipe exhaust gases can be

Fig. 7.1. Layer of photo-chemical smog caused by combination of sunlight and vehicle exhaust

monitored and can feedback the monitoring data. The gas sensor for such applications has to withstand extreme temperatures from exhaust pipe or outside. The gas sensor should be unaffected by corrosion even in presence of high water vapor concentrations. Other desirable quantities are high sensitivity, selectivity and fast response time.

7.5 HVAC

Heating, ventilation and air conditioning (HVAC) [25] is the technology of indoor and vehicular environmental comfort with a goal of providing acceptable indoor air quality. HVAC is a significant part of Residential structures, industrial skyscrapers, hospitals, on-board vessels and marine environments. Ventilation is a key part of HVAC technology which is the process of replacing the air for maintaining good air

quality. Air in closed spaces may have issues like moisture, odors, smoke, bacteria, CO_2 and depleted oxygen content. Ventilation provides removal of all these contaminants and circulates air inside a building. Stagnation of air is prevented by ventilation all the time.

Such HVACs are used throughout industry for a good air quality and healthy environment at all manned places.These air handling systems transport various kinds of gases, some combustible as well as some toxic from one source area to other part of building. The transport of such gases may prove to be a serious issue in case of any mishap. For avoiding any dangerous situation to arrive, a gas detecting device is of utmost importance. By early detection of potentially harmful gases, an appropriate action can be taken timely. On detection of such gases, an automatic shutdown of HVAC systems can prevent worse from happening.

For gas sensors to be deployed in the air ducts, few important key characteristics a sensor must possess are listed:

- Firstly it should be able to withstand the high speed air inside the ducts, of the order of 23-68 mph.
- Secondly, the sensor has to be highly sensitive to detect low concentrations of harmful gases since they might have gotten mixed with replaced air causing dilution.
- The issue of uneven mixing and bending of ducts and non-uniform air flow has to be addressed by increasing sensing area and more sampling channels.
- Due to presence of dust and dirt in air, the sensing screen exposed to air may undergo reduced sensitivity. Therefore regular maintenance and accessibility of sensors is important.

8. RESULTS AND DISCUSSION

8.1 Device Configurations

The wafers used in this research were fabricated by graphene Supermarket.com online facility, using CVD thin film technology with 0.4nm graphene films. The oxide thickness was 90nm think, and the silicon wafer was 1cm^2 surface and 1mm thickness. The wafer with mono-layer graphene was first tested for different configurations without presence of gas. The testing for all the configurations was done on Keithley nano-characterization System.

8.1.1 Resistive Configuration

The device was tested as a resistive sensing device. The sheet resistance of mono-layer graphene thin film is theoretically around 600Ω, while on testing with Keithly Characterization system, the sheet resistance of mono-layer graphene film was found to be 950Ω. The sheet resistance is altered with the gas application.

8.1.2 Capacitive Configuration

The sensor was tested as a capacitive device where the capacitance changes in the presence of gas. Here the Capacitance was measured like a two parallel plate capacitor with dielectric in between. The Silicon substrate acting as one plate and the graphene layer was acting as another. Layer of silicon dioxide was the insulating material acting as dielectric. The C-V curve was obtained for a sweep voltage from -1V to 1V in steps of 0.05 V. Figure 8.1 shows the experimental set up for measuring the C-V curve of the device.

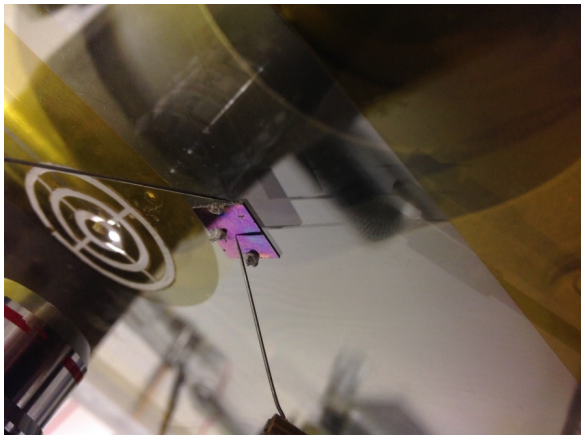

Fig. 8.1. The setup for C-V curve measurement

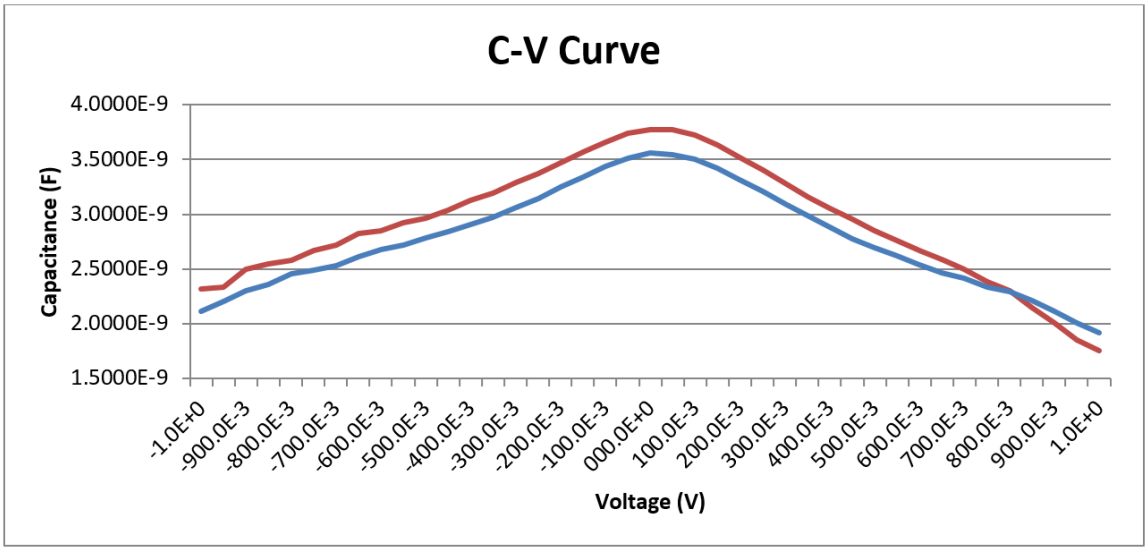

Fig. 8.2. The C-V curves. Two different data were received within a short time interval of 1 minute.

Figure 8.2 shows the C-V data for two successive measurements within a short time interval. In the figure, the upper curve was taken first and the lower one was taken after a time interval of around 1 minute. The lowering of capacitance in a time interval of 1 minute for the same device is accredited to effect of light from the surroundings. Photons emitted from surrounding light get accumulated on the

device and it records lower values of capacitance for the same sweep voltages. From this founding, we can infer, our gas sensing device is sensitive to light and light can be an add-on parameter for future research and experiments.

Figure 8.3 gives the average capacitance distribution with the voltage applied. The curve in Figure 8.3 provides measurement for capacitance at a given voltage. Therefore, the change of capacitance with the applied gas can be determined when compared with the non-gas measurements. The slope of the curve gives the sensitivity of the sensor.

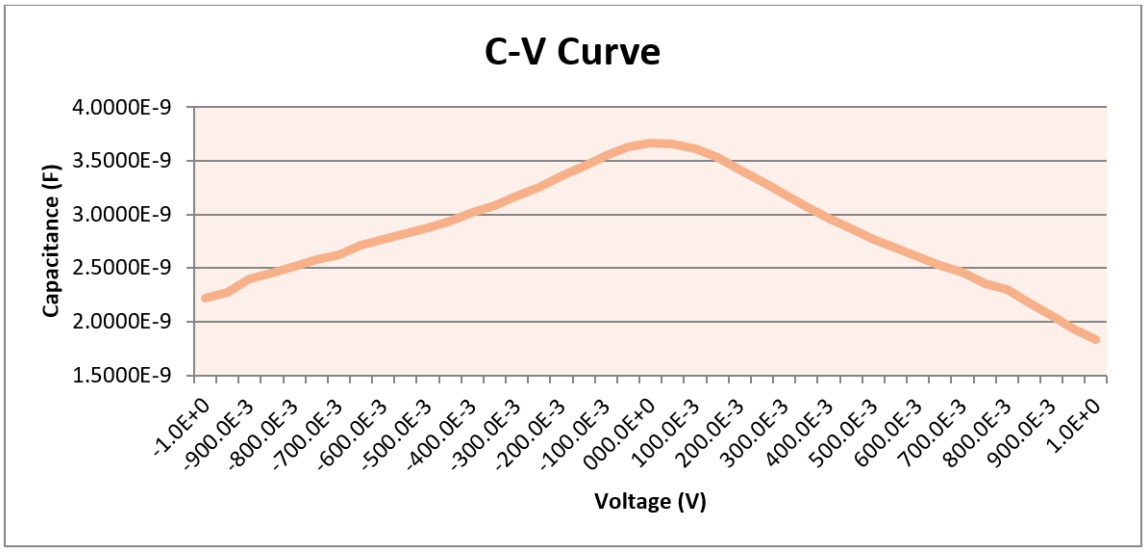

Fig. 8.3. The average C-V curve.

The capacitance of a two-parallel plate is given by,

$$C = \frac{\epsilon_o \epsilon_r A}{d} \tag{8.1}$$

where, A = Area of the parallel plates

d = distance between the plates

$$\epsilon_o = Electrical\ permittivity\ of\ the\ vacuum\ = 8.85 * 10^{-12} Fm^{-1}$$

$$\epsilon_r = Relative\ permittivity\ of\ the\ dielectric(Silicondioxide)3.9$$

For our device,

$$C = \frac{3.9 * 8.85 * 10 - 12 * 0.0001}{10^{-6}} = 3.5nF, \tag{8.2}$$

which agrees with the experimental results at 0V applied as shown in Figure 8.2. The change of the voltage with either polarities show identical different C-values from the device.

We can infer from the graphs in Figures 8.2 and 8.3, the capacitance of the device goes down as we apply either negative or positive voltages to the two-parallel plate capacitor. When a negative voltage is applied, as we can see in Figure 8.4, electrons are kicked in from the mono-layer graphene to the silicon substrate through SiO_2, creating some current, which leads to lowering of capacitance.

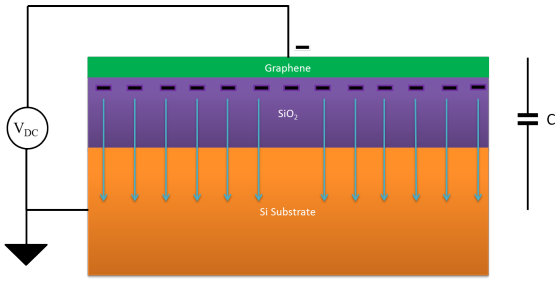

Fig. 8.4. Dynamics of charge carriers when negative voltage is applied

On the contrary, when a positive voltage is applied across the two terminals, positive charge carriers drift through the SiO_2 and thicken the depletion layer at the junction of silicon and silicon dioxide as shown in Figure 8.5. The depletion layer acts as a dielectric and results in formation of another capacitor. The capacitance of the device is the resultant capacitance connected in series. This explains the curve when a positive voltage is applied; the capacitance is lower than its counter-part on the negative voltage side.

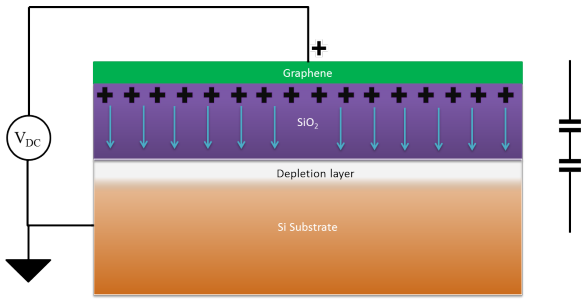

Fig. 8.5. Dynamics of charge carriers when positive voltage is applied

8.1.3 The FET Configuration

A thin film of gold was deposited over the graphene thin film on the wafer in order to form a channel at the center. A mask was prepared to do so and the thin film deposition was done using sputtering technique. The FET characteristics were recorded using Keithley characterization system. For testing purpose, gate, source and drain terminals were to be formed using epoxy contacts. Figure 8.6 gives the FET configuration of the sensor.

Output Characteristics

The drain current-drain to source voltage characteristics was estimated at a constant gate to source voltage. The channel for the flow of electrons in the FET is within the graphene sheet. Figure 8.7 gives the drain characteristics of the device. The positive gate to source voltage leads to higher drain current. The charge carriers flow from source to drain through a channel, which is mono-layer graphene in our case. When the gate-to-source terminals are in reverse bias condition, we can confirm from the graph, as we keep on increasing the reverse bias voltage V_{GS} from 0V to -3V, the depletion layer thickens resulting in more resistance and decreased current.

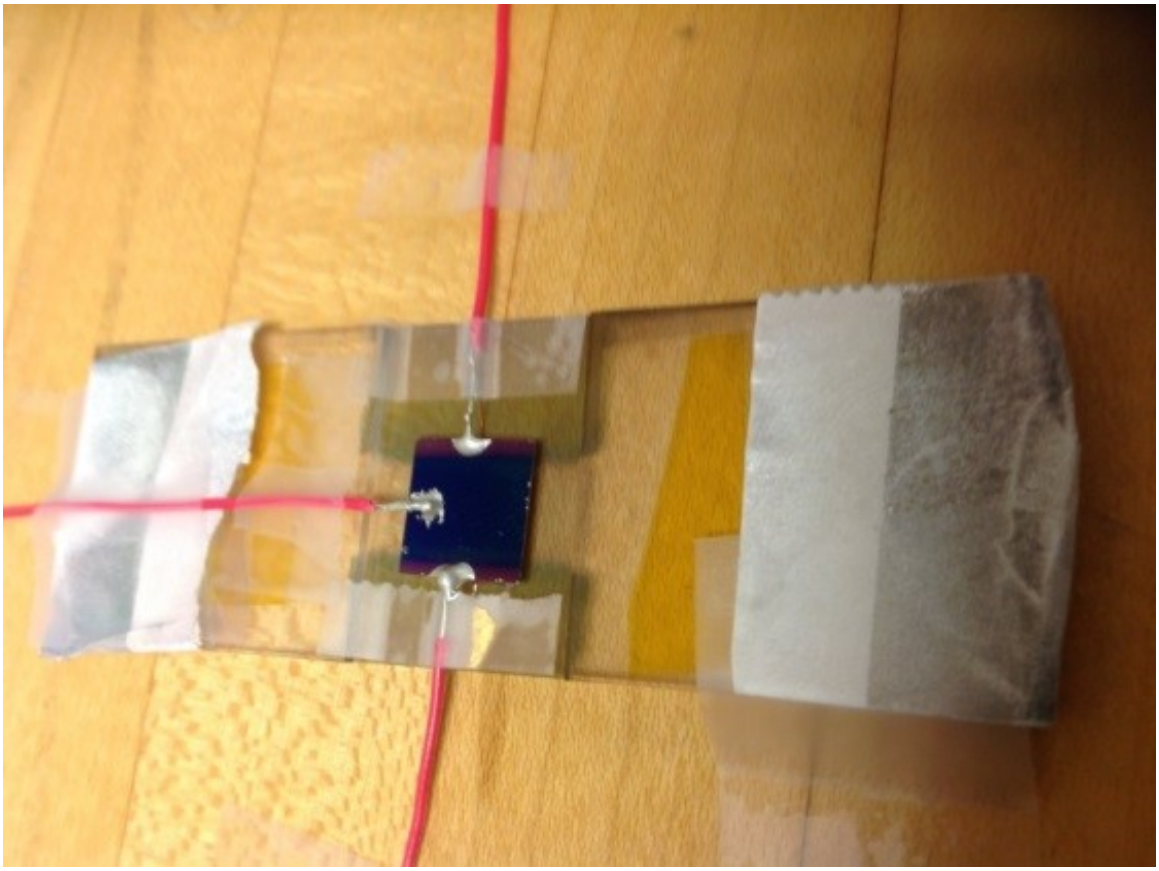

Fig. 8.6. The FET Configuration device

Transfer Characteristics

The transfer characteristics relate to the drain current (I_d) response to the input gate-source driving voltage (V_{GS}). The gas sensor was tested for its transfer characteristics in an FET configuration in the absence of the gas. The drain and source of the FET were formed using gold metal deposition using sputtering technique. Similarly the gate was also formed with gold metal. The transfer characteristics were observed with changing gate voltage from -3 V to 3 V for different drain voltages. Table 1 gives the drain current and voltages at different gate to source voltages.

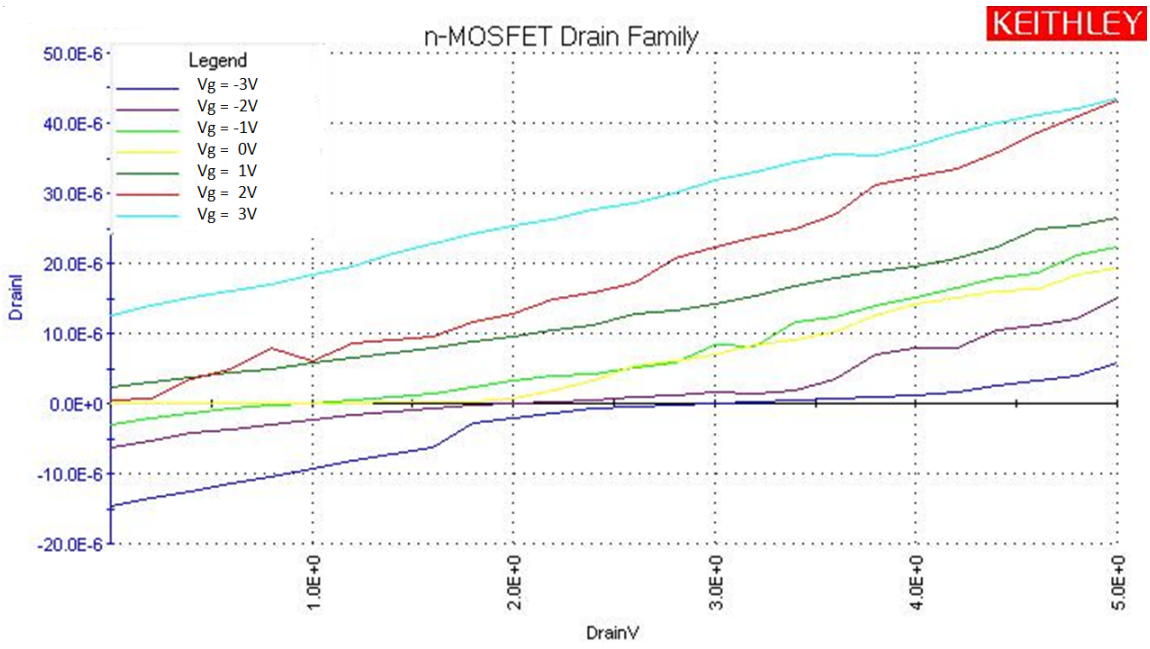

Fig. 8.7. Output characteristics of FET device.

Table 8.1
Drain currents at different drain voltages measured at various gate to source voltages

#	$I_d(\mu A)$ at	$I_d(\mu A)$ at	$I_d(\mu A)$ at	$I_d(\mu A)$ at	$I_d(\mu A)$ at	$I_d(\mu A)$ at
$\mathbf{V_{GS}}$	$V_d = 5V$	$V_d = 4V$	$V_d = 3V$	$V_d = 2V$	$V_d = 1V$	$V_d = 0V$
-3V	5	2	0	-2	-9.5	-14.5
-2V	15	8	2	0	-2	-6
-1V	22	15	9	1	0	-3
0V	20	14	8	3	0	0
1V	27	20	15	10	5	0.5
2V	43	32	22	13	5.5	2.5
3V	44	38	32	25	19	12.5

Sputtering specifications for electrodes: Electrodes area was sputtered using a RF Sputtering System at 30mA current for 90 seconds. Figure 8.6 gives the transfer characteristics of the sensing device. The drain current was recorded and found to be ranged from 0.5μA to 44 μA.

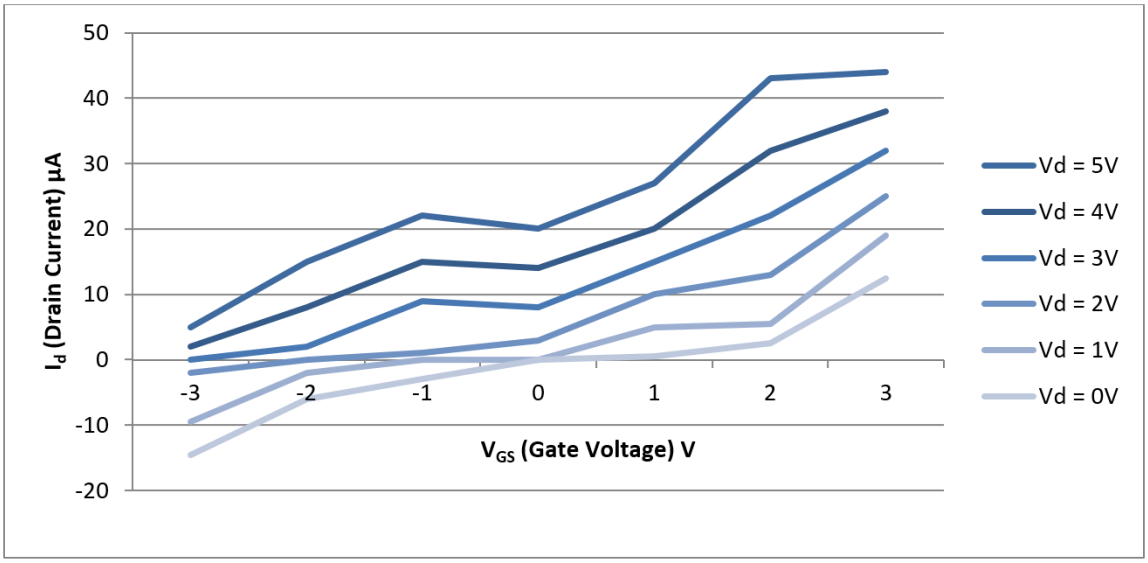

Fig. 8.8. Transfer characteristics of FET device.

It is also clear from Figure 8.6 that higher drain voltage is applying higher electric field to the channel carriers, leading to higher drain currents. As we can see in the graph, as the drain-to-source voltage is increased from 0V to 5V, flow of current also increases. The forward trans-conductance (g_m), which is given by change in drain current (ΔI_d) over change in gate voltage (Δ V_d) at a given V_{GS}, is attributed to the non-linearity of the operating regions of the channel.

8.2 Effect of Carbon Dioxide Gas Application at Different Concentrations

8.2.1 Sensor Testing in Presence of 100% CO_2

For gas sensing, the reading could not be taken on the Keithley Characterization system since there is no option of closing it in a chamber filled with gas. In this situation, a gas chamber was formed and used for testing purposes. A small size chamber was used to be better controlled with gas application. Figure 8.9 shows the gas chamber with the sensor inside. The change in resistance of the mono-layer

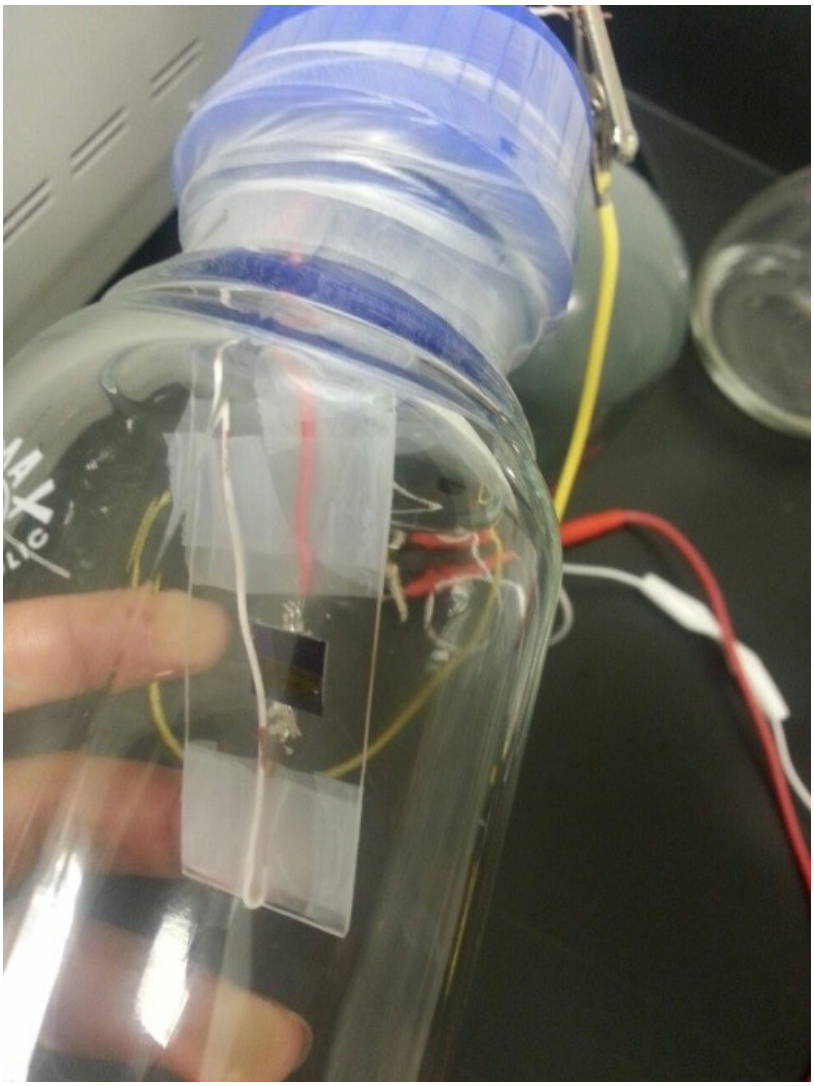

Fig. 8.9. The gas chamber with the sensor in.

graphene sheet in presence of gas was noted using a multi-meter across the wafer contacts, which were made on the wafer using Silver Epoxy as shown in the Figure 8.10.

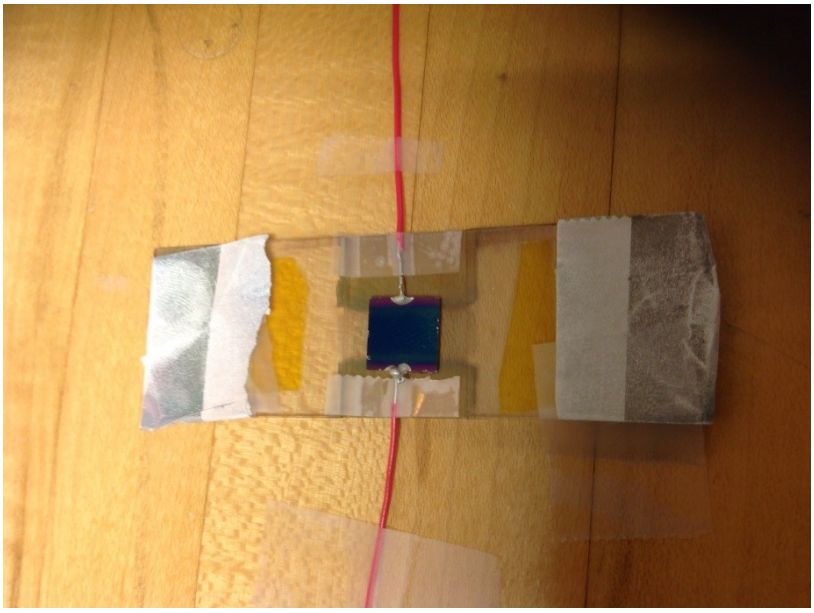

Fig. 8.10. The sensor with metal contacts

The wafer was tested for 100% CO_2 gas. The change in the sheet resistance of graphene was recorded to be around 600 Ω. Table 8.2 gives the resistive values with the gas applications.

Table 8.2
Change in resistance in presence of 100% CO_2 gas

#	**Repetition**	**Initial R(Ω)**	**Final R(Ω)**	**Recovered R(Ω)**
CO_2 100%	1	1179	595	950
CO_2 100%	2	950	724	850
Average		1064.5	659.5	900

Figure 8.11 shows the fall time and rise time for the gas sensor resistive device. The gas was applied at t=0second. The gas was kept for near 2 minutes, then the gas flow was stopped, and the sensor was exposed to the air. It is clear the linearity of the fall time with gas application, and the recovery time with the absence of the gas. The green curve is the average of the blue and red characteristics. The red curve which was measured after completing the blue data curve (near 4 minutes) lags the blue curve, indicating that the sensor has not reached its full recovery, exhibiting a resistance drop of near 230 Ω (1179Ω-950Ω).

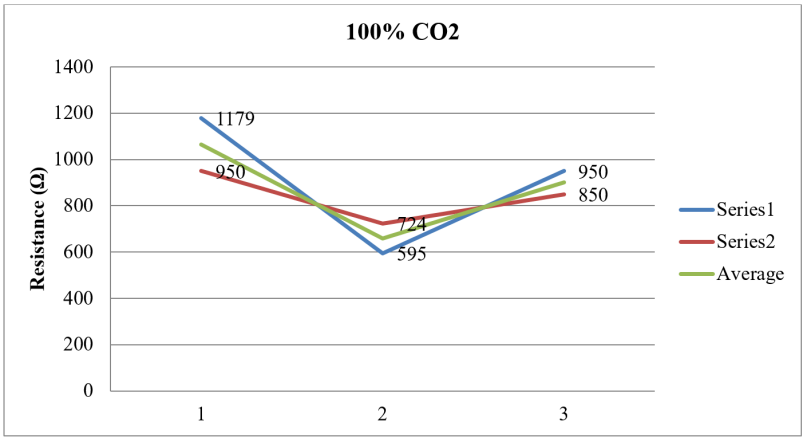

Fig. 8.11. The 100% concentration gas application data for the resistive device sensor

The precision in repeatability of the sensor was also confirmed with the readings recorded. The measured electrical resistance change was evaluated with a defined parameter of sensitivity. The sensitivity of the sensor is defined as the ratio of change in resistance and initial resistive value.

$$Sensitivity(\%) = \frac{FinalResistance - InitialResistance}{InitialResistance} = \frac{1179 - 595}{595} * 100 = 49\% \tag{8.3}$$

Therefore, for 100% CO_2 the sensor showed a change in resistance as much as 49%.

8.2.2 Sensor Testing in the Presence of 5% CO_2

The sensor sensitivity was measured by applying 5% CO_2 concentration. The sensor was tested a resistance change around 3.38% was estimated. The sensor was found to be precise for 5% CO_2 concentration as depicted figure 8.12 and tabulated in Table 8.3.

Table 8.3
The 5% concentration data of the resistive gas sensor

#	Repetition	Initial R(Ω)	Final R(Ω)	Recovered R(Ω)
CO_2 5%	1	1099	1124	1079
CO_2 5%	2	1079	1124	1073
CO_2 5%	3	1079	1113	1074
Average		1083.7	1120.3	1075.3

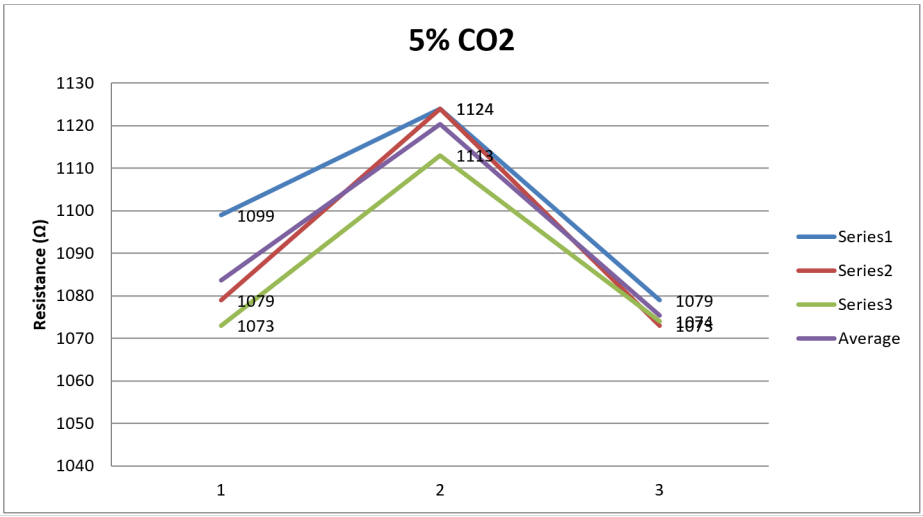

Fig. 8.12. The 5% concentration data repeated three times. The purple color gives the average of the three successive data. Again the fall time and recovery time show linearity in the sensor sensitivity.

8.2.3 Sensor Performance Comparison: 100% Vs 5% CO_2

As shown in figure 10, the gas sensor is highly sensitive to 100% CO_2 gas and shows a rapid change in its resistance as the supply of the gas started and similarly resumes rapidly recovery as well. The resistance is seen to be decreasing, which means the gas is making the graphene film more conductive in the presence of 100% CO_2. Noticing the effect of 5% CO_2 on the gas sensor, it is shown to be increasing the resistance of the graphene film. The change in resistance and hence the sensitivity of the sensor is much less for 5% CO_2 compared to 100% CO_2 gas. The difference in the conductivity of graphene film due to 5% and 100% CO_2 lies in the adsorption phenomenon that takes place while gas sensing occurs. The molecules which get adsorbed on the sensing surface change the local carrier concentration which leads to change in resistance. The poor response for 5% CO_2 can possibly be related to unavailability of active sites for its adsorption due to its very low concentration. This came in agreement to what was investigated by [2].

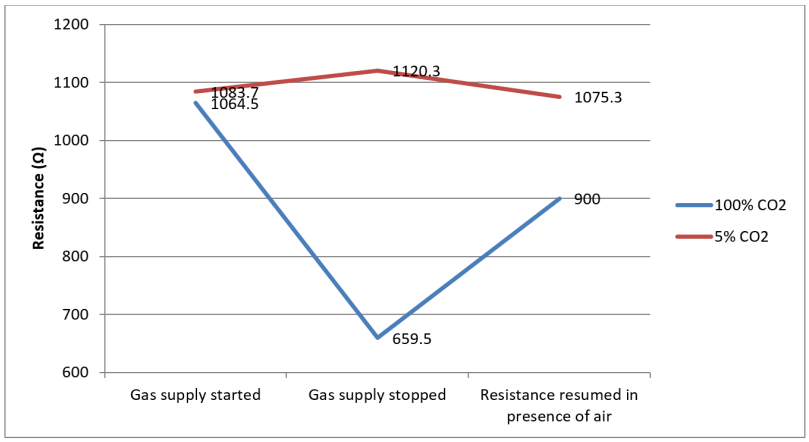

Fig. 8.13. The comparison curves between two different CO_2 concentrations

8.2.4 Dynamic Variation of Resistance for 5% CO_2

The dynamic characteristics of the wafer were recorded for 5% CO_2. Figure 8.14 shows rise time of the dynamic resistance of the sensor.

- when the gas supply is started and reaches its saturation value of resistance
- when gas supply is stopped and resumes to its stable resistance value.

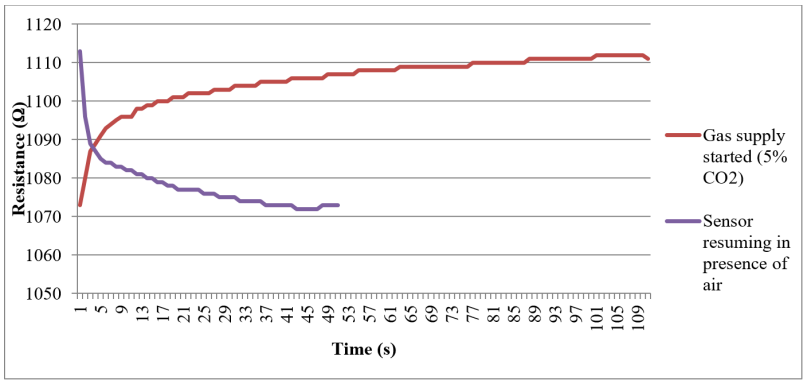

Fig. 8.14. Dynamic characteristics of sensor in resistive configuration in presence of 5% CO_2

The rise time is the time required for the response to rise from 10% to 90% of its final value was calculated for the sensor output which came out to be 62 seconds. Similarly, the fall time, which is the time taken for the response to fall from 90% to 10% was calculated and came out to be 18.5 seconds.

8.2.5 Gas Sensing Signature Array

Based on the data recorded for the gas sensing performed for CO_2 gas for two different concentrations i.e. 5% and 100%, the gas sensing signature array can be designed. The $GSSA_{CO2}$ shown below exhibits the sensors signature values for carbon dioxide gas for two different concentrations.

$$GSSA_{\mathrm{CO2}} = \begin{pmatrix} \Delta R_{\mathrm{t_0\ c_1}} & \Delta R_{\mathrm{t_1\ c_1}} & \Delta R_{\mathrm{t_2\ c_1}} \\ \Delta R_{\mathrm{t_0\ c_2}} & \Delta R_{\mathrm{t_1\ c_2}} & \Delta R_{\mathrm{t_2\ c_2}} \end{pmatrix}$$

$$GSSA_{\mathrm{CO2}} = \begin{pmatrix} 1064.5 & 810 & 659.5 \\ 1083.7 & 1108 & 1120.3 \end{pmatrix}$$

Where, t_0, t_1, t_2 are the time instances, and the concentrations c_1 and c_2 are 100% and 5% CO_2 respectively. This array can be utilized to code the gas sensor as an embedded system device for the detection of various gases with different concentrations.

8.3 Gold Nano-particle Formation

For the formation of Gold nano-particles over the mono-layer graphene coated wafer, a process with two steps was performed.

Sputtering of Au thin film: Gold thin film was deposited on the graphene coated Silicon wafer. A rate of roughly 3Å/sec i.e. a 3Åthick layer per second of sputtering is formed using magnetron sputtering system. Sputtering for duration of 30 seconds was performed on the wafer which resulted in a 9 nm thick layer of Gold. The base pressure of the system was about 108 torr.

Xenon flash annealing: The sputtered layer is then converted in to thermodynamically stable nano-particles. This is done by Xenon Flash annealing which is a technique of use of intense pulsed light for de-wetting of thin films. Two flashes of 3 ms and 30 J/cm^2 energy were shown on the sample at a gap of 2 ms between each flash. The sample was placed at a 1 cm distance from the flash.

8.3.1 Scanning Electron Microscopy

In the next step, imaging on the sample using JEOL 7800F field emission scanning electron microscope was performed to actually view the nano-particles formed. Figure 8.15 (a) and (b) show images take from SEM at 33,000x zoom and 45,000x zoom.

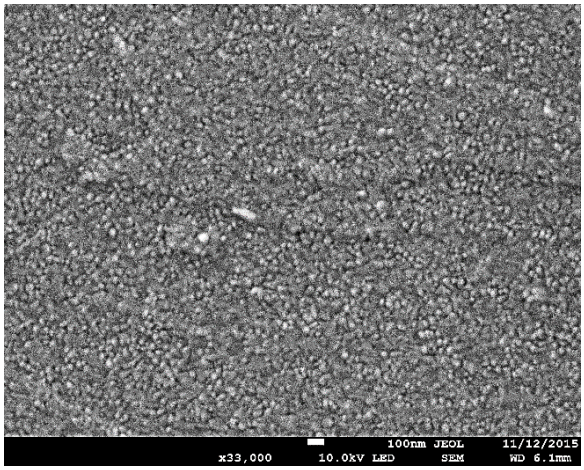

(a) 33,000 times zoomed image

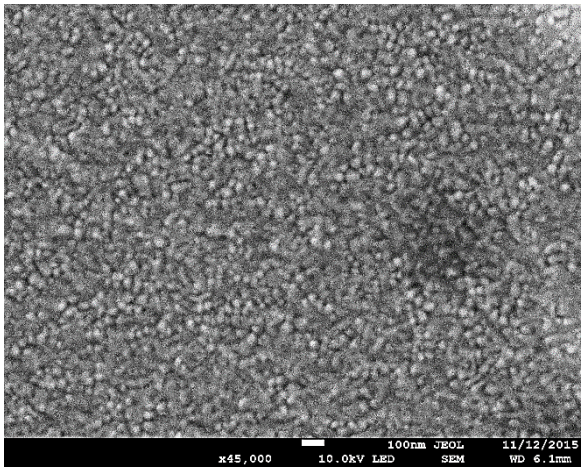

(b) 45,000 times zoomed image

Fig. 8.15. SEM imaging of AuNPs formed on Silicon wafer with mono-layer graphene on top using a JEOL 7800F field emission scanning electron microscope.

8.3.2 Raman Spectroscopy

The wafer coated with graphene mono layer was run for raman spectroscopy and the spectrum obtained is shown Figure 8.16.

The spectrum shows a clearly visible peak for graphene, which confirms presence of graphene on the wafer.

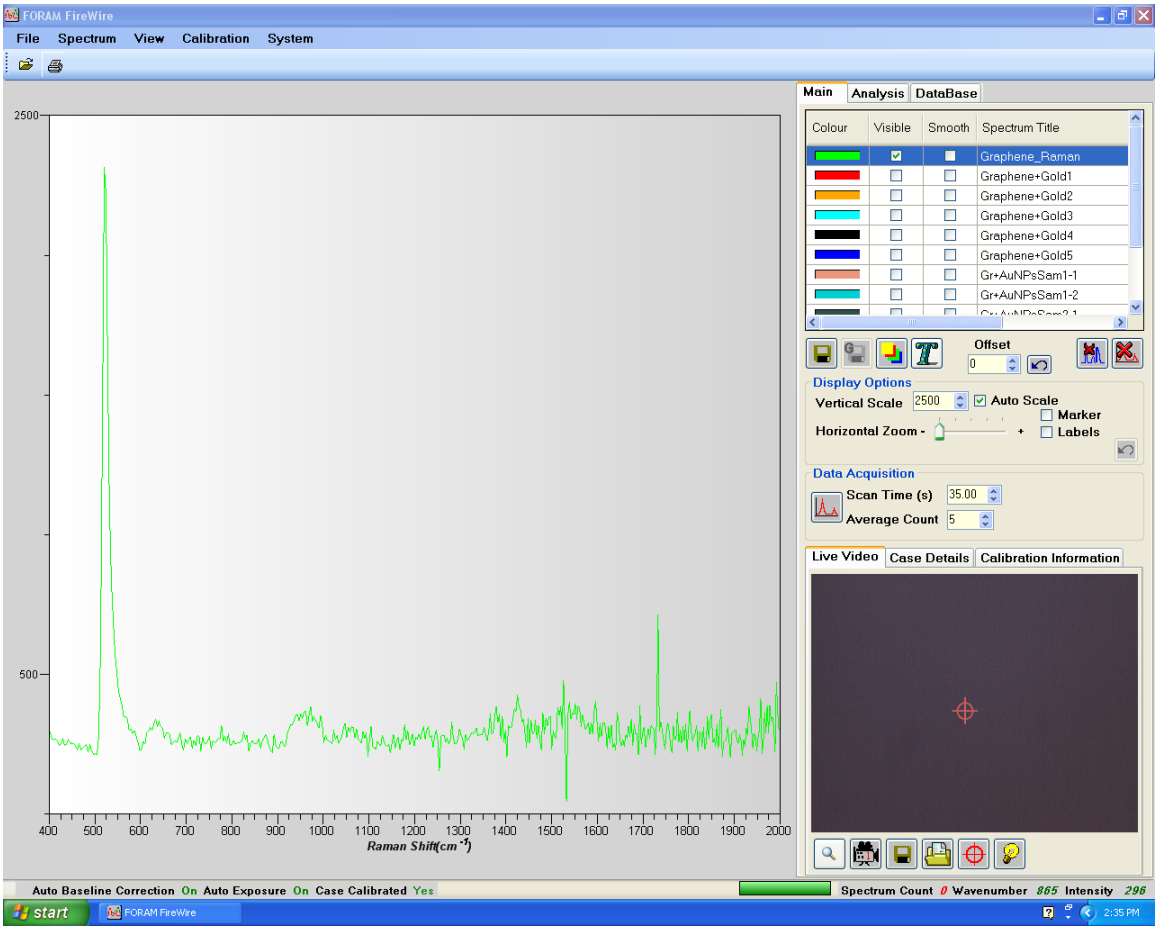

Fig. 8.16. Raman spectra for gas sensor with mono-layer graphene, collected with 532nm excitation

Likewise, the wafer was run for AuNPs to show the presence of the gold nano-particles. Figure 8.17 shows the spectrum obtained after performing raman spectroscopy on it. The graphene is clearly located on the wafer surface, and a peak along with other peaks for gold nano-particles in one spectrum clearly appeared. This confirms the presence of both graphene as well as gold nano-particles on the same wafer.

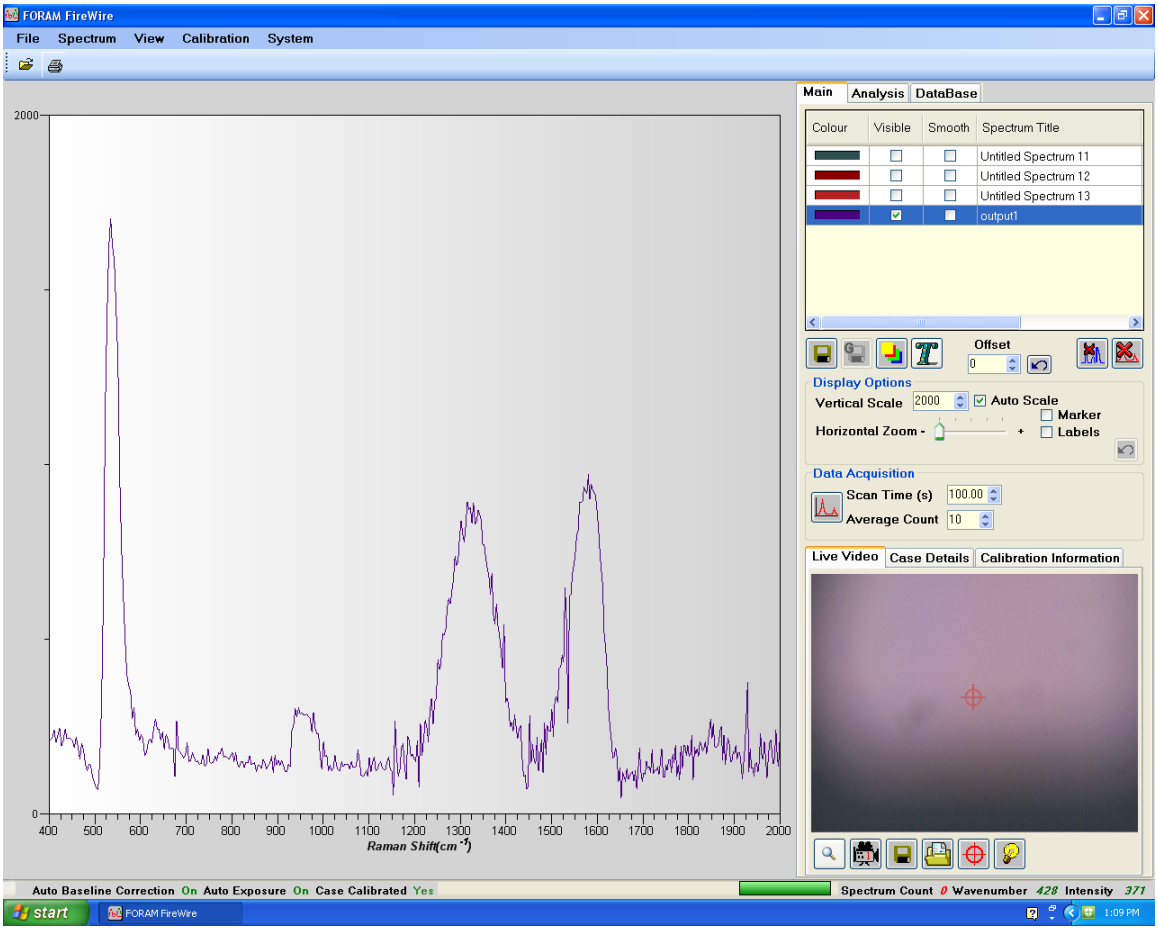

Fig. 8.17. Raman spectra for gas sensor with mono-layer graphene decorated with AuNPs, collected with 532nm excitation

8.3.3 X-Ray Diffraction of Samples

X-Ray diffraction patterns were obtained using a Bruker D8 discover X ray diffraction instrument. Figure 8.18 depicts X Ray diffraction test result peak for sample with just graphene on it. A sample with no nano-particles and just a graphene layer was run on X Ray diffraction. The results confirm the presence of a Mono-layer Graphene film on the Silicon wafer. Had there been two layers of graphene, we would have been able to see a peak for presence of graphene.

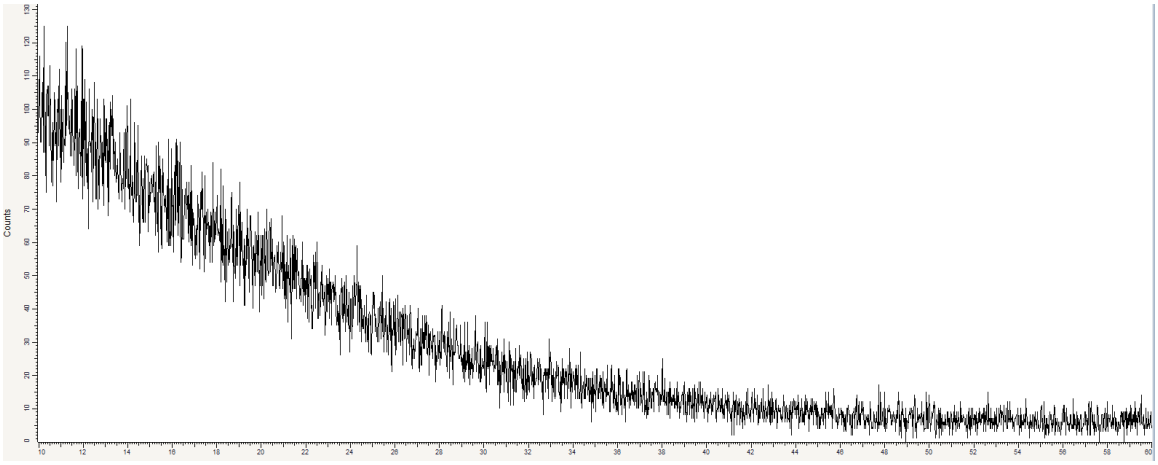

Fig. 8.18. X-Ray diffraction of wafer with graphene mono-layer

In the next step the wafer with Gold nano-particles on it run on X Ray diffraction systems. X Ray diffraction test result show peak for sample with Gold nano-particles over graphene.The results show a definitive presence of gold nano-particles on the wafer as can be seen in Figure 8.19.

8.4 Simulation Results

8.4.1 Operational Amplifier Simulation on Cadence Software

Schematic of Op-amp without feedback circuit (open loop gain): The schematic shown in Figure 8.21 is an operational amplifier at transistor level, drawn using the Virtuoso schematic editor in Cadence. The values of the length and width have been calculated. The other components have values as follows:

Load capacitor (C_L)= 1 pF

V_{dd}= 1.5V

W/L ratios for M_1=7

M_2= 7

M_3= 84

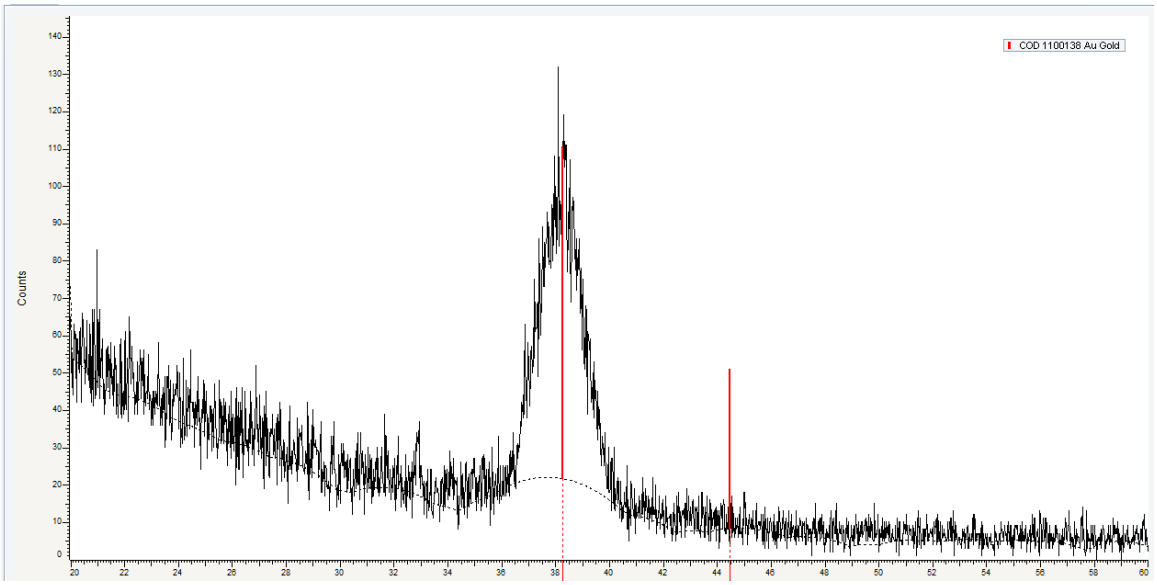

Fig. 8.19. X-Ray diffraction of wafer with graphene mono-layer

M_4= 84

M_5= 9

M_6= 9

Current source (I_{dc}) = 50 μ A

Inverting input (V_{ini}) = 800 mV DC supply

Non-inverting input (V_{inn}) = 100μ V AC supply

Figure 8.22 shows output for op-amp with open loop gain. The gain of an operational amplifier is mathematically given by,

$$Gain(A_v) = \frac{1.4579}{0.00001} = 145790 \tag{8.4}$$

Two stage amplifier was designed on cadence software. Figure 8.23 shows schematic of a two stage amplifier at transistor level.

The output waveform for op-amp with feedback circuitry are shown in Figure 8.24. The circuit is simulated for an inverting voltage of 500mV. The non-inverting voltage is given as a pulse input. The values of the non-inverting voltage swing from

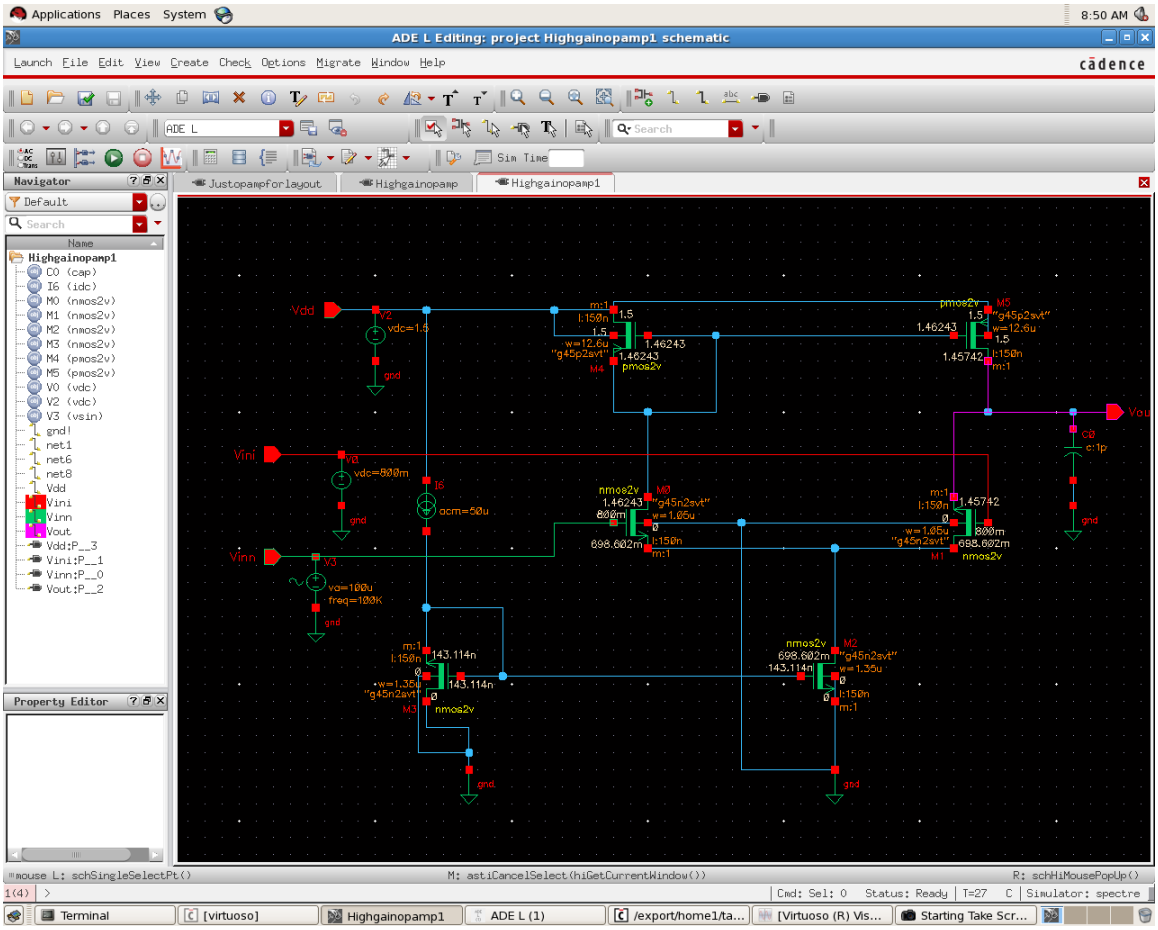

Fig. 8.20. Cadence schematic of a single stage Operational Amplifier

400mV to 600mV. The pulse width is 500ns and period is 1000ns. The rise time and fall time are both specified to be 60ns. V_{ss} was given as -1.5V.

For calculation of gain of the op-amp, the circuit was simulated with an inverting voltage of 1.4V and a non-inverting voltage of 1.40005V. For a differential voltage of 0.00005V, the gain of the op-amp was calculated.

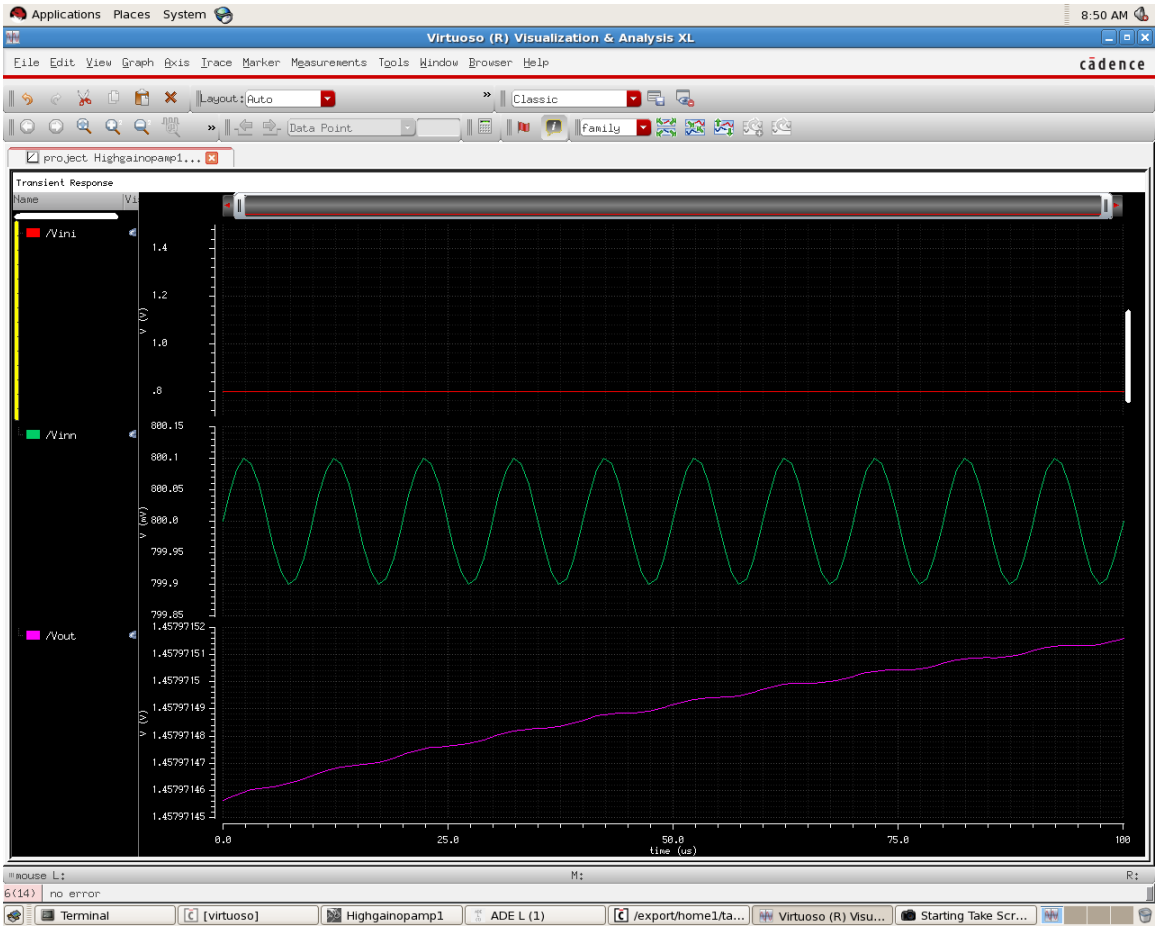

Fig. 8.21. Simulation of a single stage op-amp with open loop gain

Schematic of Op-amp with Offset Cancellation Circuitry

The schematic shown in Figure 8.25 is drawn using the virtuoso schematic editor in cadence. The clock generator circuit as well as offset cancellation circuit was added at the input of the op-amp. The schematic was simulated but we obtained no significant results. Figures 8.26 and 8.27 show the schematics of dc offset removal circuitry and clock generator respectively at the transistor level.

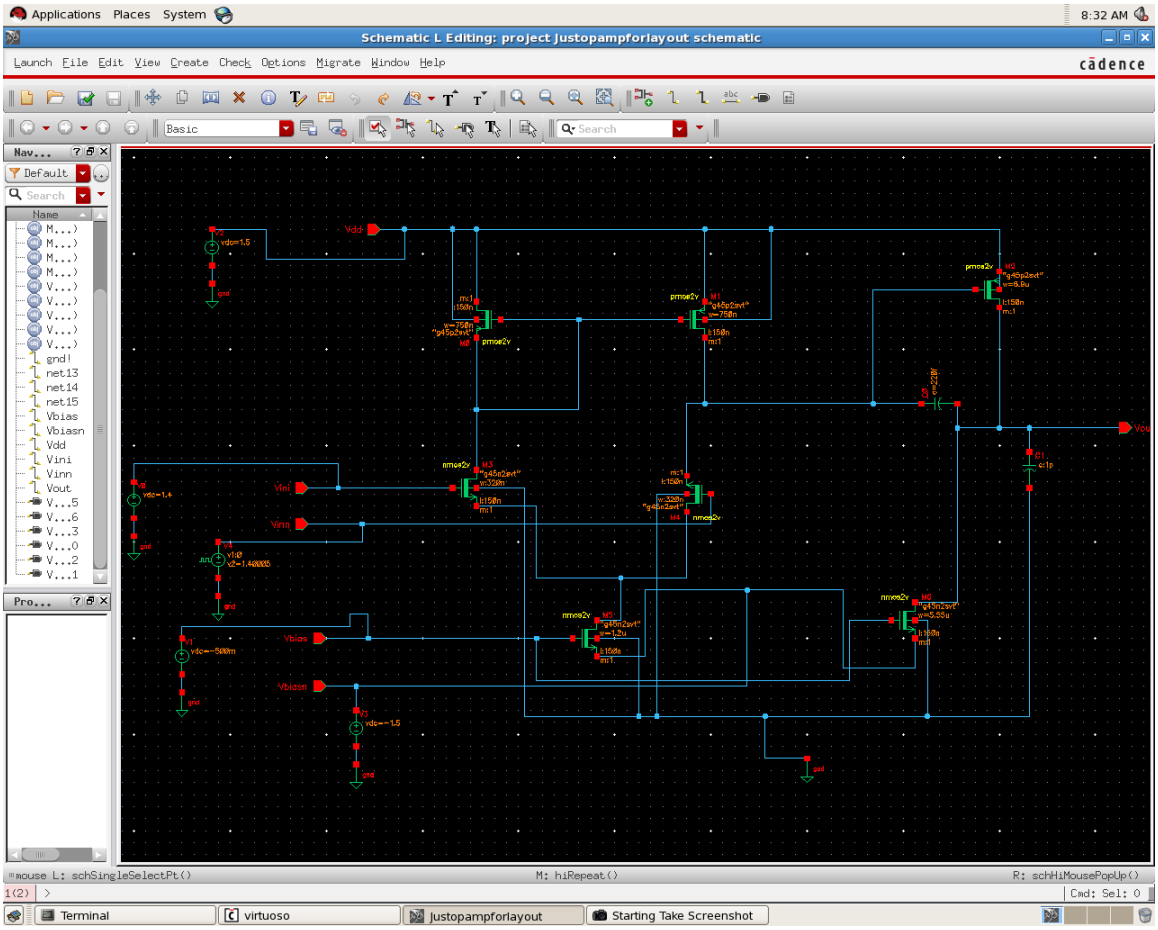

Fig. 8.22. Cadence schematic of op-amp

As shown in Figure 8.28, after the addition of offset cancellation circuitry, the offset voltage for 0 V input in both inverting and non-inverting terminals came out to be 17μV.

Cadence Layout for Operational Amplifier

The layout of the operational amplifier was designed on Cadence software and is given in Figure 8.29.

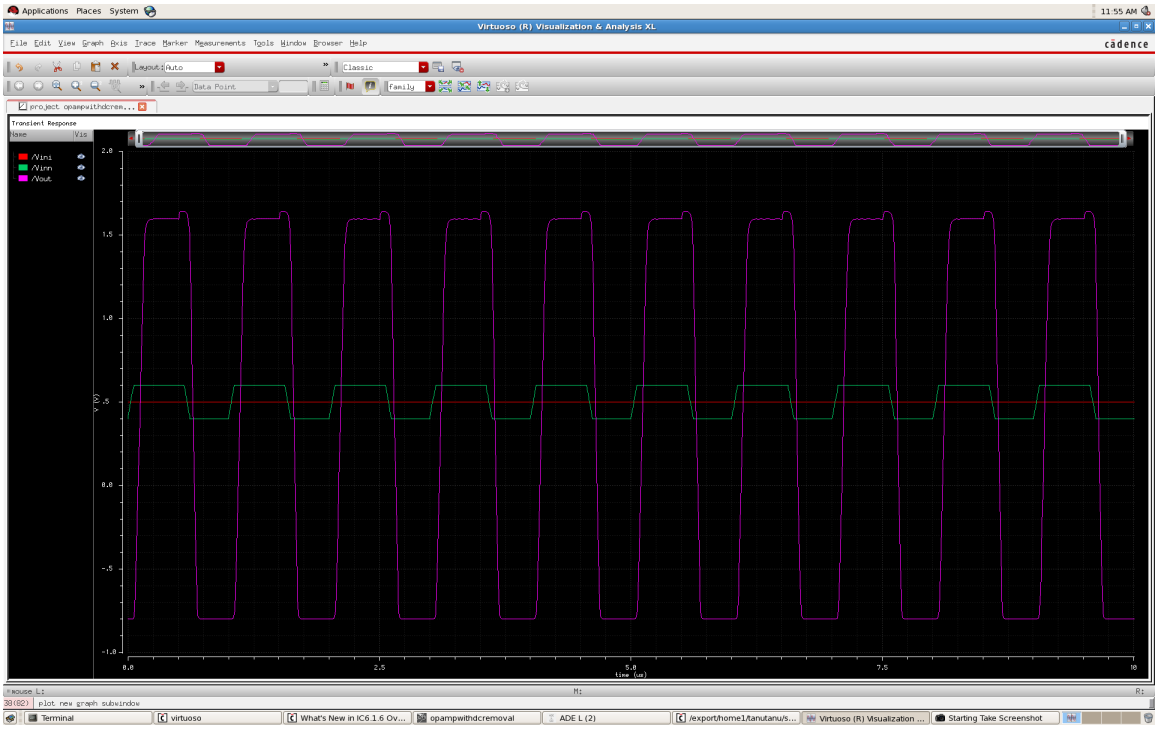

Fig. 8.23. Output waveform of operational amplifier

8.4.2 Interface Circuitry

A Wheatstone bridge is formed for converting the change in resistance values to a proportional change in voltage value. For 0.01Ω of resistance change, a voltage change of 240μV is recorded as shown in Figure 8.30.

8.4.3 Instrumentation Amplifier Simulation on LtSpice

The Instrumentation amplifiers consist of 3 operational amplifiers that were designed to achieve high gain. The circuit shown in Figure 8.31 was simulated using LtSpice software and a gain of 83 dB was achieved. The simulation was based on a change of a voltage of 240μV.

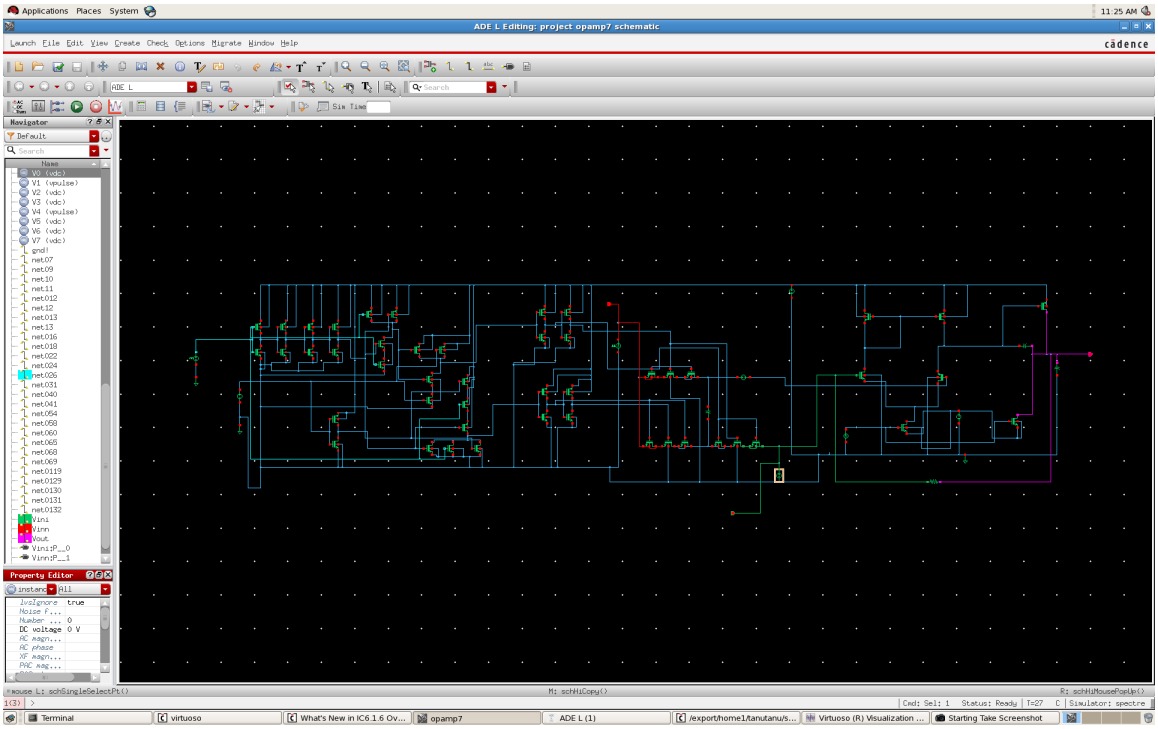

Fig. 8.24. Cadence schematic of two-stage operational amplifier with dc offset circuitry

8.4.4 Noise Reduction Results Using Guard Rings

According to [26], to isolate the input terminals with the use of guard rings, cross talk attenuation in excess of 90 db was recorded between channels in a quad instrumentation amplifier VLSI chip for a multi-channel data acquisition system. The research conducted at IUPUI for the cross talk issue, addressed the cross talk by first separating the four instrumentation amplifiers far from each other, searching for the best approach to reduce the cross talk noise issue. Addressing this research issue with practical realization of the quad amplifier on chip has led to the optimum case when these amplifiers were guarded by rings. Guard rings work as dummy collectors to collect minority carriers injected from the input terminals of the one amplifier that would otherwise be collected by the input terminals of another amplifier. The chip

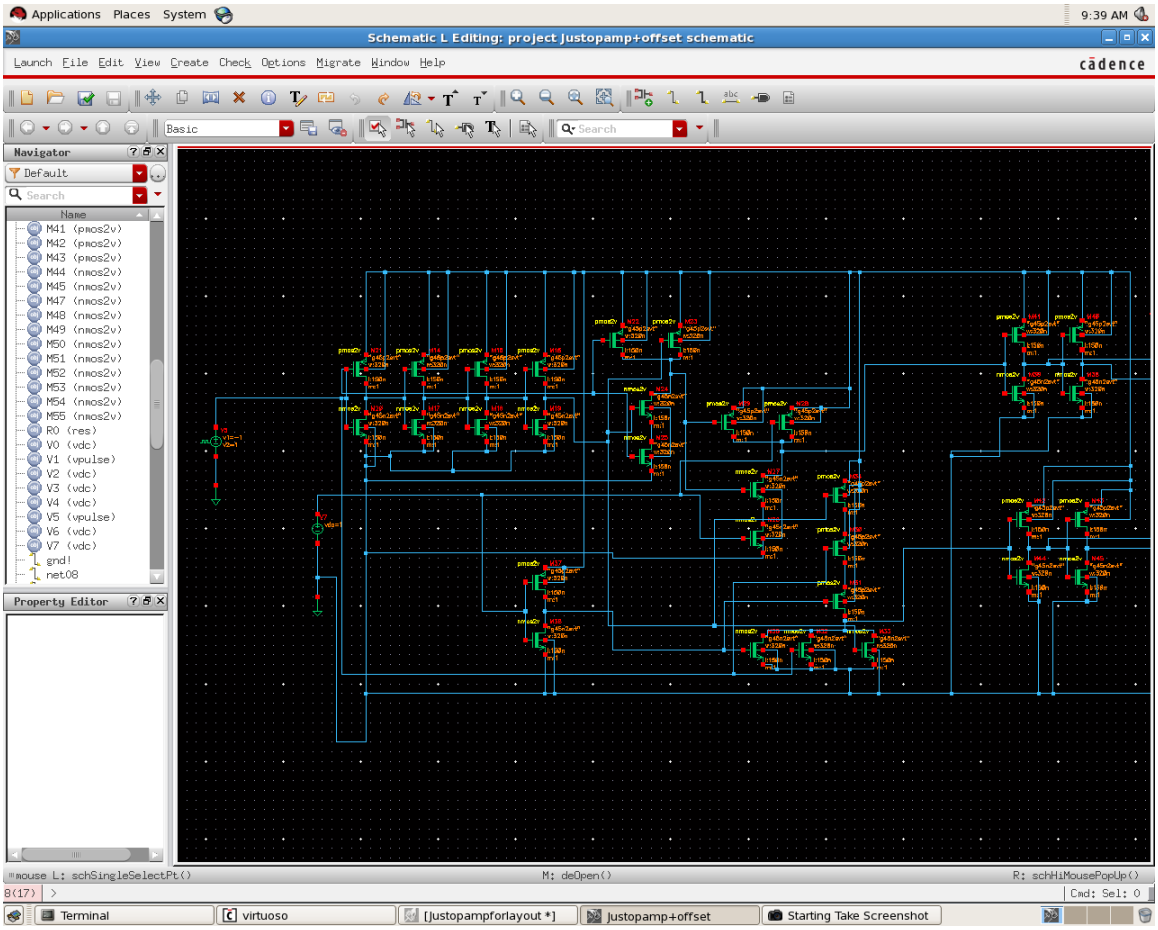

Fig. 8.25. DC offset removal circuitry schematic on cadence spectre

was fabricated by MOSIS service and tested for the minimum noise performance. Using guard rings, as low as 90 dB noise attenuation was reported. Using guard rings, as low as 90 dB noise attenuation was reported.

8.5 IoT Capable Sensing Using FRDM K64F MCU

Wireless functionality of gas sensor was developed using FRDM K64f microcontroller board. In resistive configuration, the change in resistance due to presence of gas was fed into the Wheat stone bridge. The output from the Wheat stone bridge

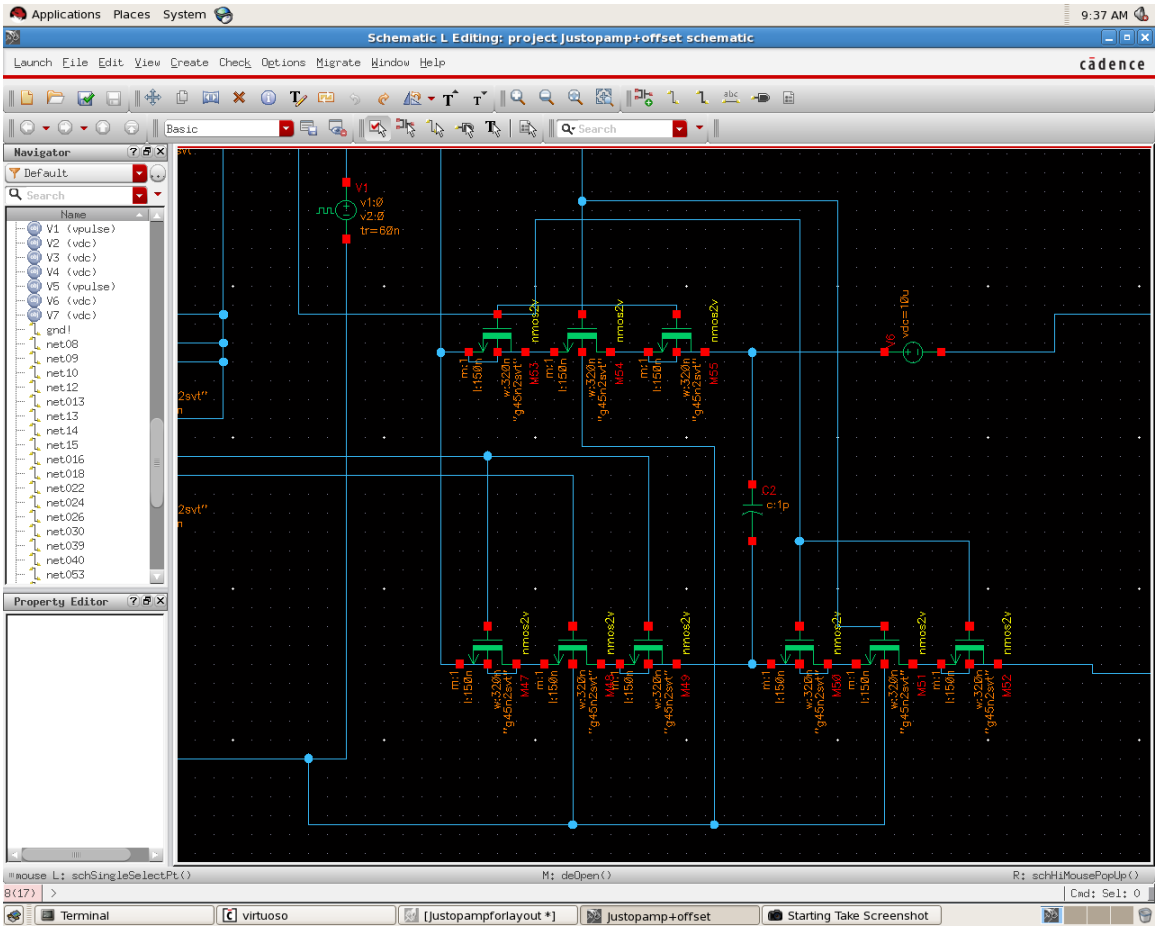

Fig. 8.26. Clock generator schematic on spectre cadence

was fed into the op-amp in a differential mode. Operational amplifier LM741 was used to amplify the voltage signal. The entire setup was designed on a bread board as displayed in Figure 8.32.

For a change in resistance of 100Ω in one arm of the wheat stone bridge, a change in voltage of 119 mV was received. Differential amplifier was fed with a this voltage and an output of 1.85 V was obtained. The Pspice simulation for this part of system is shown in Figure 8.33. The output of the amplifier was fed into the FRDM K64f micro controller board at analog-in pin. When the voltage received by the micro-controller board was higher than a certain threshold voltage specified in the code, a

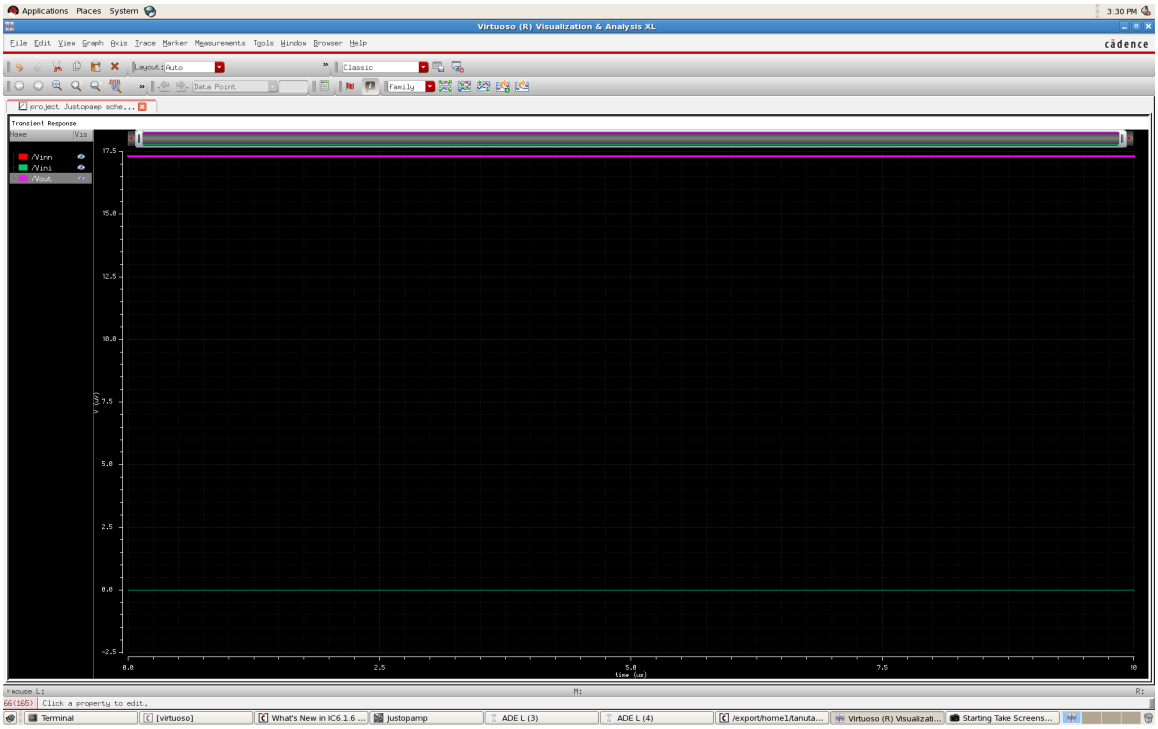

Fig. 8.27. Cadence simulation output after offset removal circuitry

message was sent via gmail to the specified user as can be seen in the screen-shot in Figure 8.34.

FRDM K64f can be coded for matching the values with the gas sensing signature array. According to the match, the gas name will be sent to the receiver via email/message.

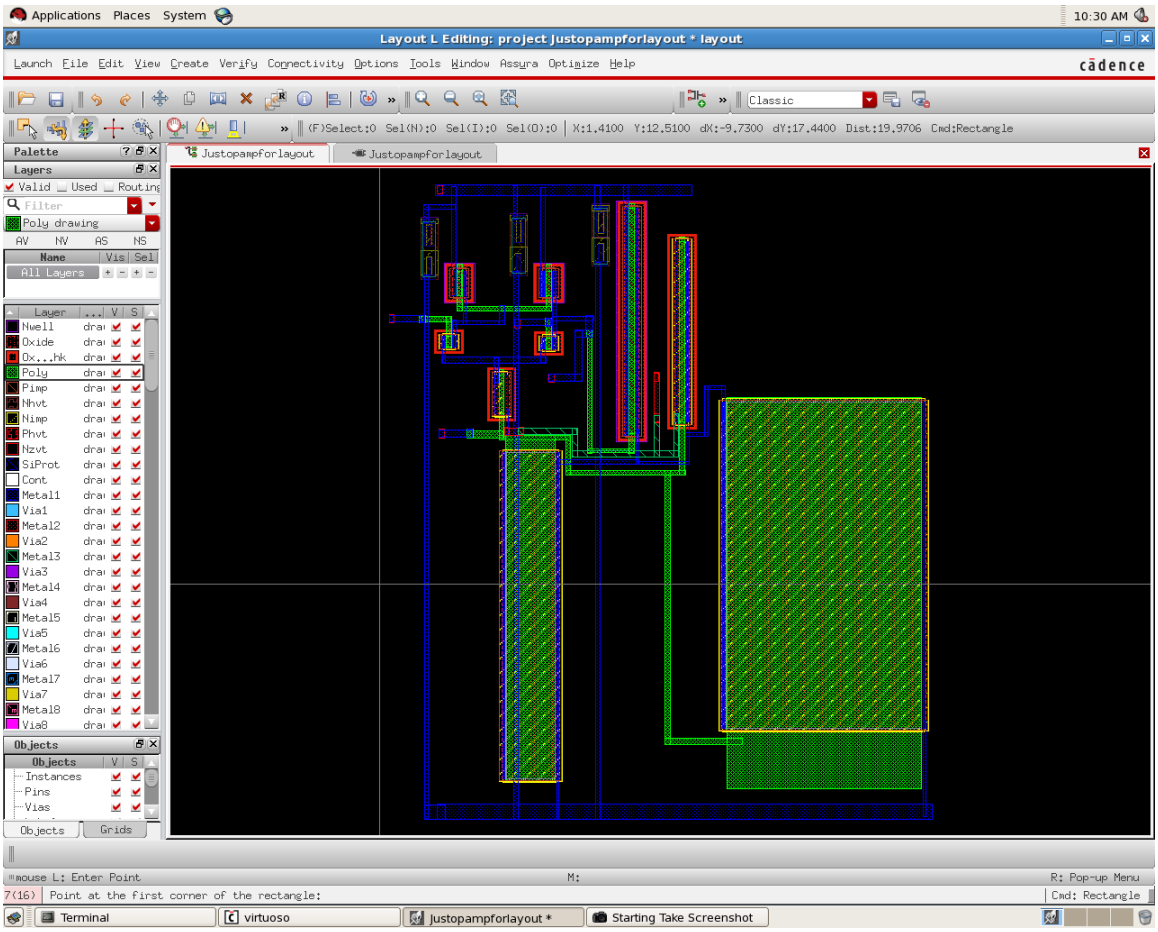

Fig. 8.28. Cadence Virtuoso layout of Operational Amplifier

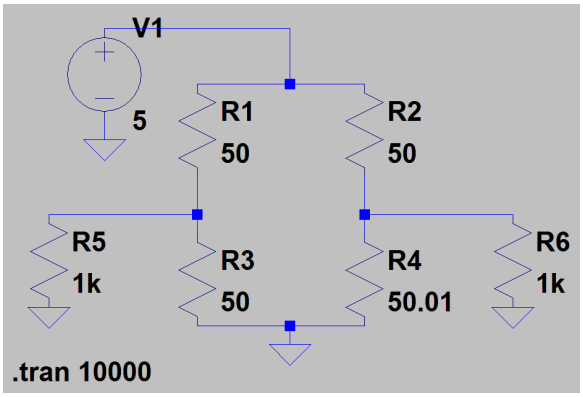

Fig. 8.29. A simple Wheat Stone Bridge

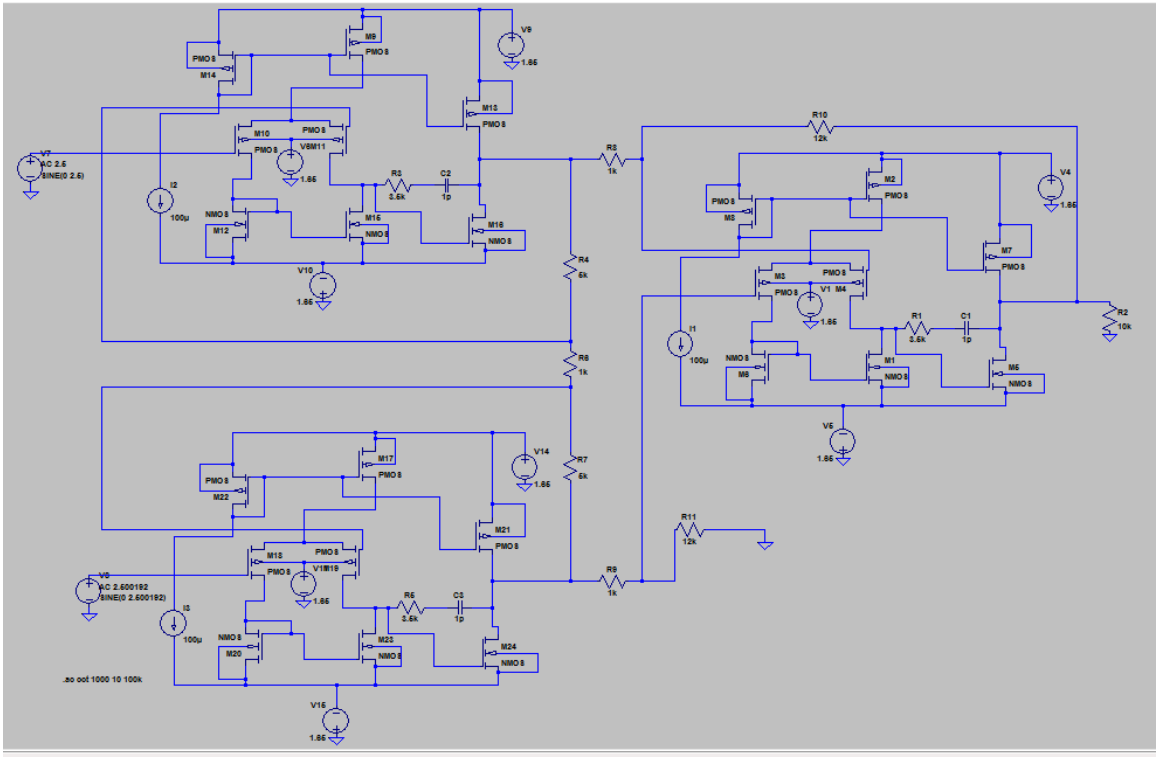

Fig. 8.30. Circuit simulation of Instrumentation Amplifier on LtSpice software

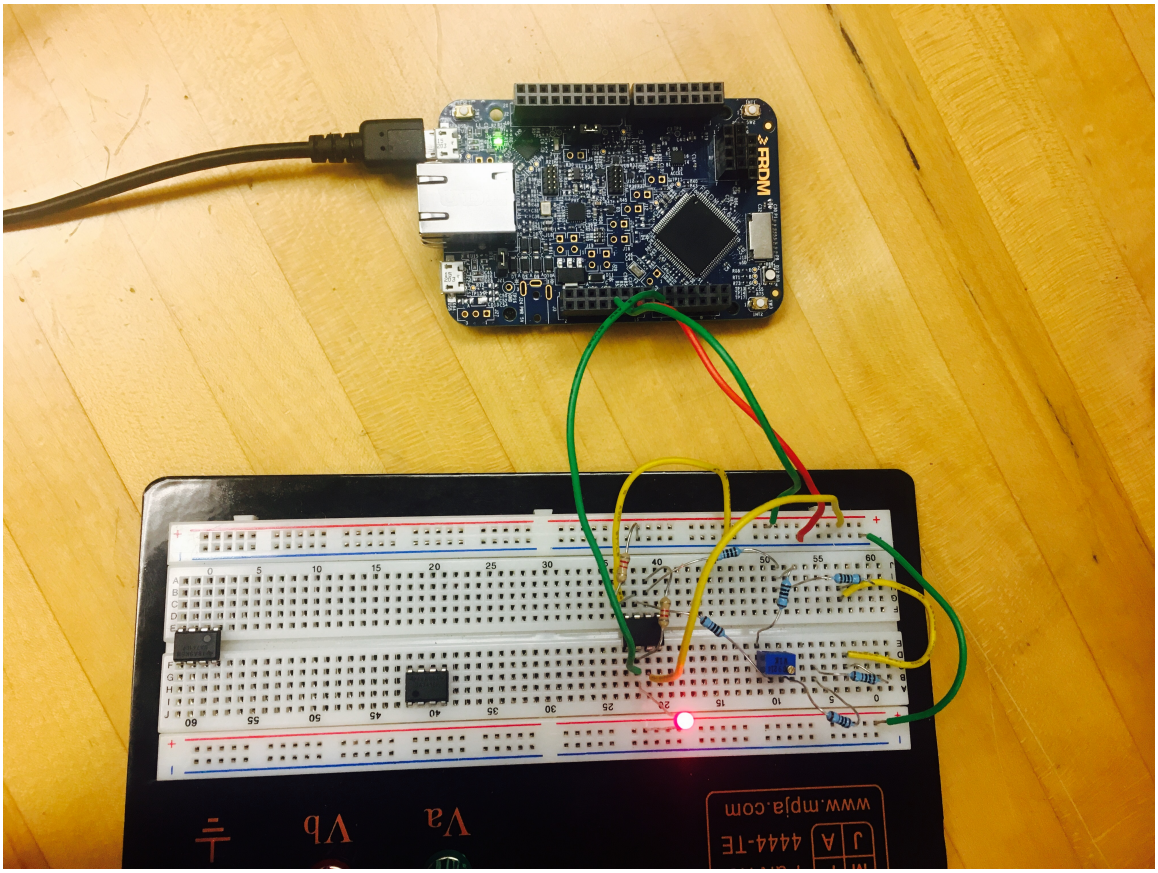

Fig. 8.31. Picture of wireless embedded system integrated device

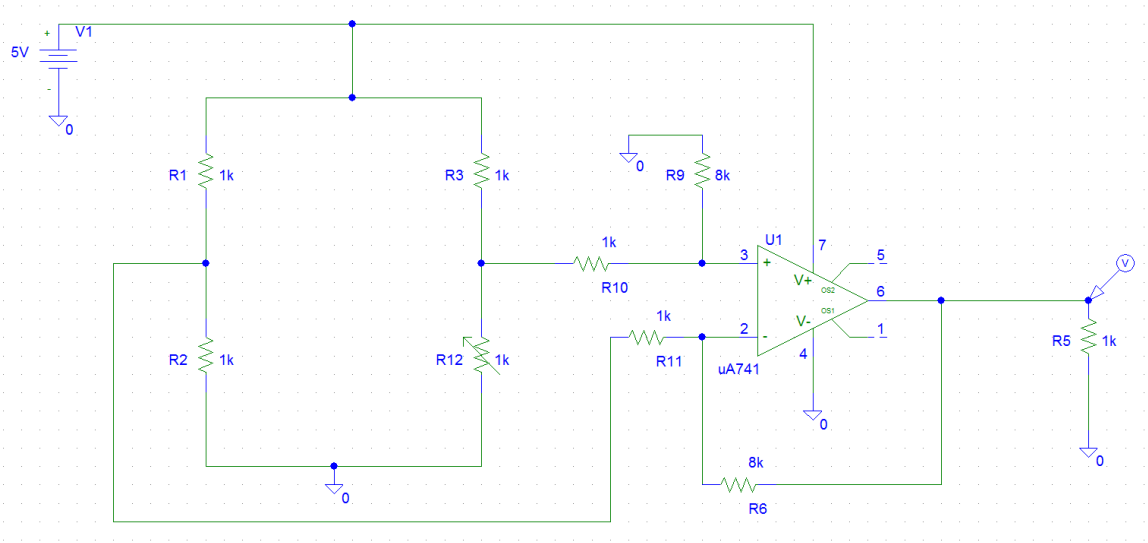

Fig. 8.32. Pspice simulation of the Embedded system integrated device

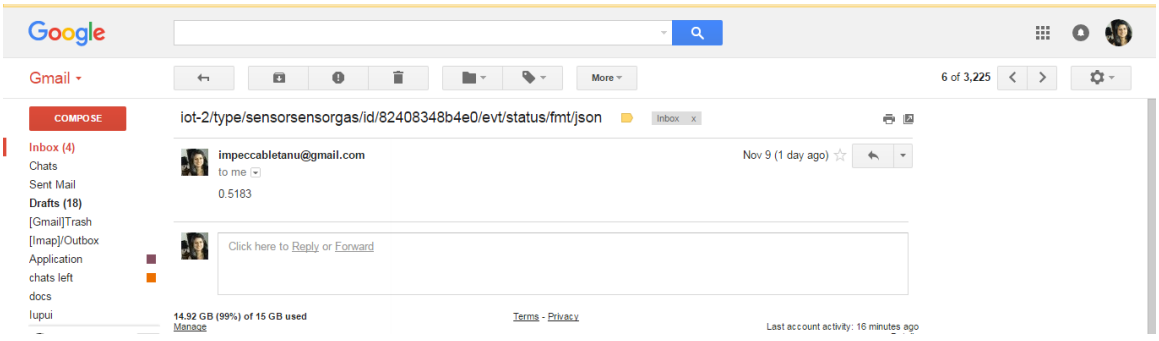

Fig. 8.33. Screenshot of the email received by the user

9. CONCLUSION AND FUTURE WORK

The nanotechnology gas sensor with graphene materials and gold nano-particles has shown high sensitivity as compared to existing gas sensing devices using semiconducting materials and other nanotechnology materials. The use of graphene mono-layer and the thermal energy provided by the Xenon dewetting, have led to catalyzed effect and enhanced the further sensitivity of the device. The resistive model in the presence of gas proved to be a sufficient model for proving the hypothesis of the study. The apparatus used in this research have provided accurate characteristics for the gas sensing devices. The device characteristics included change in resistance, concentration of the gas, rise time, fall time, and recovery time. The processing unit consisting of the bridge circuit, instrumentation/operational amplifiers with offset cancellation techniques have showed low input offset voltage that can be processed with operational amplifier and the signal is accommodated for IoT capability. The embedded system device used in this study features Ethernet connectivity.

The developed sensor was modeled with the three methods, resistive, capacitive, and FET. However, most of the estimation was based on the resistive model, the capacitive and FET models were used for the fabricated device before gas application. They proved the functionality of the device. The difficulty with the use of complicated characterization system with gas cylinders, make it more appropriate for the resistive model. A gas array made of two different CO_2 concentrations at different time instances were obtained by means of resistive estimation. The developed device may be fabricated in the array form with detecting more than two concentrations, to identify gas distribution and the selectivity of the target gas from a gas mixture. Testing data for more gases can be collected and sensor array can be populated further. Different metal nano-particles such as Palladium, Titanium, Copper and Silver may be utilized for the sensor array gas system in this application for improved selec-

tivity, and this is reserved for future development. For device array system, cross talk may be a serious noise issue within a microchip. The study here elaborated on the use of guard rings to minimize the cross talk between the instrumentation amplifiers (processing units). The design of these guard rings and their fabrication is reserved for future considerations. Figure 9.1 shows a processing unit with four nano-particle sensing device array.

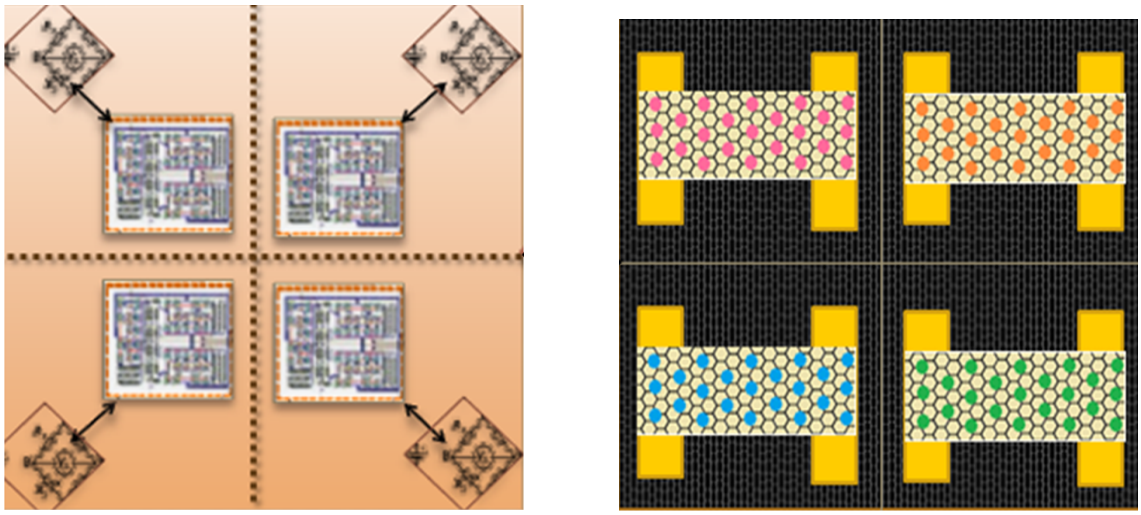

(a) Four processing units separated by guard rings

(b) Multi-nanoparticle sensing array

Fig. 9.1. Multi-sensing assemblies and interfaced processing unit separated by guard rings

LIST OF REFERENCES

LIST OF REFERENCES

[1] X. Liu, S. Cheng, H. Liu, S. Hu, D. Zhang, and H. Ning, "A survey on gas sensing technology," *Sensors*, vol. 12, no. 7, pp. 9635–9665, 2012.

[2] A. Misra, "Carbon nanotubes and graphene-based chemical sensors," *CURRENT SCIENCE*, vol. 107, no. 3, pp. 419–429, 2014.

[3] C. A. Redlich, J. Sparer, and M. R. Cullen, "Sick-building syndrome," *The Lancet*, vol. 349, no. 9057, pp. 1013–1016, 1997.

[4] T. Okumura, N. Takasu, S. Ishimatsu, S. Miyanoki, A. Mitsuhashi, K. Kumada, K. Tanaka, and S. Hinohara, "Report on 640 victims of the tokyo subway sarin attack," *Annals of emergency medicine*, vol. 28, no. 2, pp. 129–135, 1996.

[5] K. Buchholt, *Nanostructured materials for gas sensing applications*. Linköping University Electronic Press, 2011.

[6] P. Gouma, "Nanoceramic sensors for medical applications," *American Ceramics Society Bulletin*, vol. 91, no. 7, pp. 26–32, 2012.

[7] K. Kalantar-Zadeh, *Sensors: an introductory course*. Springer Science & Business Media, 2013.

[8] F. Léonard, "Crosstalk between nanotube devices: contact and channel effects," *Nanotechnology*, vol. 17, no. 9, p. 2381, 2006.

[9] W. C. Crone, "A brief introduction to mems and nems," in *Springer handbook of experimental solid mechanics*, pp. 203–228, Springer, 2008.

[10] G. M. Scheuermann, L. Rumi, P. Steurer, W. Bannwarth, and R. Mulhaupt, "Palladium nanoparticles on graphite oxide and its functionalized graphene derivatives as highly active catalysts for the suzuki- miyaura coupling reaction," *Journal of the American Chemical Society*, vol. 131, no. 23, pp. 8262–8270, 2009.

[11] K. P. Loh, Q. Bao, P. K. Ang, and J. Yang, "The chemistry of graphene," *Journal of Materials Chemistry*, vol. 20, no. 12, pp. 2277–2289, 2010.

[12] S. Kochmann, *Graphene as a sensor material*. Dissertation, Universitat Regensburg., 2014.

[13] Z. Ao, J. Yang, S. Li, and Q. Jiang, "Enhancement of co detection in al doped graphene," *Chemical Physics Letters*, vol. 461, no. 4, pp. 276–279, 2008.

[14] X. Qin, Q. Meng, and W. Zhao, "Effects of stone–wales defect upon adsorption of formaldehyde on graphene sheet with or without al dopant: a first principle study," *Surface Science*, vol. 605, no. 9, pp. 930–933, 2011.

[15] Wikipedia, "Graphene — wikipedia, the free encyclopedia," 2015. [Online; accessed 11-November-2016].

[16] Wikipedia, "Carbon nanotube — wikipedia, the free encyclopedia," 2016. [Online; accessed 11-November-2016].

[17] M. Pumera, A. Ambrosi, A. Bonanni, E. L. K. Chng, and H. L. Poh, "Graphene for electrochemical sensing and biosensing," *TrAC Trends in Analytical Chemistry*, vol. 29, no. 9, pp. 954–965, 2010.

[18] I. F. Rivera, R. K. Joshi, and J. Wang, "Graphene-based ultra-sensitive gas sensors," in *Sensors, 2010 IEEE*, pp. 1534–1537, IEEE, 2010.

[19] M. Čekada, "Properties and characterization of thin films," *Surface Properties and Engineering of Complex Intermetallics*, vol. 3, p. 1, 2010.

[20] K. Instruments *et al.*, "Making iv and cv measurements on solar/photovoltaic cells using the model 4200-scs semiconductor characterization system," *Keithley Application Note Series*, no. 2876, 2007.

[21] E. Akbari, V. K. Arora, A. Enzevaee, M. T. Ahmadi, M. Saeidmanesh, M. Khaledian, H. Karimi, and R. Yusof, "An analytical approach to evaluate the performance of graphene and carbon nanotubes for nh3 gas sensor applications," *Beilstein journal of nanotechnology*, vol. 5, no. 1, pp. 726–734, 2014.

[22] ARMmbed, "Frdm k64f development board," 2016, https://developer.mbed.org/platforms/FRDM-K64F/. [Online; accessed 05-November-2016].

[23] A. Daneshkhah, S. Shrestha, M. Agarwal, and K. Varahramyan, "Poly (vinylidene fluoride-hexafluoropropylene) composite sensors for volatile organic compounds detection in breath," *Sensors and Actuators B: Chemical*, vol. 221, pp. 635–643, 2015.

[24] Wikipedia, "Smog — wikipedia, the free encyclopedia," 2016, https://en.wikipedia.org/w/index.php?title=Smog&oldid=748948172. [Online; accessed 11-November-2016].

[25] Wikipedia, "Hvac— wikipedia, the free encyclopedia," 2016, https://en.wikipedia.org/w/index.php?title=HVAC&oldid=748482778. [Online; accessed 11-November-2016].

[26] M. E. Rizkalla, M. El-Sharkawy, and P. Salama, "Use of guard rings in solving cross talk problems between analog vlsi based instrumentation amplifiers," in *Electrical, Electronic and Computer Engineering, 2004. ICEEC'04. 2004 International Conference*, pp. 427–430, IEEE, 2004.

APPENDIX

A. APPENDIX DEMONSTRATE CODE

The main code used for sending sensing data from the sensor to the user's email address using IBM IoT platform is given.

```
#include "MQTTClient.h"
#include "MQTTEthernet.h"
#include "rtos.h"
#include "K64F.h"        // Update this to the next number
//*before* a commit
#define _APP__SW__REVISION__"18"
// Configuration values needed to connect to IBM IoT Cloud
#define ORG "hcx5hr"
// ygou5cFor a registered connection, replace with your org
#define ID "82408348b4e0"
// For a registered connection, replace with your id
#define AUTH_TOKEN "My_sen07"
// NEvLnuhK5EDI9gy+h5For a registered
//connection, replace with your auth-token
#define TYPE "sensorsensorgas"
//tanutanusensor For a registered connection,
//replace with your type
#define MQTT_PORT 1883
#define MQTT_TLS_PORT 8883
#define IBM_IOT_PORT MQTT_PORT
#define MQTT_MAX_PACKET_SIZE 250
InterruptIn sw2(SW2); // INTERRUPT FOR BUTTON PRESSED
```

```
23 AnalogIn ain(A0);    // to take the analog input
24 float f = 0.0 ;
25 void sw2_release(void) // irq handler
26 {
27    f = ain.read();
28    //printf("value is: \%f \n",f);
29 }
30 bool quickstartMode = true;
31 char org[11] = ORG;
32 char type[30] = TYPE;
33 char id[30] = ID;         // mac without colons
34 char auth_token[30] = AUTH_TOKEN;
35 // Auth_token is only used in non-quickstart mode
36 bool connected = false;
37 bool mqttConnecting = false;
38 bool netConnected = false;
39 bool netConnecting = false;
40 bool ethernetInitialising = true;
41 int connack_rc = 0;         // MQTT connack return code
42 int retryAttempt = 0;
43 int menuItem = 0;
44 int blink_interval = 0;  // to blink led during mqtt
45 //packet transfer
46 char* ip_addr = "";
47 char* gateway_addr = "";
48 char* host_addr = "";
49 int connectTimeout = 1000;
50 int connect(MQTT::Client<MQTTEthernet, Countdown,
51 MQTT_MAX_PACKET_SIZE>* client, MQTTEthernet* ipstack)
```

```
52 // the connect function is use
53 //to establish connection with IBM Watson platfrom
54 {
55  const char*iot_ibm =".messaging.internetofthings.
56  ibmcloud.com";
57  char hostname[strlen(org) + strlen(iot_ibm) + 1];
58  sprintf(hostname, "%s%s", org, iot_ibm);
59  EthernetInterface& eth = ipstack->getEth();
60  ip_addr = eth.getIPAddress();
61  gateway_addr = eth.getGateway();
62     // Construct clientId - d:org:type:id
63  char clientId[strlen(org) + strlen(type) + strlen(id) + 5];
64  sprintf(clientId, "d:%s:%s:%s", org, type, id);
65   // Network debug statements
66  LOG("=====================================\n");
67  LOG("Connecting Ethernet.\n");
68  LOG("IP ADDRESS: %s\n", eth.getIPAddress());
69  LOG("MAC ADDRESS: %s\n", eth.getMACAddress());
70  LOG("Gateway: %s\n", eth.getGateway());
71  LOG("Network Mask: %s\n", eth.getNetworkMask());
72  LOG("Server Hostname: %s\n", hostname);
73  LOG("Client ID: %s\n", clientId);
74  LOG("=====================================\n");
75  $\int$
76  netConnecting = true;
77  int rc=ipstack->connect(hostname,
78  IBM_IOT_PORT,connectTimeout);
79  if (rc != 0)
80     {
```

```
81        WARN("IP Stack connect returned: %d\n", rc);
82        return rc;
83      }
84      netConnected = true;
85      netConnecting = false;
86      // MQTT Connect
87      mqttConnecting = true;
88      MQTTPacket_connectData data =
89      MQTTPacket_connectData_initializer;
90      data.MQTTVersion = 3;
91      data.clientID.cstring = clientId;
92      if (!quickstartMode)
93     {
94          data.username.cstring = "use-token-auth";
95          data.password.cstring = auth_token;
96      }
97      if ((rc = client->connect(data)) == 0)
98      {
99          connected = true;
100         //displayMessage("Connected");
101         wait(1);
102         //displayMessage("Scroll with joystick");
103     }
104     else
105         WARN("MQTT connect returned %d\n", rc);
106     if (rc >= 0)
107         connack_rc = rc;
108     mqttConnecting = false;
109     return rc;
```

```
110 }
111 int getConnTimeout(int attemptNumber)
112 //no of attempts to try
113 //to estrablish connection
114 {  // First 10 attempts try within 3 seconds,
115 //next 10 attempts retry after every 1 minute
116  // after 20 attempts, retry every 10 minutes
117  return(attemptNumber<10)?3:(attemptNumber<20)?60:600;
118 }
119 void attemptConnect(MQTT::Client<MQTTEthernet, Countdown,
120 MQTT_MAX_PACKET_SIZE>* client, MQTTEthernet* ipstack)
121 {
122  connected = false;
123  // make sure a cable is connected before starting to connect
124  while (!linkStatus())
125  {
126    wait(1.0f);
127  WARN("Ethernet link not present. Check cable connection\n");
128  }
129   while (connect(client, ipstack) !=
130   MQTT_CONNECTION_ACCEPTED)
131  {
132    if (connack_rc == MQTT_NOT_AUTHORIZED || connack_rc
133    ==    MQTT_BAD_USERNAME_OR_PASSWORD)
134     return;
135         // don't reattempt to connect if
136         //credentials are wrong
137         //Thread red_thread(flashing_red);
138         int timeout = getConnTimeout(++retryAttempt);
```

```
139         WARN("Retry attempt number %d waiting %d\n",
140         retryAttempt, timeout);
141         // if ipstack and client were on the heap we
142         //could deconstruct and goto a label where
143         //they are constructed
144         //  or maybe just add the proper members to
145         //do this disconnect and call attemptConnect(...)
146         // this works - reset the system when the retry
147         //count gets to a threshold
148         if (retryAttempt == 5)
149             NVIC_SystemReset();
150         else
151             wait(timeout);
152   }
153 }
154 int publish(MQTT::Client<MQTTEthernet, Countdown,
155 MQTT_MAX_PACKET_SIZE>* client, MQTTEthernet* ipstack)
156 // publish the data on IBM Watson IoT platform
157 {
158   MQTT::Message message;
159     char* pubTopic = "iot-2/evt/status/fmt/json";
160     sw2.rise(&sw2_release);
161     // call the irq handler
162     char buf[250];
163     if(f > 0.5)
164     // if the voltage is greater than 0.5 publish the
165     //data on device type creted on watson
166     {
167      //sprintf(buf,"{\"Vol\":\"%s\}",f);
```

```
168       sprintf(buf,"{\"voltage\":%0.4f\}", f);
169       // pack the data in buffer of size 250
170        f = 0;
171        // f = 0 in order to avoide continious publishing
172      }
173      message.qos = MQTT::QOS0;
174      message.retained = false;
175      message.dup = false;
176      message.payload = (void*)buf;
177      message.payloadlen = strlen(buf);
178      LOG("Publishing %s\n", buf);
179      return client->publish(pubTopic, message);
180  }
181  char* getMac(EthernetInterface& eth,
182  char* buf, int buflen)
183  // Obtain MAC address
184  {
185      strncpy(buf, eth.getMACAddress(), buflen);
186      char* pos;
187      // Remove colons from mac address
188      while ((pos = strchr(buf, ':')) != NULL)
189          memmove(pos, pos + 1, strlen(pos) + 1);
190      return buf;
191  }
192  void messageArrived(MQTT::MessageData& md)
193  //we can use this to send some control information
194  //from app(ibm blumix) to frdmk64f
195  {
196      MQTT::Message &message = md.message;
```

```
197     char topic[md.topicName.lenstring.len + 1];
198     sprintf(topic, "%.*s", md.topicName.lenstring.len,
199     md.topicName.lenstring.data);
200     LOG("Message arrived on topic %s: %.*s\n",  topic,
201     message.payloadlen, message.payload);
202     // Command topic: iot-2/cmd/blink/fmt/json - cmd is
203     the string between cmd/ and /fmt/
204     char* start = strstr(topic, "/cmd/") + 5;
205     int len = strstr(topic, "/fmt/") - start;
206     if (memcmp(start, "blink", len) == 0)
207     {
208         char payload[message.payloadlen + 1];
209         sprintf(payload, "%.*s", message.payloadlen,
210         (char*)message.payload);
211         char* pos = strchr(payload, '}');
212         if (pos != NULL)
213         {
214             *pos = '\0';
215             if ((pos = strchr(payload, ':')) != NULL)
216             {
217                 int blink_rate = atoi(pos + 1);
218                 blink_interval = (blink_rate <= 0) ? 0 :
219                 (blink_rate > 50 ? 1 : 50/blink_rate);
220             }
221         }
222     }
223     else
224         WARN("Unsupported command: %.*s\n",
225         len, start);
```

```
226 }
227 int main()
228 {
229     quickstartMode = (strcmp(org, "quickstart") == 0);
230     //lcd.set_font((unsigned char*) Arial12x12);
231     // Set a nice font for the LCD screen
232     led2 = LED2_OFF;
233     // K64F: turn off the main board LED
234     //isplayMessage("Connecting");
235     //Thread yellow_thread(flashing_yellow);
236     //Thread menu_thread(menu_loop);
237     LOG("***** IBM IoT Client Ethernet Example *****\n");
238     MQTTEthernet ipstack;
239     ethernetInitialising = false;
240     MQTT::Client<MQTTEthernet, Countdown,
241     MQTT_MAX_PACKET_SIZE>
242     client(ipstack);
243     LOG("Ethernet Initialized\n");
244     if (quickstartMode)
245         getMac(ipstack.getEth(), id, sizeof(id));
246     attemptConnect(&client, &ipstack);
247     if (connack_rc == MQTT_NOT_AUTHORIZED || connack_rc ==
248     MQTT_BAD_USERNAME_OR_PASSWORD)
249     {
250        // red();
251         while (true)
252             wait(1.0); // Permanent failures - don't retry
253     }
254     if (!quickstartMode)
```

```
255     {
256         int rc = 0;
257         if ((rc = client.subscribe("iot-2/cmd/+/fmt/json",
258         MQTT::QOS1, messageArrived)) != 0)
259     WARN("rc from MQTT subscribe is \%d \n", rc);
260     }
261     blink_interval = 0;
262     int count = 0;
263     while (true)
264     {
265       if (++count == 100)
266         {    // Publish a message every second
267             if (publish(&client, &ipstack) != 0)
268             attemptConnect(&client, &ipstack);
269                 // if we have lost the connection
270             count = 0;
271         }
272         if (blink_interval == 0)
273             led2 = LED2_OFF;
274         else if (count % blink_interval == 0)
275             led2 = !led2;
276         client.yield(10);
277         // allow the MQTT client to receive messages
278     }
279 }
```